uOttawa

L'Université canadienne
Canada's university

Approaches for Noble Gas Isotope Application in Rock Porewater Studies

by

Ende Zuo

Under the supervision of

Dr. Ian D. Clark

A thesis submitted to the University of Ottawa

in partial fulfillment of the requirements for

Doctorate of Philosophy degree in Earth Science

Department of Earth and Environmental Sciences
Faculty of Science
University of Ottawa

Examining Committee

The following served on the Examining Committee for this thesis.

External Examiner: Tom Kotzer

Associate Principal Consultant, SRK Consulting

Adjunct Professor, University of Saskatchewan

Internal Examiner: Tom Al

Professor, Department of Earth and Environmental Sciences,

University of Ottawa

Clement Bataille

Assistant Professor, Department of Earth and Environmental Sciences, University of Ottawa

Richard Amos

Associate Professor, Institute for Environmental and Interdisciplinary Sciences, Carleton University

Supervisor: Ian Clark

Professor, Department of Earth and Environmental Sciences, University of Ottawa

Declaration of Authorship

I hereby certify that this thesis is entirely my own original work except where otherwise indicated. I am aware of the University's regulations concerning plagiarism, including those concerning consequent disciplinary actions. Any use of the works of any other author, in any form, is properly acknowledged at their point of use.

Abstract

Radioactive decay of U, Th and K contributes to noble gas radiogenic ingrowth in different geological reservoirs, which distinguish mass origin and reveal its transport pathway. Compared with minerals and fluid inclusions, porewater is more relevant in revealing the mobile mass origin and transport in the porous, deep subsurface environment. Hence, the approaches for porewater noble gas extraction and analysis are of great meaning to geochemistry and hydrogeology. However, all five stable noble gases in rock porewater are difficult to acquire because of possible air contamination during storage and difficulty of noble gas separation. This dissertation is dedicated to exploring novel noble gas extraction and analysis methods from rock porewater.

Two porewater gas extraction methods were developed for crystalline and sedimentary rocks, respectively. Temperature-controlled heating was applied to crystalline rocks. Out-diffusion in Al-foil bags was used for Ordovician sedimentary rocks. Regarding noble gas methodology, a newly designed pneumatic processing line was built to explore an iterative polished stainless steel wool trapping method to separate Kr from Ar. The iterative trapping method yields > 95% trapping efficiency for Kr and > 99% trapping efficiency for Xe. Simultaneously, comparable and steady noble gas sensitivities and noble gas isotope ratios were attained from air standard aliquots.

From heating experiments on crystalline rock porewater, the consistency of noble gas ratios between headspace gas and rock porewater illustrates that this extraction method is valid for crystalline rock. This work provides a benchmark for noble gas extraction from crystalline rock porewater. With room-temperature out-diffusion method in Al-bag, noble gas ratios and concentrations of Ordovician sedimentary rocks reveal crustal features. The measured noble gas ratios in Ordovician sedimentary cores agree with measurements previously made in the Ordovician brine samples from the western flank of the Michigan Basin. The Ordovician porewater residence time is quantitatively estimated with both He and Xe radiogenic ingrowth, yielding an average of 251 million years (m.y.), which is comparable with the previous He accumulation time estimate at the same study site that yielded 260 m.y.. The remarkable preservation of gases in Al-foil bags provides an economic and efficient possibility for noble gas out-diffusion sampling.

In summary, the exploration of porewater noble gas extraction and all five noble gas analysis methodology gives satisfying noble gas results and geological information. These original developments are of great meaning to the future work of the noble gas laboratory at the University of Ottawa.

Acknowledgments

This thesis is a summary of my hard work, study and academic growth in the last five years. Though I have encountered a lot of failure and frustration, finally I reach the finish line with the help of so many kind people.

First of all, I would like to say thanks to my supervisor Ian Clark who is always patient and inspiring. Thanks to him, I get systematically trained with hands-on experience in every section of noble gas research. He has a rigorous academic attitude and conveys his spirit to everyone who works with him. I would not have achieved this without his careful cultivation.

I greatly appreciate the help and company from Anthony Lapp during these years. He is the witness of every step of building the processing line, calibrating the two mass spectrometers, developing the noble gas analysis procedures and analyzing different kinds of samples. He is the one always there to help even on weekends and maintain the operation of the laboratory. I could not have completed my sample analysis without his selfless dedication. I also want to acknowledge Josué J. Jautzy for his cooperated sampling and his useful discussion on my papers. The quality of the paper was highly improved with his suggestions. I also say thanks to David Zal and Najem Tarek for their smooth cooperation during the crystalline core experiments. They give a lot of help and support to the experiment design and conduction.

Special thanks extend to the committee of this thesis: Dr. Tom Kotzer from SRK Consulting and the University of Saskatchewan, Dr. Tom Al and Dr. Clement Bataille from the University of Ottawa, Dr. Richard Amos from the Carleton University. It is my great honor to have them review my thesis and I appreciate their comments and suggestions to improve this thesis.

I give many thanks to my office neighbors and friends: Daniela Quintero, Victor Garcia, Shilong Liu, Yuan Wang, Shishi Chen, Shuo Liang, He Kang for their support. Last but not least, I thank my parents for their love, support and sacrifices, giving me a chance to pursue my academic dream far away from home and always being patient.

Table of Contents

List of Figures

List of Tables

List of Symbols and Abbreviations

U----------Uranium

Th----------Thorium

K----------Potassium

He----------Helium

Ne----------Neon

Ar----------Argon

Kr----------Krypton

Xe----------Xeon

SFT----------Split Flight Tube

SEM----------Secondary Electron Multiplier

SRG----------Spinning Rotary Gauge

λ ----------decay constant

Y----------mass yield of daughter element form decay of parent

DGR----------deep geologic repository

UHV----------ultra high vacuum

IUPAC----------International Union of Pure and Applied Chemistry

Chapter 1 Introduction

1.1. Noble Gas Basic Properties

1.1.1. Physical Properties

Due to their scarcity and non-reactivity, the noble gases were found relatively late in chemistry history. Noble gases were the last column added in the Periodic Table (Ozima & Podosek, 2002). Helium (He) was identified by several observers who found a previously unknown line in the spectrum of the solar chromosphere during the 1868 eclipse. Other noble gases were discovered mainly by Rayleigh and Ramsay at the end of the 19^{th} century. They published a paper to announce the discovery of a new element and named it argon (Ar) in 1895. Then in September 1898, Ramsay and Morris Travers conducted fractional distillation experiments on liquid air, in which they identified other three noble gas elements: neon (Ne), krypton (Kr) and xenon (Xe) (Ozima & Podosek, 2002).

He, Ne, Ar, Kr and Xe are chemical elements with atomic numbers 2, 10, 18, 36, 54, atomic weights 4.0026, 20.179, 39.948, 83.80, 131.30, respectively. They are all colorless, odorless inert gases. He is monatomic gas under standard conditions, the first element in the noble gas group in the periodic table with a volume fraction of 5.24 ppm in the air. Ne is also monatomic gas under standard conditions, with about two-thirds the density of air and with a volume fraction of 18.18 ppm. Ar is the third-most abundant gas in the Earth's atmosphere with an abundance of 0.934%, which is a bit contradictory with the alias of noble gases, rare gases. Ar is the most abundant noble gas in the Earth's crust, comprising 0.00015% of the crust. Nearly all of the Ar in the Earth's atmosphere is radiogenic ^{40}Ar, derived from the decay of ^{40}K in the Earth's crust. Kr occurs in trace amounts in the atmosphere and its concentration is 1.14 ppm in the air. Xe is the heaviest stable noble gas found in the Earth's atmosphere in trace amounts and its abundance is 0.087 ppm in the air. The main physical and chemical properties of the noble gases are listed in Table 1.1.

Table 1.1 Physical and chemical properties of He, Ne, Ar, Kr and Xe

(Ozima and Podosek, 2002)

	Units	He	Ne	Ar	Kr	Xe
Atomic number	-	2	10	18	36	54
Atomic weight	amu	4.00260	20.18	39.95	83.80	131.30
Triple point	K	-	24.6	83.8	116.0	161.3
Normal boiling point	K	4.2	27.1	87.3	119.8	165.0
Critical point	K	5.3	44.5	151.9	209.4	289.7
Triple point pressure	torr	-	324	516	548	612
Heat of fusion at triple point	cal/mole	-	80	281	391	549
Heat of vaporization at NBP	cal/mole	19	414	1558	2158	3020
Van der Waals const. a	1^2-atm	0.03412	0.211	1.345	2.318	4.194
Van der Waals const. b	1	0.0237	0.01709	0.03219	0.03978	0.05105
Atomic radius	10^{-8} cm	-	1.55	1.88	1.98	2.18
Ionization energy	eV	24.48	21.56	15.76	14.00	12.13
Ionization crosssection (80eV electrons)	10^{-17} cm^2	3.1	7	36	51	75
Polarizability	10^{-24} cm^3	0.201	0.39	1.62	2.46	3.99

1.1.2 Chemical Properties

Firstly, as the name indicated, noble gases are chemically inert, which means they do not form chemical compounds in natural conditions on the earth. This is attributed to their filled outer valence shell as elements occupying the last column of the Periodic Table. While Kr and Xe can theoretically react with highly electronegative elements (e.g. F and O), those are already bound to more reactive elements than Kr and Xe. Therefore in the natural terrestrial system, the noble gases are considered as non-reactive elements.

Secondly, because of their chemical inertness, noble gases are very scarce on the Earth. This means the noble gases have a quite low background in the environment, which makes a small amount of material added to reservoirs obvious and observable. Hence, the radiogenic and fissiogenic ingrowth of the noble gases in the geological reservoirs can make prominent changes in noble gas isotopic features.

These two main chemical properties grant the noble gases effective geological tracers of groundwater resources and geochronometers of residence time estimate.

1.2 Theoretical Review

1.2.1 Generation of Geogenic Noble Gases

In the crust, except for the atmospheric origin, trapped noble gases in crustal rocks are of a geogenic origin. Geogenic origin constitutes the major component of noble gas inventory in the crust. The contribution from the trapped atmospheric origin in the solid crust can be assumed to be insignificant, particularly for geogenic He and Ar. Regarding the small production rate of Ne, Kr and Xe isotopes, the atmospheric component is still necessary to be taken into account in geogenic ingrowth calculation. The production mechanisms of geogenic noble gases are different and the production rates are various. The geogenic noble gas isotopes can be derived from reactions as follows:

$^{238}_{92}\mathrm{U} \rightarrow {}^{206}_{82}\mathrm{Pb} + 8^{4}_{2}\mathrm{He} + 6\beta^{-} + Q$ α decay of ^{238}U (1.1)

$^{235}_{92}\mathrm{U} \rightarrow {}^{207}_{82}\mathrm{Pb} + 7^{4}_{2}\mathrm{He} + 4\beta^{-} + Q$ α decay of ^{235}U (1.2)

$^{232}_{90}\mathrm{Th} \rightarrow {}^{208}_{82}\mathrm{Pb} + 6^{4}_{2}\mathrm{He} + 4\beta^{-} + Q$ α decay of ^{232}Th (1.3)

$^{17}_{8}\mathrm{O} + \alpha \rightarrow {}^{20}_{10}\mathrm{Ne} + n$ α interaction on ^{17}O (1.4)

$^{18}_{8}\mathrm{O} + \alpha \rightarrow {}^{21}_{10}\mathrm{Ne} + n$ α interaction on ^{18}O (1.5)

$^{19}_{9}\mathrm{F} + \alpha \rightarrow {}^{22}_{10}\mathrm{Ne} + n$ α interaction on ^{19}F (1.6)

$^{22}_{11}\mathrm{Na} + e^{-} \rightarrow {}^{22}_{10}\mathrm{Ne}$ electron capture of ^{22}Na (1.7)

$^{40}_{19}\mathrm{K} + e^{-} \rightarrow {}^{40}_{18}\mathrm{Ar}$ electron capture of ^{40}K (1.8)

$^{238}_{92}\mathrm{U} \rightarrow {}^{86}_{36}\mathrm{Kr} + {}^{150}_{60}\mathrm{Nd} + 2n$ ^{238}U spontaneous fission (1.9)

$^{238}_{92}\mathrm{U} \rightarrow {}^{136}_{54}\mathrm{Xe} + {}^{100}_{42}\mathrm{Mo} + 2n$ ^{238}U spontaneous fission (1.10)

In the crust, radiogenic ^{4}He (also known as α particles) are dominantly produced from α decay of U and Th radioactive isotopes (Equation 1.1, 1.2 and 1.3). Hence ^{4}He

production rate is directly proportional to the concentration of U and Th elements in the crust. The α yields for ^{238}U, ^{235}U and ^{232}Th are 8, 7 and 6, respectively.

A very small proportion of the U-Th produced α particles will react with ^{17}O, ^{18}O and ^{19}F to produce geogenic ^{20}Ne, ^{21}Ne and ^{22}Ne (Equation 1.4, 1.5 and 1.6) (Ballentine & Burnard, 2002). ^{22}Ne can also be produced from the electron capture of ^{22}Na (Equation 1.7). Ne isotopes production rate is related to radioelement and target-element concentrations as well as the distribution of the target elements.

^{40}Ar production in the crust is dominated by the decay of ^{40}K (Equation 1.8) and is therefore proportional to the K concentration. ^{40}Ar is produced by the electron capture of ^{40}K with a decay constant of 5.81×10^{-11} yr^{-1}. The ^{40}Ar production rate is quite large so that the Ar in the air is mostly from the crustal source.

Production of ^{86}Kr and ^{136}Xe in the crust is dominated by the spontaneous fission of ^{238}U. ^{238}U has a branched decay mode, except α decay, spontaneous fission produces other isotopes including ^{86}Kr with a yield of 0.951% and ^{136}Xe with a yield of 6.3%, respectively (Young & Thode, 1960). With a ^{86}Kr production rate that is 6.1 times smaller than that for spontaneous ^{136}Xe, U-Kr dating method is less useful than U-Xe dating method due to the lower fission yield and the usually higher initial Kr abundance compared to Xe.

1.2.2 Noble Gas Geochronometry

The stable noble gases have well-constrained atmospheric concentrations and atmospheric molar fractions. While most of the noble gases were produced during nucleosynthesis at the formation of the solar system, others continue to be produced by nuclear reactions such as α decay of U and Th, electron capture reaction and spontaneous fission in the subsurface (I. Clark, 2015). Measuring the geogenic increase/ingrowth of noble gas abundances in deep groundwater and rock porewater provides a measure of system closure time because the waters have been isolated from the atmosphere.

The decay of U and Th to stable isotopes of Pb (Equation 1.1, 1.2 and 1.3) is the basis for U-Pb, Th-Pb and U/Th-He dating methods. The U/Th-He method has been widely applied in the groundwater and porewater residence time estimate in the crust (e.g., Osenbrück et al., 1998; I. D. Clark et al., 2013; Holland et al., 2013; Zuo et al., 2021). ^{4}He production rate in the crust can be calculated according to:

$$^{4}He=8\times\left[^{238}U\right]\times(e^{\lambda_{238}t}-1)+7\times\left[^{235}U\right]\times(e^{\lambda_{235}t}-1)+6\times\left[^{232}Th\right]\times(e^{\lambda_{232}t}-1) \quad (1.11)$$

Where ^{4}He is the radiogenic ^{4}He concentration that would be produced within a rock over time t; $[^{238}U]$, $[^{235}U]$, $[^{232}Th]$ are concentrations in ppm of the parent elements; λ_{238}, λ_{235}, λ_{232} are the decay constants for the three radioisotopes, 1.55×10^{-10} yr^{-1}, 9.85×10^{-10} yr^{-1} and 4.95×10^{-11} yr^{-1}, respectively (Faure & Mensing, 2004; Yoshioka et al., 2005).

Based on the ^{4}He production rate (Equation 1.11), the U/Th-He age is expressed as:

$$t_{(U/Th-He)} = \frac{^4He_{radiogenic}}{^4He_{production\ rate}} \quad (1.12)$$

Where $^4He_{radiogenic}$ is the radiogenic ^4He measured in rock or groundwater samples, $^4He_{production\ rate}$ is calculated with the U and Th concentrations in the samples.

Since the theoretical basis was established in 1950, K-Ar dating method has been widely used for measuring the ages of K-bearing rocks and minerals. ^{40}K is a naturally occurring isotope with an abundance of $0.01167 \pm 0.00004\%$ in the environment. About 10.48% of the naturally occurring ^{40}K decay to stable ^{40}Ar by electron capture. Stable ^{40}Ar can also be produced by positron emission of ^{40}K, but the frequency is only 0.001%, which can be neglected. The K-Ar age calculation can be expressed as:

$$t_{(K-Ar)} = \frac{1}{\lambda} \ln \left[\frac{^{40}Ar^*}{^{40}K} \left(\frac{\lambda}{\lambda_e} \right) + 1 \right] \quad (1.13)$$

Where λ is the total decay constant of ^{40}K, λ_e refers to the decay to ^{40}Ar, λ_β refers to the decay to ^{40}Ca, $\lambda = \lambda_e + \lambda_\beta$; $^{40}Ar^*$ is the growth of radiogenic ^{40}Ar atoms in a K-bearing rock or mineral; ^{40}K is the atoms of ^{40}K per unit weight of a K-bearing rock or mineral. As mentioned above, K-Ar is usually suitable for K-bearing rock or minerals. When it comes to groundwater or rock porewater age calculation, the weathering level of K-bearing mineral or rock determines the extent of the radiogenic ^{40}Ar partial release into the ambient environment (e.g., Andrews et al., 1989; Seltzer et al., 2021). As a consequence, K-Ar method is deemed not accurate for groundwater and rock porewater age calculation.

The U-Xe age is calculated using the following equation (Eikenberg et al., 1993):

$$t_{(U-Xe)} = \frac{1}{\lambda_\alpha + \lambda_{sf}} \ln \left[\frac{^{136}Xe_{sf} \times \left(\lambda_\alpha + \lambda_{sf} \right)}{^{238}U \times Y_{sf} \times \lambda_{sf}} + 1 \right] \quad (1.14)$$

Where λ_α is the α-decay constant of ^{238}U which is 1.55×10^{-10} yr^{-1} (Yoshioka et al., 2005); λ_{sf} is the ^{238}U spontaneous fission decay constant 8.51×10^{-17} yr^{-1}(Yoshioka et al., 2005); Y_{sf} is the mass yield of ^{136}Xe from ^{238}U spontaneous fission, which is 6.3%;(Young & Thode, 1960); $^{136}Xe_{sf}$ is the concentration of fissiogenic ^{136}Xe (cc ^{136}Xe/g rock).

Theoretically, geogenic Ne and Kr can also be used as geochronometers. However, the geogenic Ne has complicated production routes and the ingrowth is not prominent. The geogenic Kr has a very small production rate which needs 21 Ga to make 10% increase of $^{86}Kr/^{84}Kr$ value, which makes the isotopic anomaly hard to detect. By reasons of the foregoing, geogenic Ne and Kr have not been widely used as geochronometers for groundwater and rock porewater.

1.3 Literature Review

According to their special physical and chemical properties and origin, noble gases are not only widely applied in cosmochemistry, geochemistry and oceanography (Aeschbach, 2016), but also have been extensively used as environmental tracers in the study of lakes, oceans, groundwater and porewater since the 1960s.

1.3.1 Cosmochemistry

In the solar nebular, the noble gases are very abundant and the Sun is the largest reservoir of noble gases in the solar system. Researchers got the cosmochemical profile of the solar system by investigating the composition of meteorites and the Moon (Porcelli et al., 2002). Some Ar data was attained from planetary probes for the atmosphere of Mars (Nier & McElroy, 1977). The primitive noble gas abundances and ratios of solar system bodies (except the Earth, Mars and asteroids), the atmospheres of Mercury and the moon, comets, interplanetary dust particles and elementary particles in the interplanetary medium were summarized and discussed(Wieler, 2002). Radiogenic noble gases were applied to solar system and lunar chronology (Swindle, 2002). A Martian meteorite found in northwest Africa was detected that contained no solar-like Xe but with Martian atmospheric noble gases (Marty et al., 2006). The concentrations and isotopic ratios of the cosmogenic He, Ne and Ar in the iron meteorite "Xinjiang" indicate significant cosmogenic contribution and give an exposure age of 62 ± 16 Ma (Ammon et al., 2011).

1.3.2 Noble gases in the mantle and the crust

In the research of the mantle, the noble gases can provide information on the mantle evolution processes, mass spatial distributions and chronological constraints. In the mantle-derived materials, high $^{129}Xe/^{130}Xe$ ratios were also discovered (Kaneoka & Takaoka, 1978; Staudacher & All ègre, 1982). There have been mantle variations in Xe isotopes, which provide constraints on the early degassing process. In Japanese volcanic rockss, a relatively low $^{40}Ar/^{36}Ar$ was detected, a simple model of mass fractionation explained this phenomenon and predicted an upper limit for $^{20}Ne/^{22}Ne$ of 10.3 and a lower limit for $^{40}Ar/^{36}Ar$ of 280 that was coincident with the noble gas data from volcanic materials (Kaneoka, 1980). Ne isotopes were used to constrain the convection and primordial volatile origin in the Earth's mantle (Ballentine et al., 2005). Noble gases help confirm a plume-related mantle degassing process which is the first evidence in support of an upwelling deep mantle beneath Southern Africa (Gilfillan et al., 2019). Xe isotopes provide geochemical evidence for high volatile fluxes from the mantle at the end of Archean by a relatively short burst of mantle activity (Marty et al., 2019). He ratio ($^{3}He/^{4}He$) variation in the mantle was proved not only as a result of the decay of U and Th but also can be caused by thermal diffusion in the lower mantle (Zhu et al., 2020). A strikingly high He ratio in central Panama reveals a distal connection to the Galapagos plume through a slab window (Bekaert et al., 2021).

With respect to study in the crust, the noble gases provide evidence on the crust evolution processes, the mass spatial distributions, migrations and chronological

constraints. The discovery of excess ^{129}Xe in the Harding County (New Mexico, USA) natural gases provided the first evidence for the terrestrial effects of an extinct ^{129}I isotope (Butler et al., 1963). A review was made on the production, release, transport and accumulation in the continental crust which is important instructional work (Ballentine & Burnard, 2002). Noble gas applications in tracing the fluid origin, transport and interactions in the crust were also summarized in a review paper (Ballentine et al., 2002). Deep brine samples from the Michigan basin present crustal noble gas components, and a recent reactivation of the ancient midcontinent rift system is likely the reason for the crustal noble gas features (Ma et al., 2009). Preserved ^{4}He and ^{40}Ar in the stable continental crust from the Bravo Dome natural CO_2 field (New Mexico) were applied to provide constraints on the chemical evolution of the solid Earth and atmosphere (Sathaye et al., 2016). An $^{40}Ar/^{36}Ar$ model which firstly combined Ar degassing with the thermal evolution of the Earth constrains the growth of continental crust (Guo & Korenaga, 2020). Noble gases are also coupled with other geochemical tracers to distinguish the mixture compositions of crustal geothermal fluids (e.g., Pinti et al., 2020). By comparing the noble gases isotopic compositions of crustal xenoliths and lavas, a significant modification of magmatic noble gases by the interaction with the partially melted crust was revealed (Álvarez-Valero et al., 2022). Moreover, the noble gases are commonly applied on the mass tracing and age constraints for crustal rock and water samples (Kietäväinen et al., 2014; Hendry et al., 2015; T. Wen et al., 2015; T. Wen et al., 2016; Tao Wen et al., 2017; Warr et al., 2018; Kotarba et al., 2019; Pinti et al., 2019; Li et al., 2020; Zuo et al., 2021).

1.3.3 Noble Gases Applied in Groundwater

In hydrogeology, the noble gases are prevailing tracers and their concentrations dissolved in groundwater constitute thermometers which provide a method of paleoclimate reconstruction (e.g., Mazor, 1972; Aeschbach-Hertig et al., 2000). In addition, the noble gases are also useful for determining the origin of ground ice in the Canadian Arctic (e.g., Utting et al., 2012; Utting et al., 2013). Noble gas data can also contribute to the quantification of the mixing proportions of different water masses (Loose et al., 2016). Noble gases, especially the temperature-sensitive ones (Kr and Xe), are recognized as well-established tracers to reconstruct groundwater recharge conditions.

Concerning deep groundwater/porewater, noble gases reserved in confined circumstances provide information for mass migration path and groundwater/porewater residence time. Dating ancient porewater/groundwater is a key factor for the safety assessment for nuclear waste in deep geological repositories. In order to understand the risk of exposure to the radioactive waste, assuming that the mobile radionuclide will be transported by a deep groundwater system, it is very important to interpret the residence time of deep fluids from low-permeability rock strata to the biosphere by noble gas geochronology.

In rock samples, the deep fluids' age or residence time can be unraveled by the radiogenic ^{4}He, ^{40}Ar and ^{136}Xe isotopes produced mainly by α decay of U and Th, electron capture of ^{40}K and spontaneous fission of ^{238}U. For instance, the porewater

ages of sedimentary rock exceed 6–10 million years near the nuclear waste repository in Morsleben, Germany (Osenbrück et al., 1998). In fluid inclusions from Western Australia, from a drilled core which has an Ar-Ar plateau age of 3.0±0.2 billion years, brine age was confirmed by $^{130}Ba - {}^{130}Xe$ dating to be 3.8±1.1 billion years (Pujol et al., 2011). Holland et al. (2013) used Ne and Xe isotopes to date paleo groundwater in deep crystalline rock, showing enrichments in $^{21}Ne/^{22}Ne$ up 13 times to the ratio in air, and $^{136}Xe/^{130}Xe$ 25% greater than the atmospheric ratio (Holland et al., 2013). With the noble gas isotopic excesses, they calculate a minimum mean residence time for crystalline brine of about 1.5 billion years, which is the oldest groundwater discovered on the Earth (Holland et al., 2013).

Generally speaking, noble gas isotopes can be applied in many aspects in the study of groundwater/porewater. They have been proven as powerful tools in hydrogeological and geochemical studies.

1.4 Issue Statement

1.4.1 Novel Noble Gas Sampling Method

Because of the large diffusivity of noble gases, the storage of deep rock cores for noble gas analysis is difficult. The usual storage method for rock samples is stainless steel chambers which are efficient but very costly. One of the aims of this dissertation is to explore a novel storage method for noble gases in rock porewater.

Site characterization activities were conducted for a nuclear waste deep geological repository (DGR) in Kincardine, Ontario, Canada. Six boreholes were drilled in the course of the DGR site characterization program. The core samples were vacuum-sealed in Mil PRF-131K CLASS 1 vapor barrier foil bags following two N_2 flushes of the bag, then stored at the site at 4 ℃. These Al-foil bags are made of OPP/PE/Al foil/PE compacted material. With time, the gas components of the porewater in the rock samples have slowly degased. At the time of gas sampling, the rock samples had degassed for approximately 7 years at Bruce nuclear site. During the 7 years degassing period, substantial degassing has occurred which had created sufficient space to allow sampling. Collecting noble gases of rock porewater from Al-foil bags would be a more economical sampling method and the integrity of Al-foil bags over several years, providing their integrity for retaining all gases can be demonstrated.

1.4.2 All Noble Gas Processing and Analysis Line

In the Noble Gas and Tritium Laboratory at the University of Ottawa, the methodology and procedure for He-Ne analysis have been well developed and tested on the Thermo Scientific Helix SFT^{TM} (Split Flight Tube) noble gas mass spectrometer. However, the analysis methodology for all five stable noble gases (He, Ne, Ar, Kr, Xe) still requires development with the existing processing line.

To measure all five stable noble gases, purification and separation are the key success factors. Currently, there are two dominant materials for noble gas trapping and

separation, one is activated charcoal (Lott & Jenkins, 1984), the other one is polished stainless steel (Lott III, 2001). Because polished stainless steel is not capable to capture He within the lowest temperature a helium compressor can reach (Lott III, 2001) (Figure 1.1), most laboratories are using activated charcoal traps which are temperature-controlled by helium compressors. It is relatively easy to separate Ne from He and separate Xe from Kr, but it is difficult to separate Kr from Ar because of the extremely high abundance of Ar compared with other stable noble gases. The high abundance of Ar results in the layered effect which means Ar is frozen below Kr at the Kr trapping temperature during the noble gas trapping process. Subsequently, partial Ar will be released together with Kr from the coldhead at the temperature to thaw Kr. The separation of Kr from Ar has been one of the main challenges for noble gas researchers around the world.

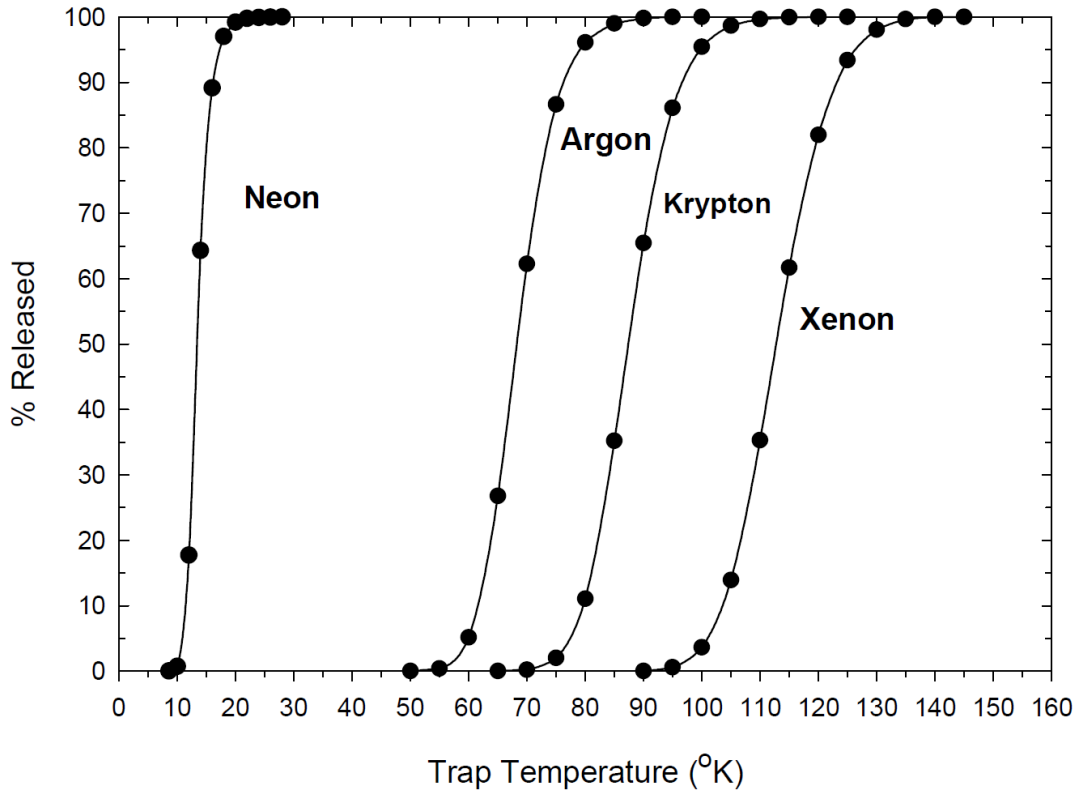

Figure 1.1 Percentage of Ne, Ar, Kr, Xe release profile as a function of polished stainless steel temperature (Lott III, 2001).

In addition, the coldhead in the Noble Gas Laboratory at the University of Ottawa is a custom-made ARS (Advanced Research Systems) activated charcoal cryogenic trap that is particularly suitable for He-Ne separation. The adsorption capacity of the coldhead is not able to deal with the superabundant Ar in air standards and geological samples. Therefore, a methodology that can handle Ar individually from other noble gases is badly needed.

1.4.3 Noble Gas Extraction from Rock Porewater

In deep sedimentary and crystalline rocks, the porewater content is rather low because of very small porosity. Regarding the rock samples for noble gas analysis, extracting noble gases from porewater without disturbing mineral-retained gas is very important. Especially for sedimentary rock, gas components vary between those in porewater and the minerals. This is attributed to the different and unknown origins of the minerals that formed sedimentary rock. The minerals may reserve geochemical information from their parent body. Hence, it is important to find a methodology that only releases porewater rather than the gas phase in the minerals and fluid inclusions.

Generally, room-temperature out-diffusion and heating are the mainstream methods to degas noble gases from rock porewater. Room-temperature diffusion needs a well-sealed container with long-time integrity that can prevent noble gas losses from the container and keep them for long period. So it is critical to find a type of container which is gas-tight and economic. According to the usual practice, metal material is normally used to constitute the container for noble gas samples. However, the conventional container is the stainless steel chamber which is very costly with a Nupro gas shut-off valve on it. It is meaningful to try a metal material bag that is gas-tight but is much cheaper than the metal chamber. The only disadvantage is a long time for the absolute degassing of dissolved gases from rock porewater.

In contrast, the heating method saves a lot of time and effort but it is necessary to figure out the exact temperature which can release rock porewater gases without

accessing gases trapped within the minerals. And a solid, gas-tight metal chamber is essential for the heating process. The advantage of the heating method is a short period for the degassing process, and the storage and maintenance for rock samples could be skipped. This can save a lot of time, effort and energy. However, the exact temperatures to release porewater noble gases for different kinds of rocks still require heating experiments to determine.

1.4.4 Noble Gas Data Interpretation

Determining the residence time of the porewaters in the Ordovician aquiclude and aquitard is central to the safety assessment for a proposed DGR in the region of the Bruce Nuclear Site. He accumulation time estimates have been made in the previous study at the same site (I. D. Clark et al., 2013). Heavy geogenic noble gas (Ne, Ar, Kr and Xe) geochronometers represent direct and reliable measurements of porewater age, based on their autochthonous origin and conservative behaviour. Geogenic noble gases can helpreconstruct noble gas concentrations in Ordovician rock porewaters of the DGR borehole profile and in associated groundwaters, to understand the origin of porewaters and their mechanism of emplacement by detecting the excesses in radiogenic Ne, Ar, Kr, Xe isotopes. Based on their respective and unique modes of formation, the excesses of radiogenic isotopes are used to estimate Ordovician porewater age /residence time in the crust.

1.5 Objectives

According to the instruments in our lab and the issues illustrated before. The objectives of my research are:

1. To build a noble gas isotope analysis system and develop a methodology for analysis of He to Xe.

2. To benchmark noble gas extraction from crystalline rock porewater using a new method with heating under vacuum.

3. To develop a methodology for noble gas analysis in archived sedimentary rocks from Bruce Nuclear Site.

And 4. The final objective of this thesis is to develop a new geochronometer—^{136}Xe in sedimentary aquitards and aquicludes.

References

Aeschbach-Hertig, W., Peeters, F., Beyerle, U., & Kipfer, R. (2000). Palaeotemperature reconstruction from noble gases in ground water taking into account equilibration with entrapped air. *Nature, 405*(6790), 1040-1044.

Aeschbach, W. (2016). New perspectives for noble gases in oceanography. *Journal of Geophysical Research: Oceans, 121*(8), 6550-6554.

Álvarez-Valero, A., Sumino, H., Burgess, R., Núñez-Guerrero, E., Okumura, S., Borrajo, J., & Rodríguez, J. L. (2022). Noble gas variation during partial crustal melting and magma ascent processes. *Chemical Geology, 588*, 120635.

Ammon, K., Leya, I., & Lin, Y. (2011). Noble gases in the Xinjiang (Armanty) iron meteorite – – A big object with a short cosmic - ray exposure age. *Meteoritics & Planetary Science, 46*(6), 785-792.

Andrews, J., Hussain, N., & Youngman, M. (1989). Atmospheric and radiogenic gases in groundwaters from the Stripa granite. *Geochimica et cosmochimica acta, 53*(8), 1831-1841.

Ballentine, C. J., Burgess, R., & Marty, B. (2002). Tracing fluid origin, transport and interaction in the crust. *Reviews in Mineralogy and geochemistry, 47*(1), 539-614.

Ballentine, C. J., & Burnard, P. G. (2002). Production, release and transport of noble gases in the continental crust. *Reviews in Mineralogy and geochemistry, 47*(1), 481-538.

Ballentine, C. J., Marty, B., Lollar, B. S., & Cassidy, M. (2005). Neon isotopes constrain convection and volatile origin in the Earth's mantle. *Nature, 433*(7021), 33-38.

Bekaert, D. V., Gazel, E., Turner, S., Behn, M. D., De Moor, J. M., Zahirovic, S., . . . Hammerstrom, A. (2021). High 3He/4He in central Panama reveals a distal connection to the Galápagos plume. *Proceedings of the National Academy of Sciences, 118*(47).

Butler, W., Jeffery, P., Reynolds, J., & Wasserburg, G. (1963). Isotopic variations in terrestrial xenon. *Journal of Geophysical Research, 68*(10), 3283-3291.

Clark, I. (2015). *Groundwater geochemistry and isotopes*: CRC press.

Clark, I. D., Al, T., Jensen, M., Kennell, L., Mazurek, M., Mohapatra, R., & Raven, K. (2013). Paleozoic-aged brine and authigenic helium preserved in an Ordovician shale aquiclude. *Geology, 41*(9), 951-954.

Eikenberg, J., Signer, P., & Wieler, R. (1993). U-Xe, U-Kr, and U-Pb systematics for dating uranium minerals and investigations of the production of nucleogenic neon and argon. *Geochimica et cosmochimica acta, 57*(5), 1053-1069.

Faure, G., & Mensing, T. M. (2004). *Isotopes: Principles and Applications, 3rd Edition*.

Gilfillan, S., Györe, D., Flude, S., Johnson, G., Bond, C. E., Hicks, N., . . . Haszeldine, R. (2019). Noble gases confirm plume-related mantle degassing beneath Southern Africa. *Nature communications, 10*(1), 1-7.

Guo, M., & Korenaga, J. (2020). Argon constraints on the early growth of felsic continental crust. *Science advances, 6*(21), eaaz6234.

Hendry, M., Solomon, D., Person, M., Wassenaar, L., Gardner, W., Clark, I., . . .

Hasegawa, T. (2015). Can argillaceous formations isolate nuclear waste? Insights from isotopic, noble gas, and geochemical profiles. *Geofluids, 15*(3), 381-386.

Holland, G., Lollar, B. S., Li, L., Lacrampe-Couloume, G., Slater, G., & Ballentine, C. (2013). Deep fracture fluids isolated in the crust since the Precambrian era. *Nature, 497*(7449), 357-360.

Kaneoka, I. (1980). Rare gas isotopes and mass fractionation: an indicator of gas transport into or from a magma. *Earth and Planetary Science Letters, 48*(2), 284-292.

Kaneoka, I., & Takaoka, N. (1978). Excess 129Xe and high 3He/4He ratios in olivine phenocrysts of Kapuho lava and xenolithic dunites from Hawaii. *Earth and Planetary Science Letters, 39*(3), 382-386.

Kietäväinen, R., Ahonen, L., Kukkonen, I. T., Niedermann, S., & Wiersberg, T. (2014). Noble gas residence times of saline waters within crystalline bedrock, Outokumpu Deep Drill Hole, Finland. *Geochimica et cosmochimica acta, 145*, 159-174.

Kotarba, M. J., Sumino, H., & Nagao, K. (2019). Origin of hydrocarbon and noble gases, carbon dioxide and molecular nitrogen in Devonian, Pennsylvanian and Miocene strata of the Polish Lublin and Ukrainian Lviv basins, southern part of the Upper Silesian Coal Basin and western part of the Carpathian Foredeep (Poland). *Applied Geochemistry, 108*, 104371.

Li, Y., Qin, S., Wang, Y., Holland, G., & Zhou, Z. (2020). Tracing interaction between

hydrocarbon and groundwater systems with isotope signatures preserved in the Anyue gas field, central Sichuan Basin, China. *Geochimica et cosmochimica acta, 274*, 261-285.

Loose, B., Jenkins, W. J., Moriarty, R., Brown, P., Jullion, L., Garabato, A. C. N., . . . Meredith, M. P. (2016). Estimating the recharge properties of the deep ocean using noble gases and helium isotopes. *Journal of Geophysical Research: Oceans, 121*(8), 5959-5979.

Lott, D., & Jenkins, W. (1984). An automated cryogenic charcoal trap system for helium isotope mass spectrometry. *Review of scientific instruments, 55*(12), 1982-1988.

Lott III, D. E. (2001). Improvements in noble gas separation methodology: A nude cryogenic trap. *Geochemistry, Geophysics, Geosystems, 2*(12).

Ma, L., Castro, M. C., & Hall, C. M. (2009). Crustal noble gases in deep brines as natural tracers of vertical transport processes in the Michigan Basin. *Geochemistry Geophysics Geosystems, 10*.

Marty, B., Heber, V. S., Grimberg, A., Wieler, R., & BARRAT, J. A. (2006). Noble gases in the Martian meteorite Northwest Africa 2737: A new chassignite signature. *Meteoritics & Planetary Science, 41*(5), 739-748.

Mazor, E. (1972). Paleotemperatures and other hydrological parameters deduced from noble gases dissolved in groundwaters; Jordan Rift Valley, Israel. *Geochimica et cosmochimica acta, 36*(12), 1321-1336.

Nier, A., & McElroy, M. B. (1977). Composition and structure of Mars' upper atmosphere: Results from the neutral mass spectrometers on Viking 1 and 2.

Journal of Geophysical Research, 82(28), 4341-4349.

Osenbrück, K., Lippmann, J., & Sonntag, C. (1998). Dating very old pore waters in impermeable rocks by noble gas isotopes. *Geochimica et cosmochimica acta, 62*(18), 3041-3045.

Ozima, M., & Podosek, F. A. (2002). *Noble gas geochemistry*: Cambridge University Press.

Pinti, D. L., Castro, M. C., López-Hernández, A., Hernández, M. A. H., Shouakar-Stash, O., Richard, L., . . . Ramírez-Montes, M. (2019). Signature of ongoing brine reinjection on noble gas isotopes and fluid chemistry at Las Tres Vírgenes geothermal field, Mexico. *Journal of Volcanology and Geothermal Research, 377*, 33-42.

Pinti, D. L., Shouakar-Stash, O., Castro, M. C., Lopez-Hernández, A., Hall, C. M., Rocher, O., . . . Ramírez-Montes, M. (2020). The bromine and chlorine isotopic composition of the mantle as revealed by deep geothermal fluids. *Geochimica et cosmochimica acta, 276*, 14-30.

Porcelli, D., Ballentine, C. J., & Wieler, R. (2002). An overview of noble gas geochemistry and cosmochemistry. *Reviews in Mineralogy and geochemistry, 47*(1), 1-19.

Pujol, M., Marty, B., & Burgess, R. (2011). Chondritic-like xenon trapped in Archean rocks: A possible signature of the ancient atmosphere. *Earth and Planetary Science Letters, 308*(3-4), 298-306.

Sathaye, K. J., Smye, A. J., Jordan, J. S., & Hesse, M. A. (2016). Noble gases preserve

history of retentive continental crust in the Bravo Dome natural CO2 field, New Mexico. *Earth and Planetary Science Letters, 443*, 32-40.

Seltzer, A. M., Krantz, J. A., Ng, J., Danskin, W. R., Bekaert, D. V., Barry, P. H., . . . Severinghaus, J. P. (2021). The triple argon isotope composition of groundwater on ten-thousand-year timescales. *Chemical Geology, 583*, 120458.

Staudacher, T., & Allègre, C. J. (1982). Terrestrial xenology. *Earth and Planetary Science Letters, 60*(3), 389-406.

Swindle, T. D. (2002). Noble gases in the Moon and meteorites: Radiogenic components and early volatile chronologies. *Reviews in Mineralogy and geochemistry, 47*(1), 101-124.

Utting, N., Clark, I., Lauriol, B., Wieser, M., & Aeschbach‐Hertig, W. (2012). Origin and flow dynamics of perennial groundwater in continuous permafrost terrain using isotopes and noble gases: case study of the Fishing Branch River, Northern Yukon, Canada. *Permafrost and Periglacial Processes, 23*(2), 91-106.

Utting, N., Lauriol, B., Mochnacz, N., Aeschbach-Hertig, W., & Clark, I. (2013). Noble gas and isotope geochemistry in western Canadian Arctic watersheds: tracing groundwater recharge in permafrost terrain. *Hydrogeology Journal, 21*(1), 79-91.

Warr, O., Lollar, B. S., Fellowes, J., Sutcliffe, C. N., McDermott, J. M., Holland, G., . . . Ballentine, C. J. (2018). Tracing ancient hydrogeological fracture network age and compartmentalisation using noble gases. *Geochimica et cosmochimica acta, 222*, 340-362.

Wen, T., Castro, M. C., Ellis, B. R., Hall, C. M., & Lohmann, K. C. (2015). Assessing compositional variability and migration of natural gas in the Antrim Shale in the Michigan Basin using noble gas geochemistry. *Chemical Geology, 417*, 356-370.

Wen, T., Castro, M. C., Nicot, J.-P., Hall, C. M., Pinti, D. L., Mickler, P., . . . Larson, T. (2017). Characterizing the noble gas isotopic composition of the Barnett Shale and Strawn Group and constraining the source of stray gas in the Trinity Aquifer, north-central Texas. *Environmental Science & Technology, 51*(11), 6533-6541.

Wen, T., Castro, M. C., Nicot, J. P., Hall, C. M., Larson, T., Mickler, P., & Darvari, R. (2016). Methane Sources and Migration Mechanisms in Shallow Groundwaters in Parker and Hood Counties, Texas-A Heavy Noble Gas Analysis. *Environmental Science & Technology, 50*(21), 12012-12021.

Wieler, R. (2002). Noble gases in the solar system. *Reviews in Mineralogy and geochemistry, 47*(1), 21-70.

Yoshioka, T., Tsuruta, T., Iwano, H., & Danhara, T. (2005). Spontaneous fission decay constant of 238U determined by SSNTD method using CR-39 and DAP plates. *Nuclear Instruments and Methods in Physics Research Section A: Accelerators, Spectrometers, Detectors and Associated Equipment, 555*(1-2), 386-395.

Young, B. G., & Thode, H. (1960). Absolute yields of the xenon and krypton isotopes in U238 spontaneous fission. *Canadian Journal of Physics, 38*(1), 1-9.

Zhu, H., Li, X., & Xu, Y. (2020). A helium stratified and ingassed lower mantle: resolving the helium paradoxes. *Acta Geochimica, 39*(1), 4-10.

Zuo, E., Lapp, A., Jautzy, J. J., & Clark, I. D. (2021). Crustal Noble Gas Isotopic Characteristics in Low-Permeability Ordovician Sedimentary Rock, Eastern Flank of the Michigan Basin. *ACS Earth and Space Chemistry*.

Chapter 2 Establishment of Noble Gas Processing Line and Calibration of Helix SFT Noble Gas Mass Spectrometer

2.1 Establishment of the Processing Line

The processing line was built by colleagues and the author in the Noble Gas and Tritium Laboratory at the University of Ottawa. As shown in Figure 2.1, the processing line is divided into low-vacuum (on the left) and high-vacuum (on the right) sections by a solid orange bar in the middle of the figure.

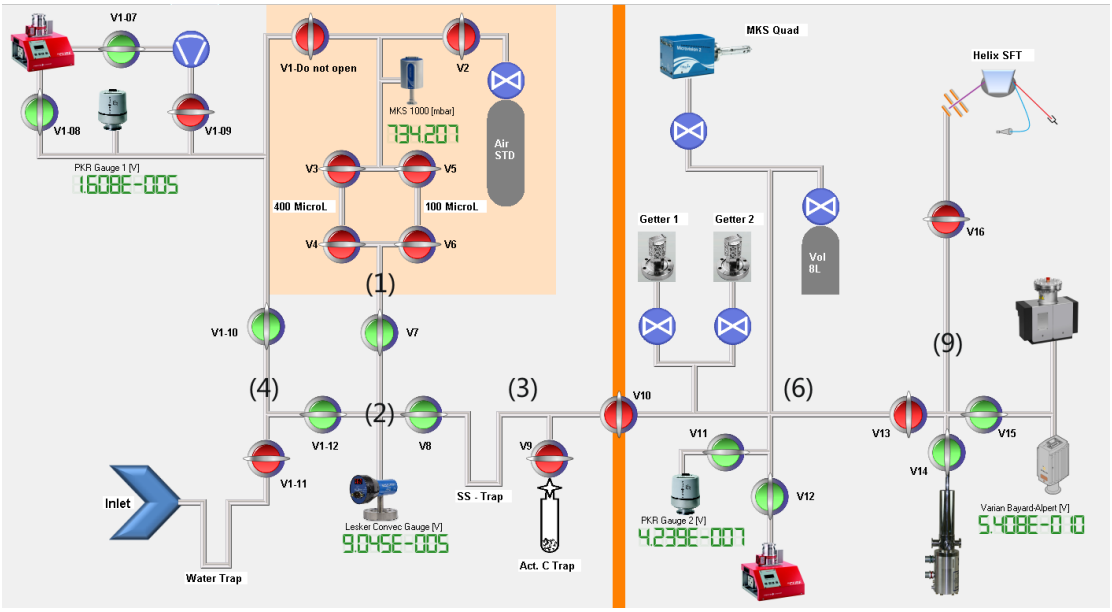

Figure 2.1 Noble gas processing line at the University of Ottawa

On the left side of the solid orange bar, from top to bottom and left to right, the low-vacuum section includes a diaphragm pump, a turbo pump, the sample inlet section, an air standard tank, two air standard pipettes, polished stainless steel trap and activated charcoal finger trap. The roles of the low-vacuum section are conducting preliminary purification of the sample and chopping the sample into appropriate volumes. The two air standard pipettes are constituted by four VCR automatic valves, and their volumes are 0.1 cm^3 and 0.4 cm^3, respectively.

On the right side of the solid orange bar, between V10 and V13, this section is the high-vacuum section which contains an MKS Quadrupole mass spectrometer, two SEAS getters, an 8-liter volume expansion tank and a turbo pump. The MKS Quadrupole is used for monitoring the background of the processing line. The SAES ST 172 getters (Zr-V-Fe), one at room temperature (293 K) and the other at 573 K, remove N_2, O_2, H_2, hydrocarbons and other active gases (e.g., CO, CO_2). Then noble gases are captured on the polished stainless steel and activated charcoal finger traps.

The section on the right of V13 (Figure 2.1) is the ultra-high vacuum section. This section contains the inlet to the Helix SFT noble gas mass spectrometer, an ion pump and a custom-made ARS activated charcoal cryogenic cooler which is mounted with indium O-ring for a better seal and lower thermal conductivity to acquire faster thermal cycling at a rate of 10 K/min. The noble gases released from the polished stainless steel and activated charcoal finger traps are adsorbed on the ARS cryogenic cooler for finer separation at specific temperatures.

The valves in green and red in this processing line are pneumatic and controlled by the Q-tegra software (Figure 2.1). The green color means the valve is open. In opposition, the red color means the valve is closed. The valves in blue color are manual ones that control the air standard tank, the SAES getters, the volume extension tank and the MKS quadrupole mass spectrometer.

2.2 Leak Test and Volume Calculation

Following the component assembly, the processing line was evacuated thoroughly and baked at 200 ℃ for several days to remove the moisture adhere on the stainless steel tubing inner surface. After baking, the large leaks were solved by acetone test. The microscopic leaks were diagnosed by a helium leak detector, one of the best and most accurate types of vacuum leak testing and leak detection. Helium is used as a tracer by being sprayed on the outside of a test part and joints while the inside of the part is being evacuated by the leak detector. The helium leaking through the test part enters through the system and this partial pressure is measured and the results are expressed as an alarm.

Subsequently, the volume measurements of every part were conducted with both air standard and Ar. As shown in Figure 2.1, the processing line was roughly divided into parts according to the distribution of valves. A known-volume spike part was attached to the sample inlet to help calculate the volume of every part. Most parts were filled with air and the volumes are calculated according to the gas law (Equation 2.1). With the gas spread further in the processing line, the volume of the adding parts can be calculated with Equation 2.2. However, the volumes of the SAES getters and the MKS quadrupole mass spectrometer were measured with argon because they will react with some components in the air. Two or three measurements were made on every part of the processing line and the data is summarized in Table 2.1.

$$P_1V_1 = P_2(V_1 + V_2) = P_3(V_1 + V_2 + V_3)\cdots\cdots \quad (2.1)$$

$$\Delta V = \left(\frac{P_n}{P_{n+1}} - 1\right) V_n \quad (2.2)$$

As shown in Table 2.1, the volumes of parts are presented in cm^3 measured with a Baratron pressure gauge. The measurements gave almost consistent values for the volume of every part. And the average volume of every part is also calculated as the volume would be used for chops to calculate noble gas concentrations.

Table 2.1 Volume measurements of parts of the processing line

Medium	Section	Measurement 1 (cm^3)	Measurement 2 (cm^3)	Measurement 3 (cm^3)	Average (cm^3)
Air	**Initial+Pipettes**	72.920	73.161	72.997	73.02591181
	1	17.749	17.789	17.788	17.77541191
	2	58.207	58.377	58.218	58.26737245
	4	17.037	17.035	16.989	17.0202187
	T	37.801	37.801	37.865	37.82257423
	Inlet	115.449	116.142	115.827	115.8057449
Argon	**3**	213.251	212.494	211.465	212.4033
	SST 1	31.861	31.788	NA	31.8245
	SST 2	32.033	31.912	NA	31.9722
	ACT 1	1.233	NA	NA	1.2334
	ACT 2	0.500	NA	NA	0.4999
	6	187.842	187.839	NA	187.8407
	Getter 1	471.977	472.443	NA	472.2100
	Getter 2	480.592	480.584	NA	480.5877
	Getter 2 (HOT)	303.500	313.197	NA	308.3483
	Volume Tank	7454.576	NA	NA	7454.5765
	Quad	306.081	304.597	NA	305.3389
	9	79.468	80.581	NA	80.0246
	Coldhead	15.629	15.368	NA	15.4983
	Mass Spec Inlet	117.079	117.878	NA	117.4786

NA: not available.

As for activated charcoal finger traps, the volume is calculated with the empty volume of the stainless finger and the volume of activated charcoal estimated by $V = \frac{m}{\rho}$.

2.3 Tuning and Calibration of Helix SFT Mass Spectrometer

The tuning and calibration of the noble gas mass spectrometer are crucial preparation of the noble gas research. Air aliquots were made with pipettes then purified and separated with finger traps and the ARS coldhead. Noble gases were separated from each other at the experiential temperatures from the literatures.

Separated noble gases were individually introduced in the Helix SFT mass spectrometer. Because the noble gases have different physical properties, different instrument settings of the mass spectrometer are tuned to get the best sensitivity for every noble gas. The different settings for the noble gases are summarized in Table 2.2. Generally in Table 2.2, except for acceleration voltage and trap current, all other settings are needed to be tuned to optimize the signal peak for different noble gases. Trap currents were set at 400 μA for He, 200 μA for Ne, Kr and Xe. The trap current for Ar was firstly set at 200 μA, whereas the continuous Ar measurements gave consistent but bigger Ar ratios (~300) compared with the recommended atmospheric values 295.5 (Nier, 1950) and 298.56 (Lee et al., 2006). Taking the ease of ionization of Ar and the sensitivity into account, the trap current for Ar was tuned to 125 μA. This change successfully solved the Ar ratio shift problem and the sensitivity of Ar was still considerable. For other settings, the only objective was to maximize the signal at the peak center. All noble gases were analyzed using a Faraday detector, except for ^{3}He, which was measured using an electron multiplier in ion counting mode.

Table 2.2 Helix SFT settings for different noble gas measurements

Noble Gas / Setting	He	Ne	Ar	Kr	Xe
Acceleration Voltage [KV]	4.50	4.50	4.50	4.50	4.50
Trap Voltage [V]	15.00	15.00	15.00	15.00	15.00
Trap Current [µA]	400.00	200.00	125.00	200.00	200.00
Source Current (µA)	1318.81	693.53	421.52	612.63	631.00
Ion Repeller (V)	-5.44	-4.92	-3.07	-5.44	-5.11
Electron Energy (eV)	91.97	93.43	89.28	79.15	81.95
Electron Energy (V)	90.72	92.23	87.99	77.68	80.52
Extraction Lens [%]	37.86	38.37	51.56	57.98	41.55
Horizontal Symmetry [%]	-12.60	-7.48	-6.50	-5.37	-5.03
Z-Focus [%]	46.32	36.16	85.49	46.40	46.90
Z-Symmetry [%]	-7.75	-2.47	-9.80	-5.37	-7.35
Field [V]	0.34	1.93	3.34	5.87	8.75

2.4 Noble Gas Methodology Development

To avoid damage to the mass spectrometer and interference among noble gas isotopes, for example, ^{20}Ne and $^{40}Ar^{++}$, purification and separation are requisites for noble gas analysis. However, the diversity of noble gas abundances in the air and samples makes the separation process not straigtforward. The molar fractions of He, Ne, Ar, Kr and Xe in the air are 5.24 ppm, 18.18 ppm, 9300 ppm, 1.14 ppm and 0.086 ppm, respectively (Clark, 2015). The tremendous differences among the noble gas abundances lead to the incomplete separation between two noble gases. For instance, the most common issue is the separation between Ar and Kr. Due to the extremely high concentration of Ar in air standards and geological samples, partial Ar would be frozen down at Kr trapping temperature. This phenomenon is the layered effect or matrix effect of Ar (Stanley et al., 2009). The large amount of Ar released with Kr is dangerous to the noble gas mass spectrometer and affects the measurement of Kr isotopes.

By now, the common solutions for Ar layered effect are thermal cycles (Stanley et al., 2009) or new trapping material to separate Kr from Ar (e.g., Mathouchanh & Aeschbach-Hertig, 2015). Thermal cycles mean repeating the freeze and thaw processes several times to minimize the amount of Ar frozen under Kr. However, thermal cycles need a lot of time and the new material is usually unrecyclable. A sustainable material is important to save the cost and improve the robustness of the procedure.

Before the development of the methodology, thermal cycles were tested several times. For example, two thermal cycles for Ar-Kr separation resulted in the whole procedure being around 8 hours and still a lot of residual Ar released together with Kr. Hence, a new methodology had to be developed to meet the time-saving and sustainable expectations.

According to the existing material we had in the lab, a simple method was proposed to separate Ar and Kr. The idea was to capture Kr and Xe with sequential polished stainless steel traps at liquid nitrogen temperature (77K) as much as possible, then isolate Kr and Xe from the remaining gas. Subsequently, the abundant Ar was trapped on the activated charcoal traps at liquid nitrogen temperature (77 K) and He and Ne are frozen on the ARS activated charcoal coldhead at 5 K. To this point, all noble gases were captured on the cold traps, one thing to remind is partial He, Ne and Ar were also trapped together with Kr and Xe on the polished stainless steel traps. These noble gases had to be pumped before releasing Kr and Xe to the ARS coldhead for finer separation.

There was no problem with He-Ne separation because their abundances are close. Firstly, He and Ne on the coldhead were released at 30 K and 80 K, respectively. Following He-Ne analysis, Kr and Xe were released from polished stainless steel traps by heating and adsorbed again on the ARS coldhead at 125 K. This temperature was attained from the noble gas release profile with temperature change of the ARS coldhead, at which Kr was completely captured and Ar was free. Then Kr and Xe were meticulously separated by the coldhead at 210 K. Including the freezing at the

beginning of the procedure, Kr and Xe had been frozen, thawed, frozen, thawed. These manipulations made two freeze-thaw cycles (thermal cycles) for Kr and Xe, which were favorable to the Kr separation from Ar. Last but not least, Ar is released from the activated charcoal traps and spread into the noble gas mass spectrometer after proper chops. Overall, the sequence of noble gases introduced to the mass spectrometer is He, Ne, Kr, Xe, Ar.

The advantages of this method are:

(1). Ar is solely handled and kept away from the ARS coldhead. This assures the ARS coldhead will not be overwhelmed by extremely abundant Ar. In addition, it is also helpful to the separation between Ar and Kr by reducing the Ar layered effect.

(2). Two thermal cycles assist in reducing the amount of Ar frozen with Kr. Though in the first freeze-thaw process, the two sequential stainless steel finger traps cannot freeze theoretically all Kr. But the iterative trapping achieves > 95% trapping efficiency for Kr. This trapping efficiency is comparable to other research.

(3). Compared with other published noble gas procedures, our method can shorten the all five noble gas analysis procedure to 4 hours and 30 min. Given the existing material and instruments we have in the lab, this method is both efficient in trapping, separating noble gases and time management.

In summary, this method not only handles Ar separately from other noble gases but also conducts two thermal cycles for Ar-Kr separation. Honestly, two

coldheads/cryogenic coolers operated by helium compressor are the ideal solution for all noble gas separation, while the Ar layered effect still influences Kr analysis and Kr trapping efficiency is around 98% which is not a far more obvious advantage than our iterative polished stainless steel trapping method. By far, this methodology developed is most suitable for our need for air standards and geological samples. The detailed performance of this separation method will be presented and discussed in the next chapter.

References

Clark, I. (2015). *Groundwater geochemistry and isotopes*: CRC press.

Lee, J.-Y., Marti, K., Severinghaus, J. P., Kawamura, K., Yoo, H.-S., Lee, J. B., & Kim, J. S. (2006). A redetermination of the isotopic abundances of atmospheric Ar. *Geochimica et cosmochimica acta, 70*(17), 4507-4512.

Mathouchanh, E., & Aeschbach-Hertig, W. (2015). *Krypton separation from argon for Atom Trap Trace Analysis of 85 Kr and 81 Kr.* MSc Thesis, University Paris SUD, France and University of Heidelberg, Germany.

Nier, A. O. (1950). A redetermination of the relative abundances of the isotopes of carbon, nitrogen, oxygen, argon, and potassium. *Physical Review, 77*(6), 789.

Stanley, R. H., Baschek, B., Lott III, D. E., & Jenkins, W. J. (2009). A new automated method for measuring noble gases and their isotopic ratios in water samples. *Geochemistry, Geophysics, Geosystems, 10*(5).

Chapter 3 Noble Gas Isotope Analysis (He to Xe) With an Iterative Trapping Method on a Split Flight Tube Mass Spectrometer

Ende Zuo, Anthony Lapp, Gilles St-Jean, Taylor Graham, Hugo Cornejo, Ian Clark*

Journal of Analytical Atomic Spectrometry

DOI: 10.1039/d2ja00153e

Abstract

Noble gas isotopes are being increasingly applied in groundwater and fugitive gas tracing and dating studies. Analysing all five stable noble gases is important to acquire as much geological information as possible. However, Ar-Kr separation has been a main challenge for noble gas analysis because Ar is over eight thousand times more abundant than Kr. The residual Ar released with Kr is considerable and interferes with the Kr measurement. This study explores a simple and iterative trapping method for Ar-Kr separation. This iterative trapping method improves both noble gas trapping efficiency and time of the whole procedure. The Helix SFT is a static vacuum gas-source mass spectrometer for the high-precision analysis of He by the simultaneous collection of ^{3}He and ^{4}He using a split flight tube. It is also capable of measuring isotopes of Ne up to Xe through peak jumping, although encumbered by the issue of remnant magnetism in the pole pieces which offsets the He peaks after measuring heavier noble gases. This study tested the performance of the Helix SFT using a new inversed tuning protocol that resolves the issue of remnant magnetism of the pole pieces when jumping back from higher masses for He analysis. With a newly designed pneumatic processing line and the iterative trapping method, noble gases have been successfully separated and yield satisfying results. Sensitivities of this analysis system have been determined for He (1.72×10^{-4} A/Torr) at a trap current of 400 μA, Ne (9.79×10^{-5} A/Torr) at 200 μA, Ar (2.28×10^{-4} A/Torr) at 125 μA, Kr (5.09×10^{-4} A/Torr) and Xe (1.01×10^{-3} A/Torr) at 200 μA. The 1σ precision of the isotopic ratios in air standards are $^{3}He/^{4}He$ (±1.39%),

$^{20}Ne/^{22}Ne$ (±0.26%), $^{40}Ar/^{36}Ar$ (±0.19%), $^{86}Kr/^{84}Kr$ (±0.09%), and $^{136}Xe/^{130}Xe$ (±0.22%). The iterative trapping method and the inversed tuning protocol allow the Helix SFT to measure beyond He despite the remnant magnetism of the pole pieces.

Keywords

Noble gas isotopes; Mass spectrometry; Separation, Sensitivity; Isotope ratios; Helix SFT

3.1 Introduction

Noble gas isotopes are effective tracers in geological and environmental studies (Burnard et al., 2013; Clark, 2015). Appropriate and powerful getters and cryogenic traps are crucial for noble gas purification and separation, which are the foundation for high-precision isotope ratio mass spectrometry (IRMS) analysis.

With the development of different types of cryogenic traps and chemical getters, noble gases are becoming more common geochronometers for groundwater dating as well as tracers for geological processes. In the early days, the analytical system was usually developed for a specific noble gas such as He (Sano & Wakita, 1988). A two-stage activated charcoal trap system cooled by a closed-cycle helium cold head was designed for capturing noble gases in the 1980s (Lott & Jenkins, 1984). Various types of getters and traps (e.g., Zr-Al alloy, activated charcoal and polished stainless steel) have been widely used in purifying and separating noble gases since the 1990s (Poole et al., 1997). Polished stainless steel has been proven to be an excellent trap for heavier noble gases (Ne, Ar, Kr, Xe) which can decrease processing time, reduce line blanks and memory effects, and narrow the gas release temperature profiles (Lott III, 2001). An automated programmed stainless steel cryogenic trap, a two-stage automated programmed water vapor trap and a Pd catalyst were applied to help reduce the temperature range when doing thermal cycling for noble gas separation (Stanley et al., 2009). Since 2000, noble gases extracted from water samples have been analyzed on Quadrupole, magnetic sector and mixed (Quadrupole+magnetic sector) mass

spectrometer systems with typical precisions (Beyerle et al., 2000; Kulongoski & Hilton, 2002; Stanley et al., 2009), while the complicated procedure and long processing time have been a common problem for many laboratories. When it comes to the instrument tuning, various parameters such as extraction, half plate bias and electron voltage were tuned on the Nier-type ion source of a GV Instruments SFT to get maximum sensitivity and the best peak shape for ^{4}He (Mabry et al., 2012). With a multi-aliquot measurement technique for $^{3}He/^{4}He$ analysis, better precision (0.2~0.3%, 2σ error) and long-term reproducibility (0.033%, 2σ error) were attained (Mabry et al., 2013). Work with a Thermo Scientific Helix-MC Plus has shown successful separation of ^{20}Ne from isobars: double-charged interfering ^{40}Ar, $^{1}H^{19}F$, $^{1}H_{2}{}^{18}O$, and partial separation of the ^{21}Ne peak from interfering $^{20}Ne^{1}H$ (Honda et al., 2015). The ^{21}Ne abundance was re-evaluated with an automated programmable noble gas line and Helix-MC Plus (Zhang et al., 2016). An isobar-free automatic procedure for Ne measurements, in particular for ^{22}Ne, was also developed on a Helix MC plus^{10K} (Farley et al., 2020). While rare reports and research are published on the analysis of all five noble gases. Furthermore, because Ar is far more abundant than Kr, the Ar-Kr separation is difficult due to Ar layering where minor Ar is invariably frozen at the Kr trapping temperature. It is imperative to find a simple separation procedure to reduce Ar layered effect from Kr.

The Thermo Scientific Helix SFT (split flight tube) noble gas mass spectrometer is a compact and powerful magnetic sector static vacuum mass spectrometer capable of the high-precision analysis of all noble gas isotopes. Its split flight tube with Faraday cup and electron multiplier detector is ideally suited to the simultaneous analysis of ^{3}He and

^{4}He. However, one disadvantage of measuring any element heavier than He is the remnant magnetization of the pole pieces. These pole pieces are situated around the flight tube at the magnet's entrance and exit points to refine the magnetic field for better separation of ^{3}He from ^{4}He and improve peak alignment during analysis. Magnetization of the pole pieces occurs at higher currents, due to the proximity to the main magnet. Thus, ramping the magnet current for higher masses will change the induced magnetization in the pole pieces and cause the ^{3}He/^{4}He peaks to diverge. This requires extensive time to dissipate for realignment of the He isotope peaks. The remnant magnetization has been observed to last hours through multiple peak coincidence scans (Text A1.1), measured at the helium setting following a higher mass jump, showing the peak center value shifting through time (Text A1.1). To circumvent the lengthy recovery time before subsequent helium analysis, an inverse tuning protocol has been developed in this study.

With our understanding of the noble gas separation and the remnant magnetization of the pole pieces, necessary for the simultaneous ^{3}He/^{4}He analysis, a method has been developed for the analysis of both ^{3}He/^{4}He and heavier noble gases on the Faraday cup, while ^{3}He is analyzed by secondary electron multiplier (SEM). The results suggest the Helix SFT is fully capable of measuring the full suite of noble gas isotopes with satisfying sensitivities. These insights are of great value to the large group of noble gas researchers and users currently functioning with the Helix SFT mass spectrometers, some of which also may experience remnant magnetization of the pole pieces.

3.2. Experimental Section

3.2.1. Processing line

The analytical requirements for the Helix SFT at the University of Ottawa Noble Gas and Tritium Laboratory include gas, groundwater and mineral materials from a range of environmental and geological settings. Accordingly, a multi-stage ultra-high vacuum (UHV) processing line for purifying and separating noble gas samples was developed and built in house (Figure 3.1). For noble gas purification, the system is equipped with two SAES ST 712 getters (Zr-V-Fe alloy), one at room temperature (293 K) and the other at 573 K; a water vapor trap (for high water content samples); two sequential polished stainless steel wool finger traps (SST1 and SST2 in Figure 3.1); and two activated charcoal finger traps (ACT1 and ACT2 in Figure 3.1). There is an optional expansion volume and an MKS Microvision 2 Quadrupole for more practical Ar abundance measurements, as well as general gas characterization. A custom-designed closed-cycle cryostat was manufactured by ARS (Advanced Research Systems), based on the DE-204 expander, that has been modified for reduced thermal mass and allow faster cycling times (less than 30 minutes from room temperature 293 K to 5K) as well as a smaller internal volume. This cryostat is also capable of reaching temperatures up to 353K.

Detailed information for each section is as follows:

The water vapor trap is a U-shape stainless-steel trap in an ethanol-liquid N_2 bath held at 190 K.

The ARS cryostat trap is modified from ARS DE-204 cold head. This activated charcoal cryogenic trap is mounted with an indium O-ring for a better seal and lower thermal conductivity allowing faster thermal cycling at a rate of 10K / min. But with a smaller internal volume, it can hardly handle high Ar concentration samples.

The stainless steel wool finger traps (SST1 and SST2) are filled with polished stainless steel wool and cooled with liquid N_2 at 77 K to capture Kr and Xe.

The activated charcoal traps ACT1 and ACT2 are cooled with liquid N_2 to draw Ar after Kr and Xe are captured on the polished stainless steel wool traps. ACT3 is also cooled with liquid N_2 to remove any residual Ar before He and Ne analysis.

The SAES ST 712 getters are made of Zr-V-Fe alloy to remove O_2, N_2, H_2, water vapor, hydrocarbons and other active gases (e.g., CO, CO_2).

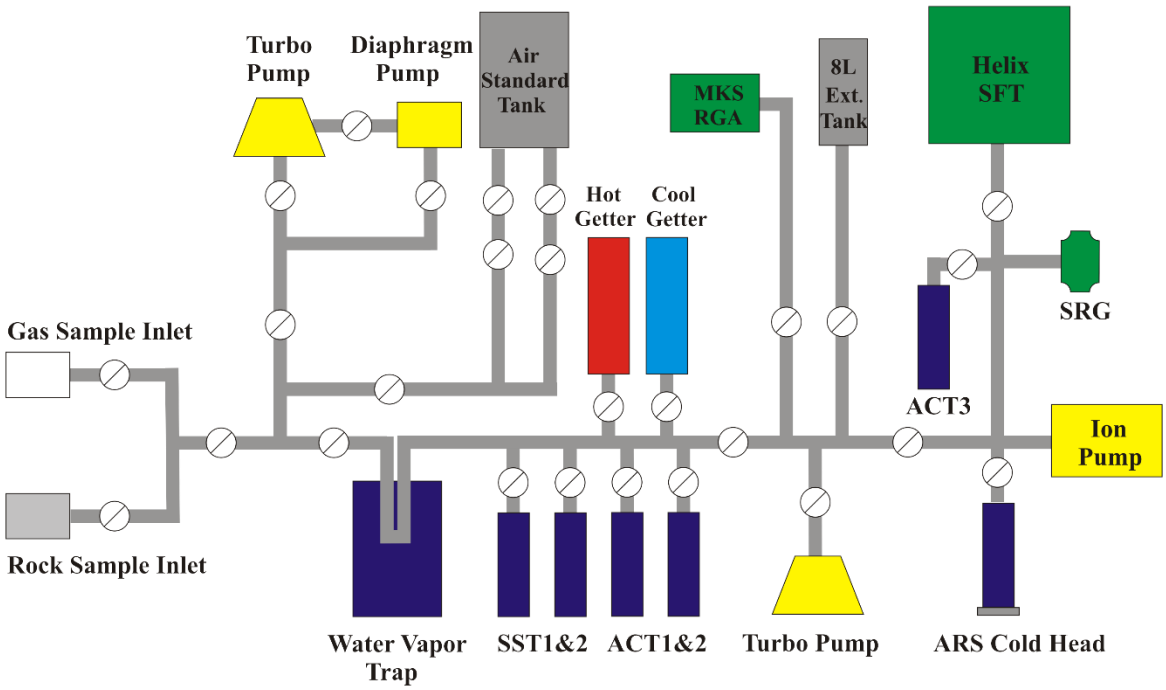

Figure 3.1 Schematic of Noble gas preparation line at University of Ottawa (SST: stainless steel trap; ACT: activated charcoal trap; SRG: spinning rotor vacuum gauge).

3.2.2. Mass spectrometer

The Thermo-Fisher Scientific Helix SFT (Split Flight Tube) static vacuum mass spectrometer is a magnetic sector mass spectrometer specially designed for the isotopic analysis of stable noble gas isotopes with enhanced capability for ^{3}He and ^{4}He. It comprises a magnetic sector analyzer with 35 cm, 120° extended geometry ion optics, and a low internal volume of 1400 cm^3. It is designed for the simultaneous collection of ^{3}He and ^{4}He for precise analysis of $^{3}He/^{4}He$ ratio. The magnetic sector is capable of analyzing masses up to 150 amu, but unlike multi-collector noble gas mass spectrometers, the Helix SFT can only measure one peak at a time beyond helium. Nonetheless, rapid cycling between specific peaks (peak jumping) allows isotope ratios to be measured. The Helix SFT has an extremely low background and low outgassing rates resulting from the close attention to surface finish, cleaning methods and the use of a high-temperature bake-out oven through the turbo and ion pump. The internal design minimizes the possibility of ion backscattering off the flight tube walls and reaching the collector. The ion source is a flange mounted "Nier" type designed for easy de-mount, filament change and cleaning.

For the low mass spur, a MasCom SEM detector is used with a set resolution at >700 (10% valley) and 75% or better ion counting efficiency, ~80% or better with inherent noise <10 cts/min. This SEM incorporates a 50 mm electrostatic analyzer for extreme abundance analysis. The maximum count rate is 1.5×10^{6} cps or ~2.4×10^{-13}A ion current (100% efficiency assumed) and electronics deflect the beam at approximately 1.6×10^{6}

cps.

On the high mass spur, is a voltage suppressed deep Faraday bucket fitted with parallel, software-switchable parallel 1×10^{11} and 1×10^{12} Ohm gain resistors feeding to an OP amplifier with a 50V limit. Resolution set for the Faraday detector is > 400 (10% peak height). The amplifiers have built-in electronic gain calibrations for consistent and fast calibrations.

3.3 Methodology

Air standard measurements were performed with a tank of clean, dry air filled in a rural area north of Ottawa in Val-Des-Monts, Quebec, Canada. The pre-evacuated tank was fitted with magnesium perchlorate and drierite to remove moisture and was left to equilibrate for 4 hours before being sealed and interfaced with the UHV processing system. The analysis system was routinely baked and pumped after analyses to ensure a low background and clean vacuum system. Following the bakeout, air standard aliquots were made with a 0.4 cm^3 pipette and released through the U-shape stainless steel water vapor trap in an ethanol-liquid N_2 bath at 190 K for the removal of residual water vapor. The air standard aliquots were then expanded into the SAES getters to remove bulk and trace atmospheric gases (i.e. N_2, O_2, CO_2, hydrocarbons).

In order to have accurate releasing temperatures of noble gases from the ARS activated charcoal cryostat, noble gas capture-release experiments were conducted (Table A1.1). Due to the high abundance of Ar in the air, the layered effect of Ar with Kr adsorption onto an activated charcoal trap must be considered (Beyerle et al., 2000; Stanley et al., 2009; Mathouchanh & Aeschbach-Hertig, 2015). To resolve this issue, we utilized two sequential polished stainless steel wool traps (SST1 and SST2 in Figure 3.1) at liquid N_2 temperature (77 K). Kr and Xe were frozen on the polished stainless steel wool traps one after the other. Repeated air standard analysis yielded the Kr trapping efficiency >95% and Xe trapping efficiency > 99%. Considering the cost, this Kr trapping efficiency is excellent compared with the 97% Kr trapping efficiency

achieved with dual polished stainless steel coldheads (Péron et al., 2020). After isolation of the stainless steel traps, Ar was isolated on the double activated charcoal traps (ACT1 and ACT2 in Figure 3.1) immersed in liquid N_2 at 77K. Afterward, He and Ne were drawn on the ARS activated charcoal cryostat at 5 K and released into the mass spectrometer at 30 K and 80 K, respectively. Subsequently, Kr and Xe were released from polished stainless steel wool traps by heating then transferred to the ARS cryostat trapped at 125 K. After pumping to remove as much residual Ar as possible, Kr and Xe were released into the mass spectrometer at 205 K and 325 K, respectively. The last step involved releasing Ar by heating the activated charcoal cold fingers (ACT1 and ACT2) and performing appropriate "chops" based on the spinning rotor vacuum gauge (SRG) reading. Since Ar was solely handled on activated charcoal traps and kept away from ARS cryostat to avoid its layered effect, the releasing profile for ^{4}He, ^{20}Ne, ^{84}Kr and ^{132}Xe of our modified ARS cryostat is shown in Fig. 3.2. All noble gases were analyzed on the static vacuum Helix SFT mass spectrometer using a Faraday detector, except for ^{3}He, which was measured using a secondary electron multiplier (SEM) in ion counting mode. The whole procedure takes about 4.5 hours and comprises two freeze-thaw thermal cycles for Ar-Kr separation. Steps involved in an air standard measurement are summarized in Table 3.1, including the details of the timing and the trap temperatures.

.

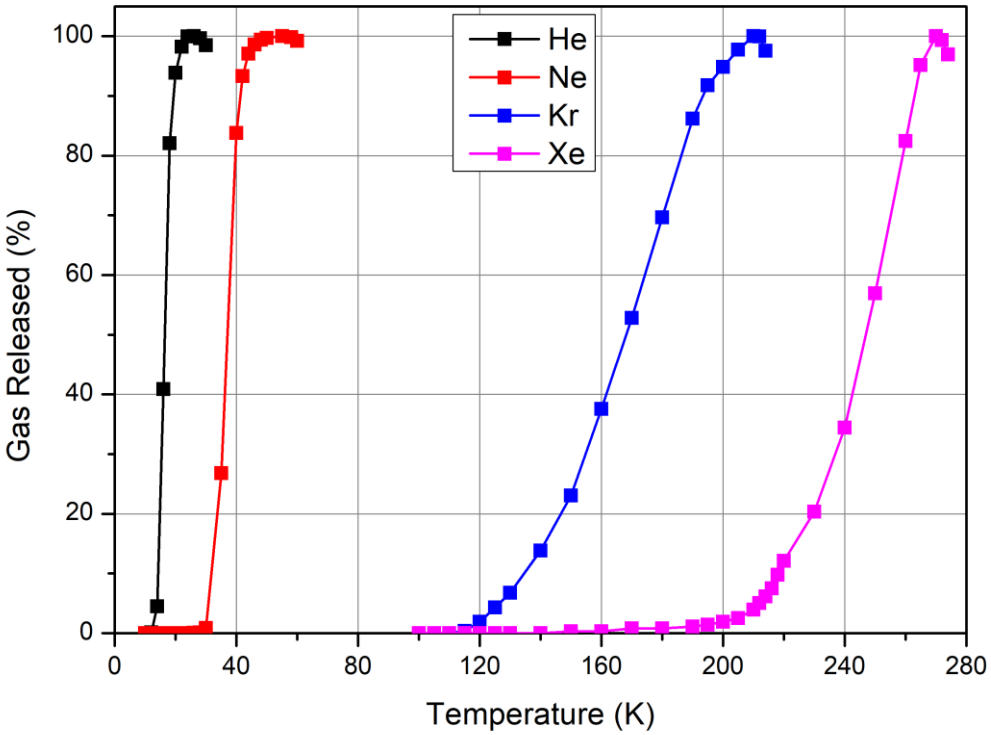

Figure 3.2 ^{4}He-^{20}Ne and ^{84}Kr-^{132}Xe releasing temperature profile of the modified ARS activated charcoal cryostat. Ar is not captured on the ARS cryostat because the layered effect between Ar and Kr increases the difficulty on separating Kr from Ar on single activated charcoal cryostat.

Table 3.1 Brief description of the noble gas analysis procedure, including trap temperatures and timing of the steps involved in air standard analysis. WVT: water vapor trap; SST: stainless steel wool trap; ACT: activated charcoal trap; LN: liquid nitrogen.

Step	**Trap**	**Trap Temperature (K)**	**Time (min)**	**Purpose**
WVT in ethanol-LN bath	WVT	190	10	Remove moisture
Gettering	SAES 1&2	293 & 573	10	Remove N_2,O_2,H_2, active gases etc.
SST 1 in LN bath	SST 1	77	10	First freeze of Kr and Xe
SST 2 in LN bath	SST 2	77	10	
ACTs in LN bath	ACTs	77	10	Draw Ar
Cyrostat to 5 K	ARS Cryostat	5	15	Capture He & Ne on Cryostat
Cryostat to 30 K	ARS Cryostat	30	20	Release and analyze He
Cryostat to 80 K	ARS Cryostat	80	20	Release and analyze Ne
Heat up SSTs	SSTs	373	30	First thaw of Kr & Xe
Cyrostat to 125 K	ARS Cryostat	125		Second freeze of Kr & Xe
Cryostat to 205 K	ARS Cryostat	205	40	Second thaw and analysis of Kr
Cryostat to 325 K	ARS Cryostat	325	40	Second thaw and analysis of Xe
Heat up ACTs	ACTs	373	30	Release Ar from ACTs
Spread Ar into Mass spec	ACTs	373	10	Chop Ar for analysis
Clean processing line	ACTs	373	5	Clean Ar in processing system

3.4 Results and Discussion

3.4.1 Analysis system performance and reproducibility

Ar is particularly abundant in the air with a molar fraction of 0.934%, while Kr has a molar fraction of only 1.14 ppmv, making it difficult to separate. As noble gases are adsorbed on cryogenic traps, the layered effect is where part of the Ar is trapped under Kr due to its abundance. It has been a challenge to separate Kr from Ar (Beyerle et al., 2000; Stanley et al., 2009; Mathouchanh & Aeschbach-Hertig, 2015), though some separation methods for these two gases have been reported with new cryogenic coldhead methods (Lott III, 2001; Stanley et al., 2009). The Kr adsorption efficiency (e.g. 51% Kr) with polished stainless steel U-shape traps is always unsatisfactory (Kulongoski & Hilton, 2002). An easy and effective separation method is then of great interest for noble gas laboratories. This study explores a separation method for Ar and Kr with an iterative application of polished stainless steel wool traps. By reverse calculation, the single polished stainless steel wool trapping efficiency for Kr is approximate 75%. And two stainless steel wool traps push the Kr trapping efficiency up to 95%. The Kr trapping efficiency of three stainless steel wool traps was also tested, but with much more residual ^{40}Ar released with Kr for a marginal increase in Kr signal intensity, trapping efficiency to 97%. Thus, two sequential polished stainless steel wool traps are the optimal compromise between the Kr trapping efficiency and residual Ar layered effect.

The signals on ^{40}Ar and ^{20}Ne peak positions with released Kr in the air standards are summarized in Table A1.2 and plotted in Figure 3.3, showing a linear trend with the release of Kr at 205 K. Here, the ^{20}Ne intensity should be dominated by doubly-charged ^{40}Ar because He and Ne are captured by the ARS cryostat at 5 K. A linear trend exists between ^{40}Ar and doubly-charged ^{40}Ar with a slope of 0.303. The intercept is 67.7 fA, which suggests a low ^{20}Ne background following the He and Ne adsorption on the activated charcoal ARS cryostat. Figure 3.3 also shows the relatively low background of ^{40}Ar during Kr analysis and confirms the effective separation between Ar and Kr.

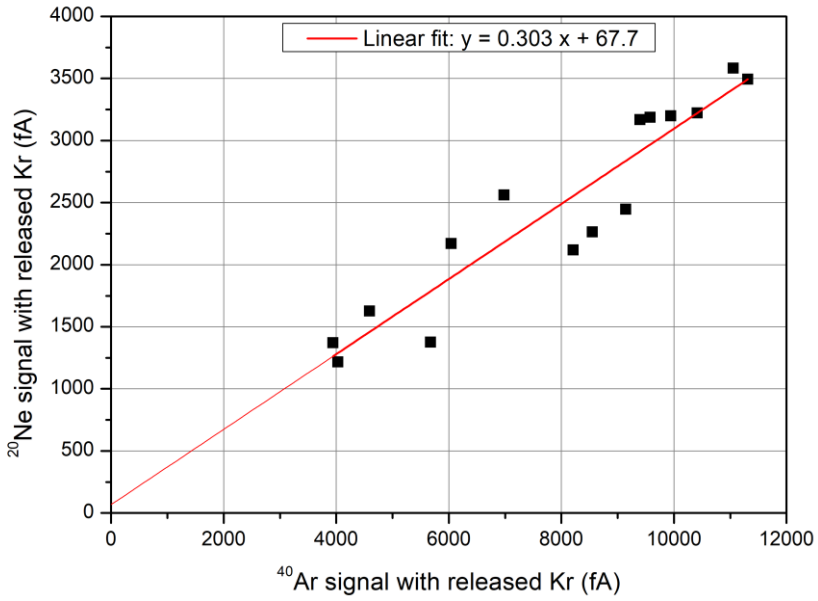

Figure 3.3 ^{20}Ne and ^{40}Ar peak signal intensity with released Kr at 205 K.

Due to the different physical properties of noble gases, different parameters of the ion source of the Helix SFT were tuned one by one to attain maximal sensitivity. The optimal settings of He, Ne, Ar, Kr and Xe are summarized and listed in Table 3.2. The noble gas sensitivities are listed in Table A1.3 and shown in Figure 3.4. The sensitivities

of noble gases are relatively consistent as shown in Figure 3.4. Among He measurements, the average sensitivity is 1.72×10^{-4} A/Torr, with a variation of $\pm7.51\times10^{-6}$ A/Torr. Among Ne measurements, the average value is 9.79×10^{-5} A/Torr, with a variation of $\pm8.14\times10^{-6}$ A/Torr. Ar measurements also have coherent sensitivities, where the average value is 2.28×10^{-4} A/Torr, with a variation of $\pm1.26\times10^{-5}$ A/Torr. Kr sensitivities have an average of 5.09×10^{-4} A/Torr and a variation of $\pm 2.42\times10^{-5}$ A/Torr. Xe measurements also have consistent sensitivities where the average sensitivity is 1.01×10^{-3} A/Torr, and the variation is $\pm 3.04\times10^{-5}$ A/Torr. As shown in Figure 3.4, the sensitivities for noble gases are related to atomic masses except for He. The analyzing system has the highest sensitivity for Xe and the lowest for Ne (Figure 3.4).

Table 3.2 The optimized instrumental settings of Helix SFT mass spectrometer for different noble gases.

Noble Gas / Setting	He	Ne	Ar	Kr	Xe
Acceleration Voltage [KV]	4.50	4.50	4.50	4.50	4.50
Trap Voltage [V]	15.00	15.00	15.00	15.00	15.00
Trap Current [µA]	400.00	200.00	125.00	200.00	200.00
Source Current (µA)	1318.81	693.53	421.52	612.63	631.00
Ion Repeller (V)	-5.44	-4.92	-3.07	-5.44	-5.11
Electron Energy (eV)	91.97	93.43	89.28	79.15	81.95
Electron Energy (V)	90.72	92.23	87.99	77.68	80.52
Extraction Lens [%]	37.86	38.37	51.56	57.98	41.55
Horizontal Symmetry [%]	-12.60	-7.48	-6.50	-5.37	-5.03
Z-Focus [%]	46.32	36.16	85.49	46.40	46.90
Z-Symmetry [%]	-7.75	-2.47	-9.80	-5.37	-7.35
Field [V]	0.34	1.93	3.34	5.87	8.75

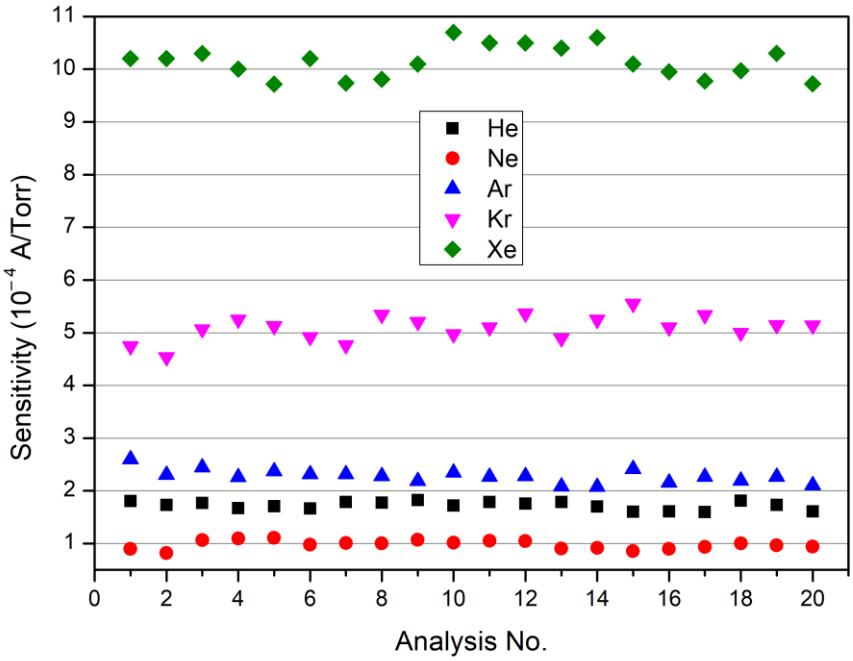

Figure 3.4 Noble gas sensitivities with experimental runs. All sensitivities are normalized to 10^{-4} A/Torr.

Noble gas isotope ratios were acquired and interpreted with the data acquisition and control software built within Qtegra. The air standard $^{3}He/^{4}He$ ratio is $1.344\times10^{-6} \pm 1.866\times10^{-8}$ (1σ) (Figure 3.5 and Table A1.4), very close to 1.343×10^{-6} from the report by the International Union of Pure and Applied Chemistry (IUPAC) (De Laeter et al., 2003). The air standard $^{20}Ne/^{22}Ne$ ratio is 9.5714 ± 0.0244 (1σ) (Figure 3.6 and Table A1.5), smaller than the published IUPAC recommended value of 9.78 (De Laeter et al., 2003). The depletion of $^{20}Ne/^{22}Ne$ indicates that the analyzing system is not influenced by the double ion-charged ^{40}Ar. Furthermore, the Ne ratios of samples will be corrected according to the relation between the air standard Ne ratios and the atmospheric value in routine analysis.

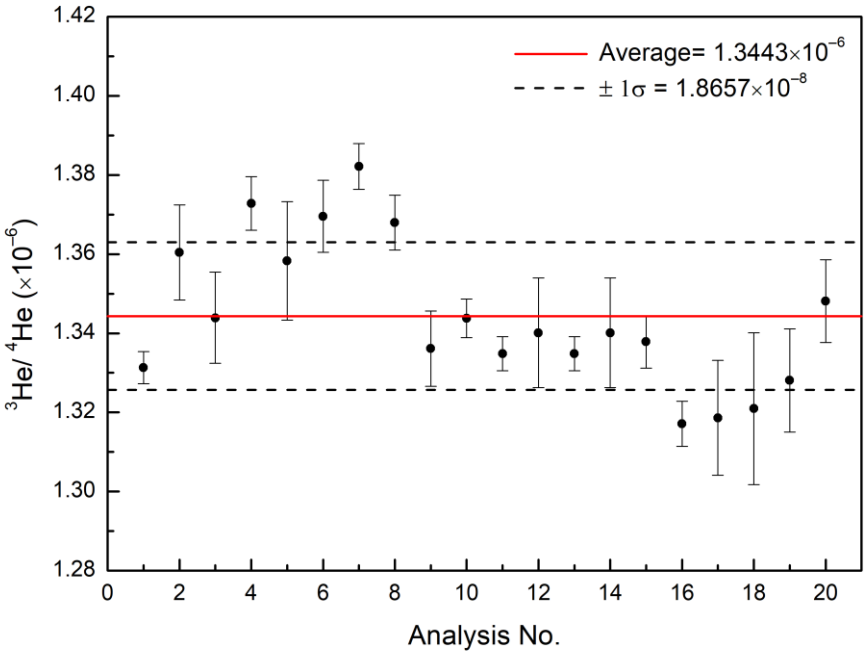

Figure 3.5 Air standard He isotope ratios with average and ±1 σ error.

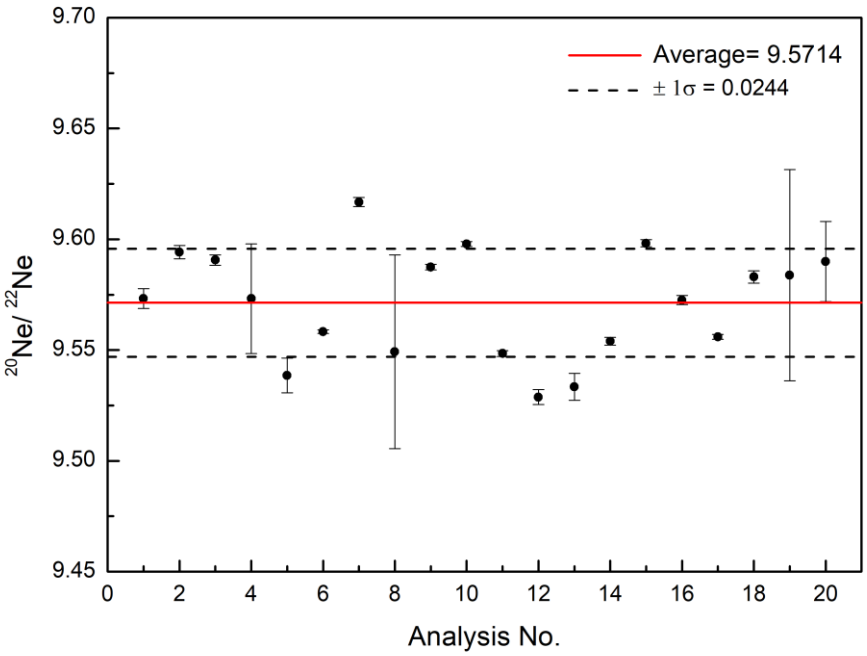

Figure 3.6 Air standard Ne isotope ratios with average and ±1 σ error.

First proposed by Nier in 1950 (Nier, 1950), the atmospheric value for $^{40}Ar/^{36}Ar$ of 295.5 ± 0.5 (1σ) has been unchallenged for a long time. Until 2006, Lee et al. applied gravimetrically prepared mixtures of highly enriched ^{36}Ar and ^{40}Ar to re-examine the atmospheric Ar ratios. A new $^{40}Ar/^{36}Ar$ value 298.56 ± 0.31 was proposed with a precision of 0.1% (Lee et al., 2006). A similar methodology with Lee et al., Valkiers et al. confirmed the new $^{40}Ar/^{36}Ar$ value of 298.7 ± 0.1 (Valkiers et al., 2008). In this study, comparable Ar ratios were attained from air standards with a value of 298.34± 0.56 (1σ) (Figure 3.7 and Table A1.6). Thus, Ar ratios of air standards are consistent and steady.

Kr isotope ratios measured in the air standards are close to published values (Figure 3.8 and Table A1.7). A $^{86}Kr/^{84}Kr$ value of 0.3046 ± 0.0003 (1σ) from air standard samples was acquired, which is close to the IUPAC recommended atmospheric value of 0.3032 (De Laeter et al., 2003). It can be concluded that our analyzing system is very reliable for the measurements of Kr ratios. The air standard Xe isotope ratios differ from the IUPAC recommended Xe values but are generally steady (Figure 3.9 and Table A1.8). The air standard $^{136}Xe/^{130}Xe$ estimated value is 2.173 ± 0.005 (1σ), which is close to the IUPAC value of 2.17571 (De Laeter et al., 2003).

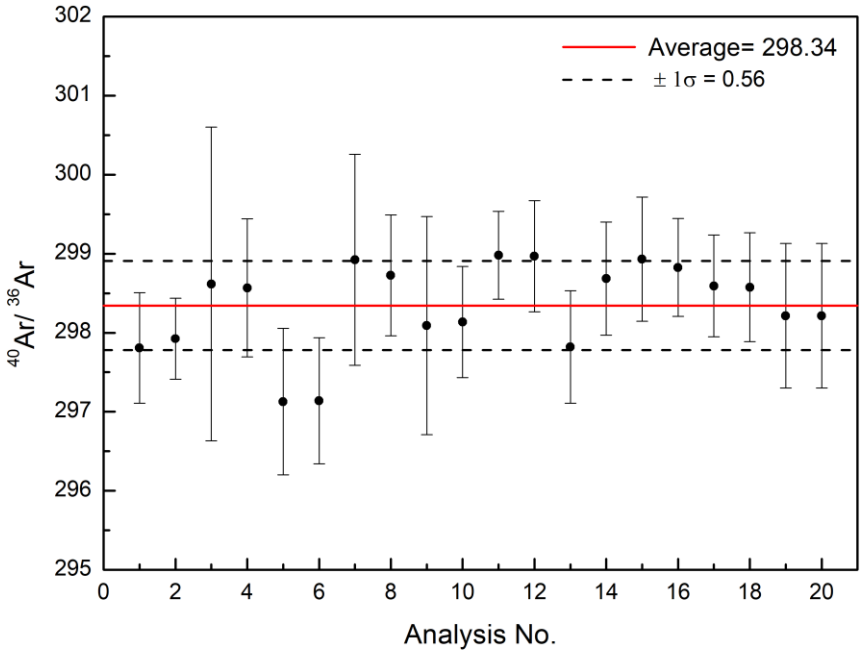

Figure 3.7 Air standard $^{40}Ar/^{36}Ar$ values with average and ±1 σ error.

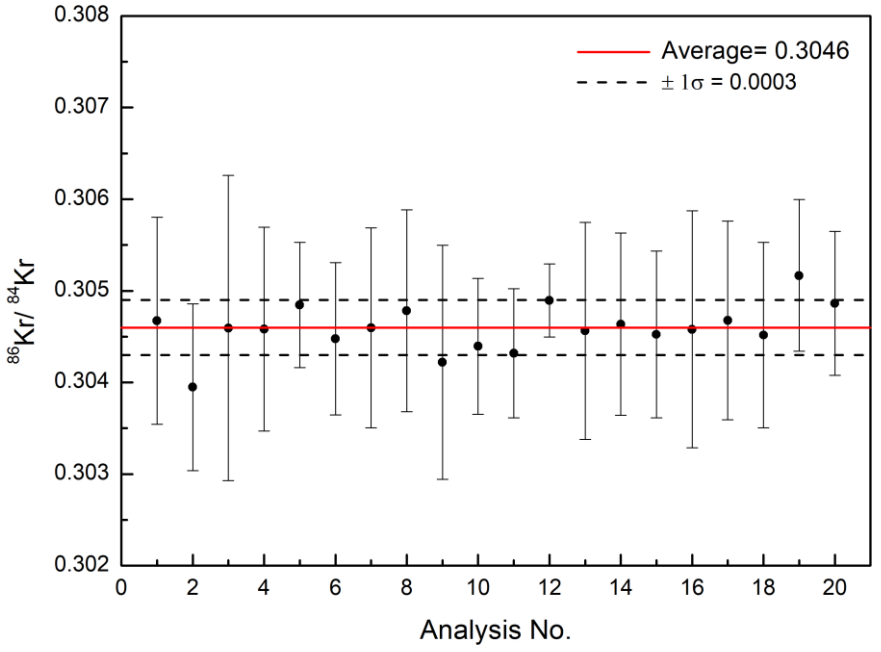

Figure 3.8 Air standard Kr isotope ratios with average and ±1 σ error.

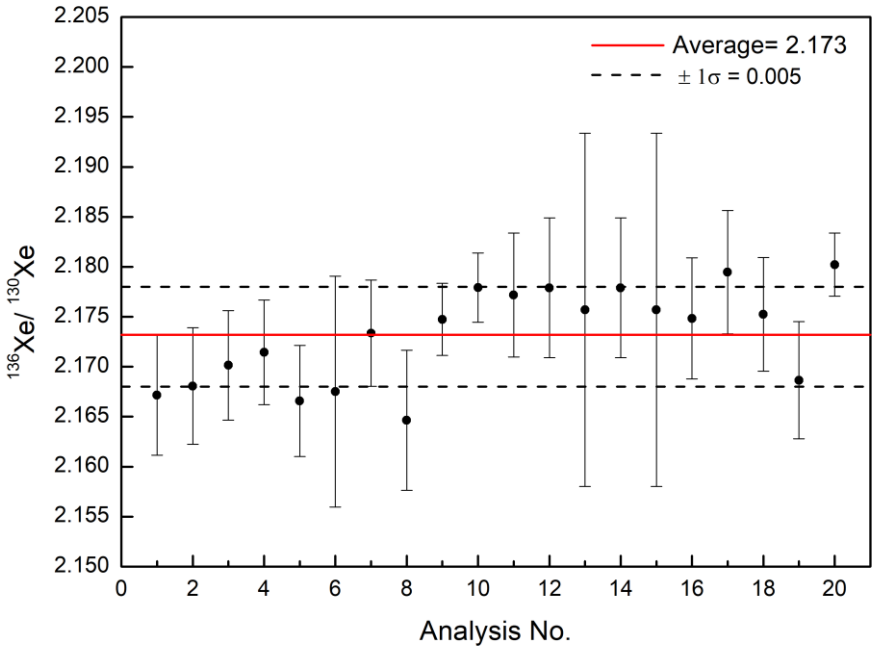

Figure 3.9 Air standard Xe isotope ratios with average and ±1 σ error.

3.4.2 Behavior and Magnetization of the Pole Piece

The remnant magnetization of the pole pieces is a common issue for Helix SFT laboratories. Users have reported the issue of pole pieces retaining a charge (remnant magnetism) after measuring heavier noble gases relative to helium. This phenomenon is attributed to the hysteresis loop for ferromagnets (Sung & Rudowicz, 2002). The hysteresis effect of demagnetization results in misaligned and unstable coincidence scans for ^{3}He and ^{4}He. We report that the same technical issue has been encountered after measuring beyond Ne and up to Xe.

The initial solution was to charge the pole piece at the magnetic field energy for Ar until the $^{3}He/^{4}He$ peaks became aligned, with a final finer peak alignment being done on the pole pieces themselves. It is hypothesized that some form of temporary residual

magnetic hysteresis (Figure 3.10) is left on the pole pieces and can last long enough for multiple analyses to take place. The pole pieces can be maintained at this level by simply resting the magnet on ^{22}Ne between analyses. Since 2014, the Helix SFT system has been operated in this manner for successfully measuring both He and Ne routinely.

However, when energizing the magnet up to Xe, we found the pole pieces become even further charged. The first time the magnetic field was tuned to Xe, the pole piece itself became physically displaced by the resulting magnetic field. Returning to Helium would show misaligned or even missing peaks. The solution was to lower the magnetic field to ^{4}He overnight and charging the pole piece on ^{40}Ar settings for 20 min the following morning prior to analyses. $^{3}He/^{4}He$ are then tuned following the same procedure as before. An even faster method for demagnetizing the pole piece was found to be restarting the instrument itself, although this presents other technical problems associated with a full system restart. Using the overnight technique to demagnetize the pole piece and remagnetize it to ^{40}Ar for 20 min, we can analyze He, Ne, Ar, Kr and Xe in a single day. A hypothesis is proposed that for the first Xe analysis on the Helix SFT, the pole pieces might have received some permanent hysteresis. The pole pieces no longer become physically displaced when peak jumping to Xe, however it does still require some fine tuning to re-align $^{3}He/^{4}He$.

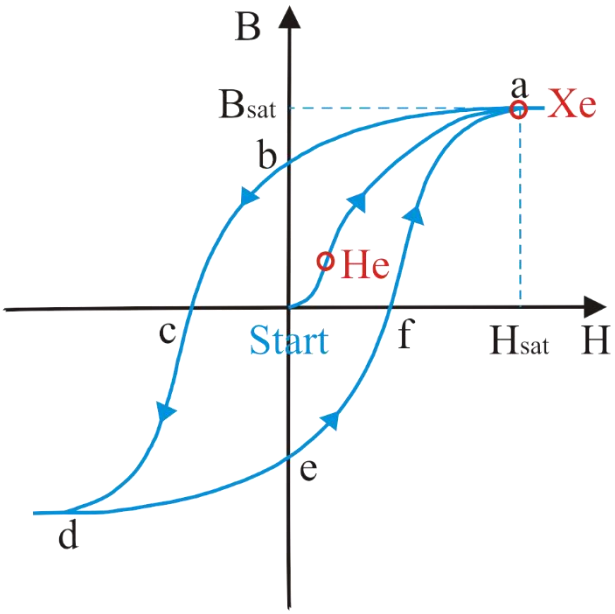

Figure 3.10 Schematic representation of a hysteresis loop for a ferromagnetic material, where a and d are the saturation point, in this study, the settings for Xe is at a maximum applied field H_{sat} and magnetization B_{sat}; b and e are retentivity points, in this study, b represent the remnant magnetization at H=0; c and f are coercivity points.

3.5. Conclusions

The performance of the UHV processing line and Helix SFT on the full suite of noble gas measurements are presented in this work. Iterative Kr trapping on polished stainless steel wool provides two freeze-thaw thermal cycles that sufficiently reduces residual Ar on the ARS cryostat, thus improving Kr sensitivity and life of the ARS cryostat. All noble gases can be effectively separated, particularly Kr from abundant Ar. Through air standard measurements, sensitivities for all noble gases are high and steady with time. By comparison with recent or IUPAC recommended noble gas ratios, this gas separation method combined with Helix SFT mass spectrometer is reliable for measuring isotopic ratios for all stable noble gases.

In addition, the magnetic memory effect of the pole pieces after heavier noble gas

analysis was solved with an inversed tuning protocol involving a daily ramping of the magnetic field to ^{40}Ar for 20 minutes to generate a baseline magnetization of the pole pieces, for which the He isotope peaks are aligned and require only minimum routine tuning. With the multi-phase inlet section, water, rock and gas samples can be analyzed with this system in high precision with minimal time spent tuning and realigning the $^{3}He/^{4}He$ peaks.

Acknowledgment

This study is part of the Ph.D. project by Ende Zuo at the University of Ottawa. Ende Zuo was the recipient of a scholarship from the China Scholarship Council for the duration of this work (No. 201606170089).

Reference

Beyerle, U., Aeschbach-Hertig, W., Imboden, D. M., Baur, H., Graf, T., & Kipfer, R. (2000). A mass spectrometric system for the analysis of noble gases and tritium from water samples. *Environmental Science & Technology, 34*(10), 2042-2050.

Burnard, P., Zimmermann, L., & Sano, Y. (2013). The noble gases as geochemical tracers: history and background *The noble gases as geochemical tracers* (pp. 1-15): Springer.

Clark, I. (2015). *Groundwater geochemistry and isotopes*: CRC press.

De Laeter, J. R., Böhlke, J. K., De Bievre, P., Hidaka, H., Peiser, H., Rosman, K., & Taylor, P. (2003). Atomic weights of the elements. Review 2000 (IUPAC Technical Report). *Pure and applied chemistry, 75*(6), 683-800.

Farley, K., Treffkorn, J., & Hamilton, D. (2020). Isobar-free neon isotope measurements of flux-fused potential reference minerals on a Helix-MC-Plus10K mass spectrometer. *Chemical Geology, 537*, 119487.

Honda, M., Zhang, X., Phillips, D., Hamilton, D., Deerberg, M., & Schwieters, J. B. (2015). Redetermination of the 21Ne relative abundance of the atmosphere, using a high resolution, multi-collector noble gas mass spectrometer (HELIX-MC Plus). *International Journal of Mass Spectrometry, 387*, 1-7.

Kulongoski, J. T., & Hilton, D. R. (2002). A quadrupole ‐ based mass spectrometric system for the determination of noble gas abundances in fluids. *Geochemistry, Geophysics, Geosystems, 3*(6), 1-10.

Lee, J.-Y., Marti, K., Severinghaus, J. P., Kawamura, K., Yoo, H.-S., Lee, J. B., & Kim, J. S. (2006). A redetermination of the isotopic abundances of atmospheric Ar. *Geochimica et cosmochimica acta, 70*(17), 4507-4512.

Lott, D., & Jenkins, W. (1984). An automated cryogenic charcoal trap system for helium isotope mass spectrometry. *Review of scientific instruments, 55*(12), 1982-1988.

Lott III, D. E. (2001). Improvements in noble gas separation methodology: A nude cryogenic trap. *Geochemistry, Geophysics, Geosystems, 2*(12).

Mabry, J., Burnard, P., Blard, P.-H., & Zimmermann, L. (2012). Mapping changes in helium sensitivity and peak shape for varying parameters of a Nier-type noble gas ion source. *Journal of Analytical Atomic Spectrometry, 27*(6), 1012-1017.

Mabry, J., Lan, T., Burnard, P., & Marty, B. (2013). High-precision helium isotope measurements in air. *Journal of Analytical Atomic Spectrometry, 28*(12), 1903-1910.

Mathouchanh, E., & Aeschbach-Hertig, W. (2015). *Krypton separation from argon for Atom Trap Trace Analysis of 85 Kr and 81 Kr.* MSc Thesis, University Paris SUD, France and University of Heidelberg, Germany.

Nier, A. O. (1950). A redetermination of the relative abundances of the isotopes of carbon, nitrogen, oxygen, argon, and potassium. *Physical Review, 77*(6), 789.

Péron, S., Mukhopadhyay, S., & Huh, M. (2020). A new dual stainless steel cryogenic trap for efficient separation of krypton from argon and xenon. *Journal of Analytical Atomic Spectrometry, 35*(11), 2663-2671.

Poole, J. C., McNeill, G. W., Langman, S. R., & Dennis, F. (1997). Analysis of noble

gases in water using a quadrupole mass spectrometer in static mode. *Applied Geochemistry, 12*(6), 707-714.

Sano, Y., & Wakita, H. (1988). Precise measurement of helium isotopes in terrestrial gases. *Bulletin of the Chemical Society of Japan, 61*(4), 1153-1157.

Stanley, R. H., Baschek, B., Lott III, D. E., & Jenkins, W. J. (2009). A new automated method for measuring noble gases and their isotopic ratios in water samples. *Geochemistry, Geophysics, Geosystems, 10*(5).

Sung, H. W., & Rudowicz, C. (2002). A closer look at the hysteresis loop for ferromagnets-A survey of misconceptions and misinterpretations in textbooks. *arXiv preprint cond-mat/0210657*.

Valkiers, S., Varlam, M., Berglund, M., Taylor, P., Gonfiantini, R., & De Bievre, P. (2008). Absolute measurements of isotope amount ratios on gases: part II. Application of the measurement models developed on real gases. *International Journal of Mass Spectrometry, 269*(1-2), 71-77.

Zhang, X., Honda, M., & Hamilton, D. (2016). Performance of the high resolution, multi-collector helix mc plus noble gas mass spectrometer at the Australian National University. *Journal of The American Society for Mass Spectrometry, 27*(12), 1937-1943.

Chapter 4 Benchmarking Dissolved He, Ne and Porewater Stable Isotopes in Crystalline Rock

Ende Zuo, Tarek Najem, David Zal, Anthony Lapp, Ian D. Clark*

Submitted to Chemical Geology.

Abstract

It has been a challenge to quantitatively extract dissolved gases and porewater from crystalline rock. Traditional crystalline rock porewater dissolved gas collecting methods always take months waiting for the out-diffusion slowly happening in the vacuum-sealed containers. While core heating for porewater extraction has been successfully tested on crystalline core, this has not been attempted for porewater dissolved gases. Though the in-situ crystalline rock seepage water sampling method was attempted, it needs a lot of effort and time to get rid of the surrounding disruption on crystalline rock porewater. This study is aimed at benchmarking an accelerated porewater noble gas extraction process for crystalline rock using a noble gas spike. To establish equilibrium between noble gases and rock porewater, the water-saturated crystalline rock core was sealed in a water-filled stainless steel container with an air-filled headspace into which a He-Ne spike was injected. The sealed chamber was then heated at 90 °C for weeks. After reaction, equilibrated headspace gas samples and rock core samples were collected and analyzed for He and Ne concentration and isotope ratios. Stable isotopes (^{2}H and ^{18}O) of saturation water and extracted water in the crystalline cores were also measured to monitor involved physical processes. We find that the noble gas ratios of He and Ne released from the rock porewater were consistent with those in air-spike mixed headspace gas, and differences between $\delta^{2}H$, $\delta^{18}O$ of saturation water and extracted water are within uncertainty. This demonstrates that heating under vacuum can release porewater and dissolved noble gases from crystalline

rock without significant isotopic fractionation and contributions from minerals and fluid inclusions.

Keywords

Crystalline rock, porewater, noble gas, equilibrium, extraction, benchmark

4.1 Introduction

With the development of drilling and sampling techniques, more and more samples have been acquired from the crust and the mantle, this inspires us to obtain more historical information about the earth from subsurface samples. Crystalline rock in the crust has been one of the accessible messengers from the earth. Noble gases in crystalline rock can be found in three primary environments: dissolved in the connected, water-filled porosity, in isolated porosity and fluid inclusions, and in mineral lattices. The physical processes for noble gas release from crystalline rock are of interest.

In the early 1980s, with the application of ultra-high-vacuum mass spectrometers that are capable of analyzing isotopic ratios of an extremely small amount of noble gases, routine noble gas investigation on crustal rocks began (Podosek et al., 1980). The measurement of noble gases found in the connected, water-filled porosity is more complicated. He and Ar isotopes measured in crystalline and sedimentary rocks in northern Switzerland showed noble gas losses happened to the rock during sampling compared with the calculated noble gas concentrations (Oxburgh et al., 1986). This kind of study illustrated the difficulties encountered on rock sample preservation before getting analyzed in the lab.

To extract porewater noble gases from rock samples, three main methods have been widely utilized until now. The first method is temperature step-wise heating on rock samples to see the released gases in mass spectrometers (Ozima & Podosek, 2002). Different research groups have different beginning temperatures and intervals, while

most are more interested in breaking the clay minerals in shales (Hassanipak & Wampler, 1996; Clauer et al., 2012). The stepwise heating method is effective but the released gases are always a mixture from several distinct sources (e.g., fluid inclusions, pores and minerals) which usually makes the data interpretation complicated. The second choice is sampling the in-situ seepage pore water from low permeability crystalline rocks with a tube or packer (Waber & Smellie, 2008; Kietäväinen et al., 2013; Purkamo et al., 2013; Warr et al., 2018). It needs considerable water content in the crystalline rocks and a lot of time (months to years) and effort to collect groundwater deep subsurface. Most commonly, gas out-diffusion experiments from conditioned rock core samples are undertaken (Waber & Smellie, 2008). Such gas out-diffusion experiments are set in the lab at room temperature in a vacuum cylinder and the out-diffusion process usually takes months (Waber & Smellie, 2008).

Stable isotopes (e.g., ^{2}H, ^{18}O) and solutes (e.g., Cl^{-}, Br^{-}) in porewater or groundwater have been investigated in crystalline rocks (Waber & Smellie, 2008; Kietäväinen et al., 2013). The groundwater geochemical parameters vary at different depths and show different characteristics at the distances between crystalline rock porewater and fracture groundwater. As well-acknowledged dating tools, noble gases have contributed to groundwater residence time estimation (Tolstikhin et al., 1996; Morikawa, 2004; Kietäväinen et al., 2014; Gerber et al., 2017; Rufer et al., 2017) and ancient hydrogeological fracture network age (Warr et al., 2018). The physical processes that happen during noble gas release from crystalline rock are also hot topics of current research. An in-situ conditional investigation was performed on the effects of drilling

and stress release on transport properties and porewater chemistry of crystalline rocks (Waber et al., 2011). Crystalline rock porosity, transport properties, and porewater composition were proved to be changed by drilling mechanical disruption and drilling fluid (Meier et al., 2015). The radiogenic noble gas release from crystalline rocks is proved correlated with rock deformation (Bauer et al., 2016). Geogenic noble gases are released during the triaxial deformation of crystalline rocks and are related to volume strain and acoustic emissions (Bauer & Hyunwoo Lee, 2017).

Deep geological repository (DGR) safety assessment and groundwater transport/evolution modellings require knowledge of groundwater and porewater geochemical compositions, as well as petrophysical and solute transport properties, to provide representative estimations of long-term system behavior. Granitic rock from the western part of the Canadian Shield is considered a potential host rock for the siting of a DGR for the storage of heat-emitting high-level nuclear fuel waste. Analysis of noble gases in crystalline rock is complicated due to the very low porosity and very low permeability of these materials. In this study, we attempt to benchmark a new method for noble gas extraction and analysis in crystalline rock porewater, based on a vacuum distillation method developed for porewater stable isotopes. This methodology can provide porewater/fissure water noble gas analysis with standards which is important for crystalline rock research.

4.2 Samples

The granitic samples were collected from Lac Du Bonnet batholith, Manitoba, the western flank of the Canadian Shield. The 75 mm-diameter cylindrical granite samples were obtained from a depth of approximately 16 m. The core samples were chopped into small pieces (15~20 cm) after being recovered from boreholes. Attributed to the geochemical interaction with groundwater, the granitic samples are in pink color. XRD testing shows that the pink granite contains 38.4% Quartz, 60.2% K-felspar, and 1.4% Mica (Selvadurai et al., 2020). The total porosity of granite is approximately 0.1% which was determined by water re-saturation experiments. The effective permeability of the granite is estimated by appeal to the geometric mean with a non-destructive methodology which gives $K=9.7\times10^{-18}$ m^2 (Selvadurai et al., 2020). All crystalline rocks were dried in an oven at 90 ℃ to a steady weight over several days to ensure pore water is removed before the noble gas in and out experiments.

4.3 Material and Methods

4.3.1 Porewater Resaturation

The benchmarking experiment for porewater stable isotopes and noble gases was conducted with full-round (75 mm diameter) granite core acquired from the Lac Du Bonnet intrusion near Pinawa, Manitoba (Selvadurai et al., 2020). A 15 cm length of core was dried by heating under vacuum until a steady weight was achieved. The dry granite sample was then isolated in a stainless steel chamber then pumped to a vacuum of 10^{-3} Torr. Subsequently, boiled deionized (DI) water was aspirated into the high vacuum chamber (Figure 4.1-a). The volume of DI water allowed to flow into the chamber was calculated to ensure the rock was fully immersed but maintaining some headspace at top of the chamber. This re-saturation process took place over a 24-hour period at room temperature to maximize resaturation of the granite core.

4.3.2 Noble Gas Spike

After the water re-saturation into the granite sample, the stainless steel chamber with the rock was transferred to the noble gas spike line (Figure 4.1-b). First of all, the valve on the stainless steel chamber was replaced with swaged standard 3/8" refrigeration Cu tube and connected to the noble gas spike line. The He & Ne spike tank consists of 0.5% He and 0.5% Ne which are balanced with N_2. The He ratio of the noble gas spike is 2.259×10^{-7}. The headspace in the metal chamber will be equilibrated with the mixture of air and noble gas spike for 20 min. Then the Cu tube is crimped with a cold-welding

clamp to seal the reaction system. The stainless steel chamber with crimped Cu tube was then transferred to an oven and baked at 90 °C for different time (e.g., several weeks) (Figure 4.1-c).

The last and most important step was taking the headspace gas sample and transferring the granite sample into the baking chamber which would be hooked to the noble gas analysis system (Figure 4.1-d). The Cu tube was crimped with a pinch-off cold-welding clamp for headspace gas sampling. The granite core was dried on the surface with Kimwipe first and transferred into a clean baking chamber as soon as possible. Before baking the porewater out, the core sample was pumped shortly on a vacuum pump until a sudden jump showed on the pressure reading. This jump is recognized as a sign that gas started to diffuse out from the inner part of the core sample.

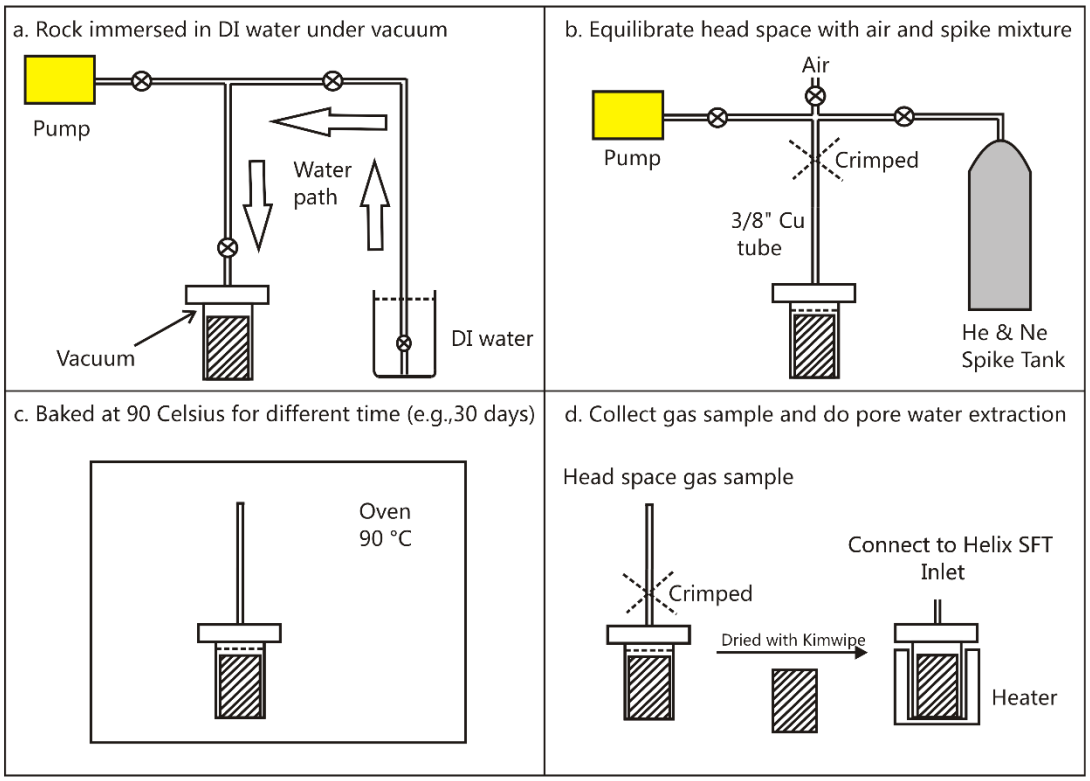

Figure 4.1 Experimental schematics for noble gas in and out crystalline rock.

4.3.3 Porewater Extraction and Isotope Analysis

Porewater extraction on saturated whole-core samples was carried out via vacuum-distillation, which involves heating the rock samples under vacuum, and the subsequent water recovery with an on-line liquid nitrogen trap. The temperature and duration of distillation are critical to ensure that as close to 100% of the porewater are collected. Testing at the University of Ottawa demonstrated that a temperature of 120°C and a duration of 6-hours at a pressure of 30 mTorr provided full porewater recovery and reproducibility (Najem et al., manuscript in preparation). Prior to extraction, a saturated core (section 4.3.1) was removed from the stainless-steel chamber, quickly surface-dried using Kimwipes, weighed, and transferred into another dry stainless-steel chamber fitted with a Swagelok valve and a custom-made Rotulex fitting. Porewater recovery was determined gravimetrically, by measuring the weight of a core and a collection vessel before and after porewater extraction.

Recovered water samples were analyzed for the stable isotopes ^{18}O and ^{2}H in Ján Veizer Stable Isotope Laboratory (University of Ottawa) using the Triple Isotope Water Analyzer (TIWA-45EP) by Los Gatos Research (LGR). Briefly, a volume of ~0.2 mL was quickly pipetted into 2 mL GC septa vials. Then, water samples were introduced without sample conversion into the OA-ICOS instrument via a PAL HTC-xt auto injector (CTC Analytics) equipped with a heated (≈85 °C) injector block (LGR), where the water samples were evaporated for isotope analysis directly on the water vapor. Liquid water samples were injected into the injector block using a Hamilton 1.2 µL,

zero dead-volume syringe. $\delta^{18}O$ and $\delta^{2}H$ values were expressed as per mil (‰ relative to Vienna Standard Mean Ocean Water (VSMOW). The routine precision (2 σ) of the ^{18}O analysis is ±0.2 ‰, and ±2.0 ‰ for the ^{2}H analysis.

4.3.4 Noble Gas Extraction and Analysis

The crystalline porewater was extracted with vacuum heating method connected to the rock sample inlet of noble gas processing line (Figure 4.2). The noble gas releasing temperature from crystalline porewater is determinant for noble gas extraction. The minerals such as quartz in the crystalline rock also retain a large amount of geogenic noble gases with unknown sources, but negligible release of He happen under heating below 350 ℃ (Lehmann et al., 2003). Hence, the equilibrated crystalline cores were vacuum heated at 150 ℃ for 12 hours to release noble gases dissolved in crystalline porewater.

Noble gas samples in Cu tubes and granitic rock porewater were purified and separated using a multi-stage ultra-high vacuum processing line (Figure 4.2) in the Noble Gas and Tritium Laboratory, at the University of Ottawa. Water vapor was removed with a U-shape polished stainless steel trap in an ethonal bath at 190 K. N_2, O_2, H_2, hydrocarbons, Ar, Kr, Xe and other active gases (e.g., CO, CO_2) were removed with two activated charcoal traps at liquid N_2 temperature (77 K) and two SAES ST 172 getters (Zr-V-Fe), one is at room temperature (293 K), and the other at 573 K.

Following purification, He and Ne were drawn down on the ARS activated charcoal

cryostat at 5 K, then individually released into the noble gas mass spectrometer at 30 K and 80 K respectively. He and Ne were analyzed on the magnetic sector static vacuum Thermo Scientific Helix SFT mass spectrometer using a Faraday detector, except for ^{3}He, which was measured using an electron multiplier in ion counting mode.

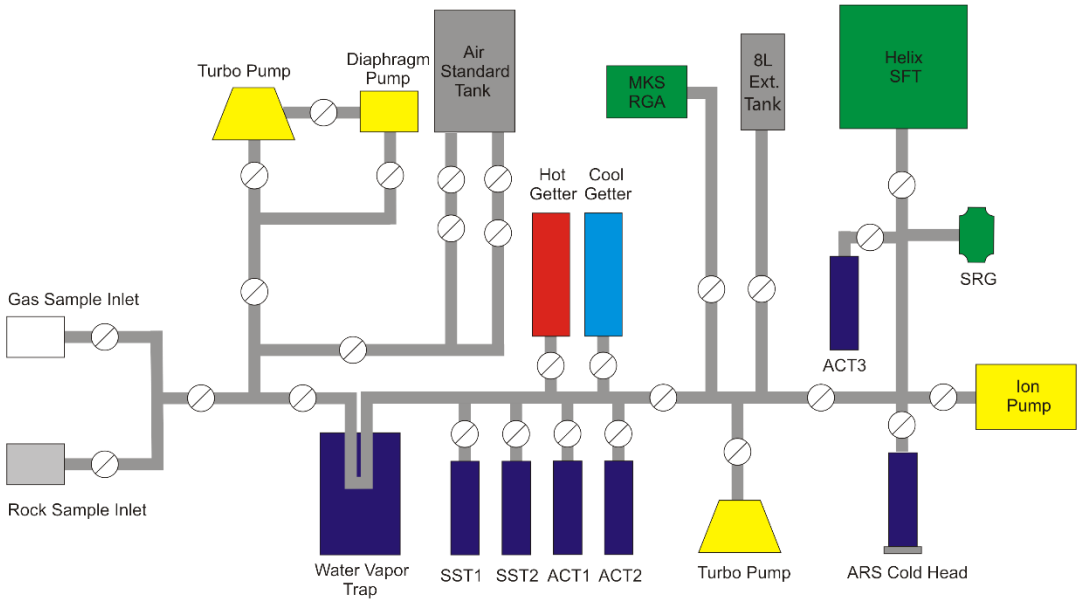

Figure 4.2 Schematic of Noble gas preparation line at University of Ottawa (SST: stainless steel trap; ACT: activated charcoal trap; SRG: spinning rotor vacuum gauge).

4.4 Results

Stable isotopes of saturation water and extracted water are presented in Table 4.1. The differences of $\delta^{18}O$ and $\delta^{2}H$ in saturation water and extracted water are minor and close to the analytical uncertainty. The difference of $\delta^{18}O$ in saturation water and extracted water ranges from 0.07‰ to 0.28‰. The difference of $\delta^{2}H$ in saturation water and extracted water ranges from 0.40‰ to 2.94‰.

Table 4.1 Stable isotopes (^{2}H and ^{18}O) of saturation water and extracted water of crystalline samples.

Sample ID	Saturation water (g)	Extracted porewater (g)	$\delta^{18}O$ (Saturation water)	$\delta^{18}O$ (Extracted water)	Difference $\delta^{18}O$	δD (Saturation water)	δD (Extracted water)	Difference $\delta^{2}H$
1	1.57	1.52	-11.61	-11.69	-0.07	-86.79	-83.85	2.94
2	0.89	0.89	-11.75	-11.93	-0.18	-85.17	-84.45	0.71
3	1.01	0.97	-11.63	-11.89	-0.26	-86.02	-85.62	0.40
4	1.38	1.38	-11.96	-12.24	-0.28	-86.03	-87.43	-1.40

He and Ne isotopic ratios of the chamber headspace gas and granite rock porewater samples are summarized in Table 4.2. From Table 4.2, it is obvious that $^{3}He/^{4}He$ and [xRa] values are not atmospheric ($Ra=1.399\times10^{-6}$). Anomalous He ratios reveal that the equilibrated system is enriched in ^{4}He relative to air. With respect to Ne ratios, they are close to the air ratios that $^{20}Ne/^{22}Ne$ and $^{21}Ne/^{22}Ne$ are 9.8 and 0.029 (Ozima & Podosek, 2002), respectively. The He ratios in headspace gas and extracted porewater confirm that the He and Ne spike mixed and equilibrated well during the experimental process.

By comparing the headspace gas and granite porewater noble gas results in every single experiment, we find that though the reaction time between gas and water phases varies from 2 weeks to 5 weeks, He and Ne ratios of crystalline rock porewater are close to those of headspace gas. This illustrates that 2 weeks is sufficient to make the gas-water interaction equilibrated. In addition, the longer reaction time did not show better consistency of noble gas ratios between the gas and water phase (Table 4.2).

Table 4.2 He and Ne isotope ratios (± 1σ) of the headspace gas and crystalline rock porewater. He ratios are normalized to atmospheric value ($Ra=1.399\times10^{-6}$) and expressed as [x Ra].

Sample ID	**Time (days)**	**$^{3}He/^{4}He$ ($\times10^{-7}$)**	**Error ($\times10^{-9}$)**	**x Ra**	**Error (x Ra)**	**$^{20}Ne/^{22}Ne$**	**Error**	**$^{21}Ne/^{22}Ne$**	**Error**
1-Gas	35	3.38	2.02	0.242	0.0014	9.67	0.004	0.0290	0.00002
1-Core	35	3.38	14.6	0.242	0.0105	9.58	0.101	0.0290	0.00107
2-Gas	34	3.82	8.09	0.273	0.0058	9.76	0.006	0.0289	0.00004
2-Core	34	3.83	4.50	0.273	0.0032	9.81	0.009	0.0286	0.00082
3-Gas	14	3.01	3.37	0.215	0.0024	9.77	0.014	0.0292	0.00002
3-Core	14	3.01	3.46	0.215	0.0025	9.80	0.007	0.0296	0.00005
4-Gas	15	2.96	2.23	0.212	0.0016	9.75	0.023	0.0293	0.00081
4-Core	15	3.00	2.63	0.215	0.0019	9.60	0.004	0.0297	0.00032

The noble gas ratio differences between headspace gas and crystalline rock porewater are calculated and compared. In regard to He ratios and [xRa], the differences between headspace gas and granite porewater are smaller than 1.5% on $^{3}He/^{4}He$ and [xRa] with a minimum difference of 0.1% and a maximum difference of 1.41%. The differences of

$^{20}Ne/^{22}Ne$ ratios between headspace gas and porewater are smaller than 1% with a minimum of 0.21% and a maximum of 0.87%. The differences of $^{21}Ne/^{22}Ne$ ratios between headspace gas and crystalline rock porewater are also smaller than 2% with a minimum difference of 0.01% and a maximum difference of 1.56%. The consistency of noble gas ratios between headspace gas and crystalline rock porewater demonstrates the thorough equilibration in the closed system and no obvious mass fractionation during extraction by vacuum distillation, due to experimental conditions, such as gas mixing, temperature change and gas dissolution in the water phase.

Table 4.3 ^{4}He and ^{20}Ne concentrations in the chamber headspace gas and crystalline rock porewater. (Errors are propagated from 1σ of measured He and Ne).

Sample ID	Headspace gas				Crystalline rock porewater			
	^{4}He ($\times10^{-4}$) concentration (cc_{STP}/cc_{gas})	Error ($\times10^{-7}$) (cc_{STP}/cc_{gas})	^{20}Ne ($\times10^{-5}$) concentration (cc_{STP}/cc_{gas})	Error ($\times10^{-7}$) (cc_{STP}/cc_{gas})	^{4}He ($\times10^{-6}$) concentration (cc_{STP}/cc_{H2O})	Error ($\times10^{-9}$) (cc_{STP}/cc_{gas})	^{20}Ne ($\times10^{-7}$) concentration (cc_{STP}/cc_{H2O})	Error ($\times10^{-9}$) (cc_{STP}/cc_{gas})
1	1.378	0.227	11.93	0.272	5.091	0.592	6.826	4.657
2	0.450	0.102	2.681	0.091	1.270	0.198	0.842	0.035
3	1.544	0.273	5.849	0.835	6.639	5.947	4.303	0.159
4	1.951	3.164	1.824	1.593	2.668	0.321	0.889	0.015

He and Ne concentrations in headspace gas and crystalline rock porewater are summarized in Table 4.3. In contrast with ratio data, He and Ne concentrations are significantly different between headspace gas and crystalline rock porewater. He and Ne concentrations in the porewater are 2~3 magnitudes smaller than that in the headspace gas. This discrepancy attributes to the extremely low solubility of He and Ne in the water phase, especially in hot water, whereas could be quantified with the Bunsen coefficient. In addition, the partial pressures of He and Ne were measured at room

temperature (293 K), a correction factor to experimental temperature (363 K) is needed when conducting mass balance calculation for noble gases between gas and porewater.

4.5 Discussion

4.5.1 Physical Processes

As the carrier of dissolved gases, it is necessary to monitor the physical processes of porewater during the vacuum distillation extraction. Benchmarking of the vacuum-distillation method revealed a full or near full recovery of the porewater from the re-saturated cores (Table 4.1), and the stable isotopes of the recovered porewater fall within the acceptable error range of their corresponding saturation waters (0.2‰ for ^{18}O and 2.0‰ for ^{2}H) (Figure 4.3). Therefore, we show that the refined core re-saturation method together with the developed vacuum distillation protocol do not introduce unwanted isotopic fractionation artifacts (Najem et al., manuscript in preparation). Consequently, the stable isotope measurements are representative of the in-situ porewater isotopes.

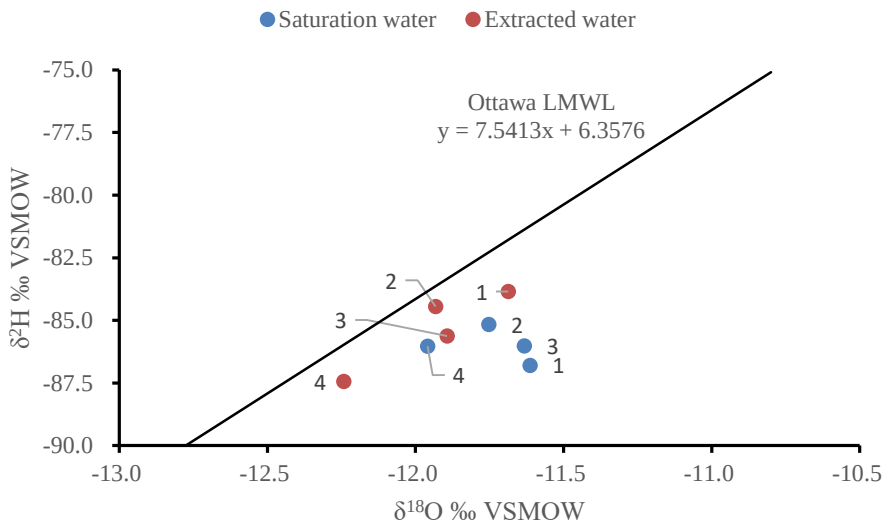

Figure 4.3 Stable isotopes (^{2}H and ^{18}O) of saturation water and extracted water of crystalline rock samples.

From Figure 4.3, we find a minor depletion in ^{18}O of water stable isotopes in extracted porewater compared with saturation water. Based on earlier experiments (Najem et al., manuscript in preparation), this is attributed to the diffusion process during the porewater resaturation under vacuum, which discriminates against the heavier isotopes of water ($^{1}H_{2}^{18}O$ and to a lesser extent, $^{2}H^{1}H^{16}O$). We conclude that any depletion artifact, however minor, are due to the re-saturation process for the benchmarking exercise and not from vacuum distillation.

The physical processes involved in the noble gas experiments are mixing of remaining headspace air and noble gas spike, gas dissolution in the water, dynamic equilibrium among crystalline porewater, water in the chamber and the headspace gas, and minor diffusion during extraction. To quantify the gas-liquid equilibrium, the solubility of He and Ne at reaction temperature (90 °C) are the key parameters.

The main factors that influence noble gas solubility in fresh water are gas partial

pressure and water temperature (Andrews, 1992). Measurements of the solubility of He, Ne were conducted in distilled water and seawater over the temperature range 0-40 ℃ (Weiss, 1971). Dissolved noble gas concentrations in high salinity Ca(Na)-Cl groundwater from the Con Mine, Canada were measured and the difference between salinity and temperature effect on Ne solubility was demonstrated (Greene et al., 2008). A compilation of He and Ne solubility data by the International Union of Pure and Applied Chemistry (IUPAC) provides the best available experimental solubility data of He and Ne in liquids (Clever, 2015). In this study, He and Ne solubilities at 90 ℃ are extrapolated from the equations in the IUPAC compacted noble gas solubility file (Clever, 2015) (.Figure 4.4 and Figure 4.5).

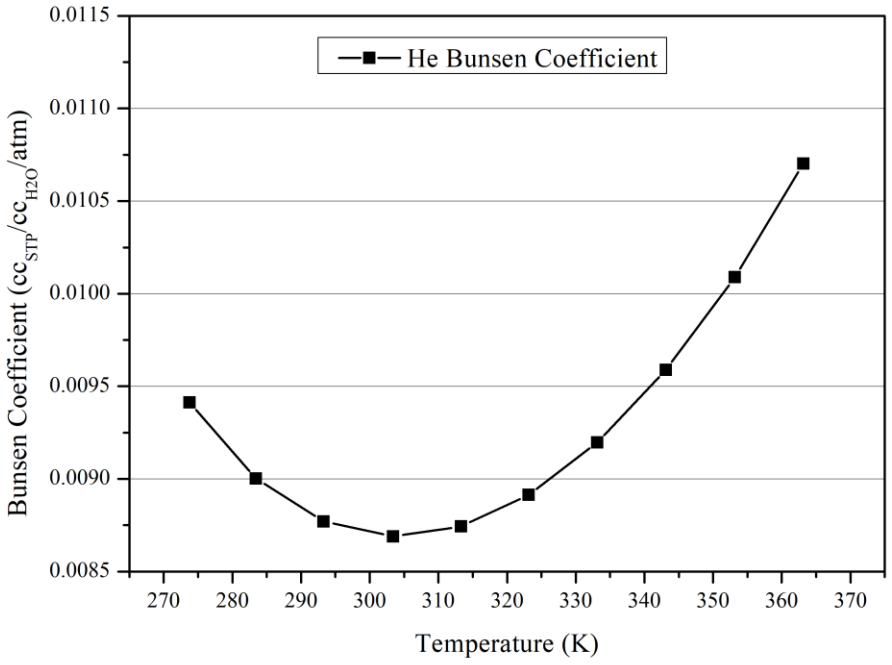

Figure 4.4 He Bunsen Coefficient (cc He/cc H_2O/atm) at different temperatures in fresh water.

$$\ln f_{He} = -41.4611 + 42.5962/(\frac{T}{100K}) + 14.0094 \times \ln(\frac{T}{100K}) \quad (4.1)$$

Equation (4.1) is the best fit for 59 He solubility measurement points (Clever, 2015). Where f_{He} is the mole fraction solubility of He at 101.325 kPa (1 atm) partial pressure of the gas. The fit in ($\ln f_{He}$) gives a standard deviation of 0.54% taken at the middle of the temperature range. From equation (4.1), He solubility expressed as Bunsen Coefficient at 90 ℃ is extrapolated as 0.010703 cc/cc_{H2O}/atm.

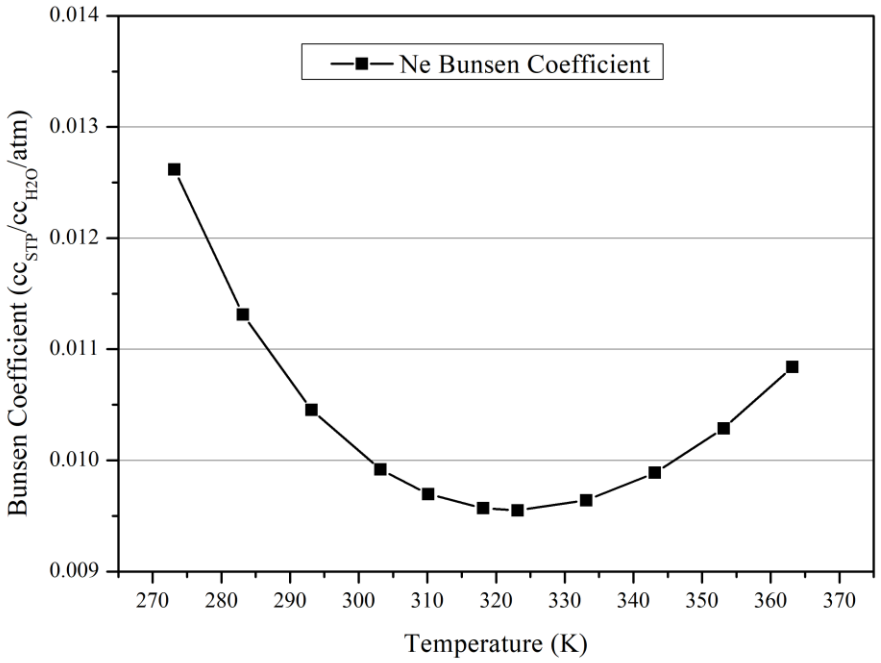

Figure 4.5 Ne Bunsen Coefficient (cc Ne/cc H_2O/atm) at different temperatures in fresh water.

$$\ln f_{Ne} = -52.8573 + 61.0494/(\frac{T}{100\ K}) + 18.9157 \times \ln(\frac{T}{100\ K}) \quad (4.2)$$

Equation (4.2) is the best fit for 59 Ne solubility measurement points (Clever, 2015). Where f_{Ne} is the mole fraction solubility of Ne at 101.325 kPa (1 atm) partial pressure of Ne. The fit in ($\ln f_{Ne}$) gives a standard deviation of 0.47% taken at the middle of the temperature range. From equation (4.2), Ne solubility expressed as Bunsen Coefficient

at 90 °C is extrapolated as 0.010839 cc/cc$_{H2O}$/atm.

After gas dissolution, equilibrium in the closed experimental system should be dominated by molecular diffusion of noble gases in gas and water (de Magalhães et al., 2017). Before the closed system equilibration, the isotope mass fractionation may occur during the process of noble gases diffusion into the crystalline rock porewater. As hydrophobic particles, the dissolution of He and Ne atoms in water results in the structural rearrangement of the water molecules, which contributes to the formation of a clathrate-type cavity (de Magalhães et al., 2017). The mechanism responsible for the noble gas fractionation is considered to be an inter-cavity hopping mechanism, which dues to the fast vibrational motion of light noble gas particles within the cavity on very short time scales (de Magalhães et al., 2017).

4.5.2 Noble gas characteristics

At the beginning of the experiment, the headspace gas was a mixture of remaining air and an aliquot of the noble gas spike which consists of 0.5% He and 0.5% Ne balanced with N_2. With the mixing process going on, the He-Ne enriched gas spike will equilibrate with remaining headspace air then with water in the chamber. Subsequently, the gas will diffuse further into the water phase and eventually penetrate the crystalline rock fissures and pores. During the whole process, water played a role as a media and carrier for noble gas transport among gas, water and rock.

In Figure 4.6 and Figure 4.7, He and Ne isotope ratios measured in the headspace gas and in porewater are the same, within analytical uncertainty. It suggests that noble gas

isotope ratios in the porewater have equilibrated with the headspace gas phase through the chamber water, and that no fractionation occurs during porewater extraction by vacuum distillation. Higher temperatures within an appropriate range are favorable for the noble gas exchange between gas and liquid phases. In this study, the experimental subject was baked at 90 °C to accelerate the diffusion progress but with no significant influence on the solubility of He and Ne (Figure 4.4 and Figure 4.5). The physical process of diffusion involved in the experiments could potentially have resulted in the mass-dependent fractionation of noble gases if equilibrium conditions had not been achieved. Equilibrium exchange would have been facilitated by the high temperature in the sealed chamber.

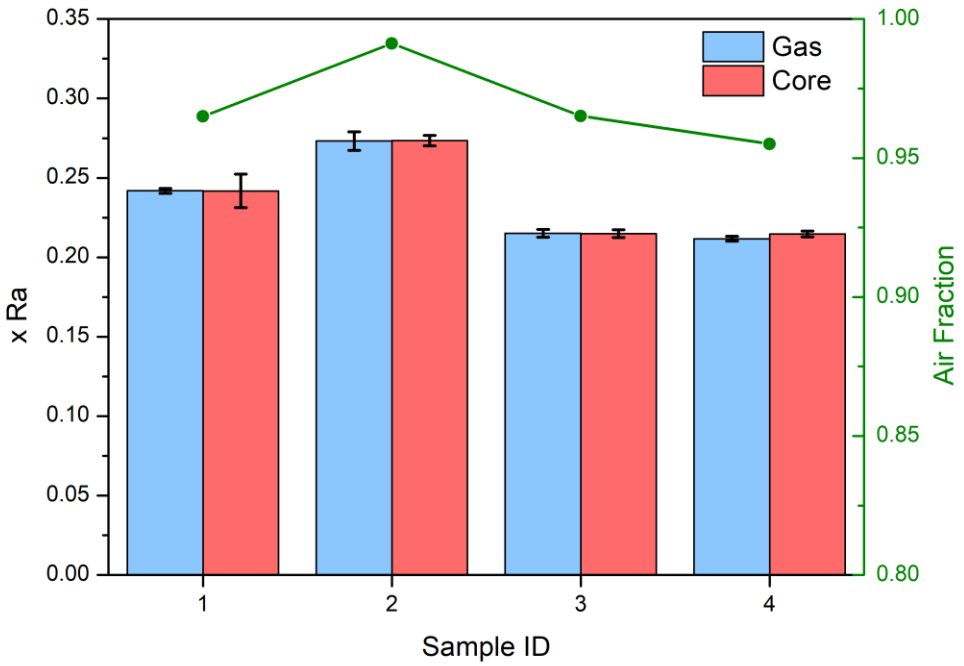

Figure 4.6 He ratios (± 1σ) and air fraction in gas mixture in the headspace gas and crystalline rock porewater. He ratios are normalized to atmospheric value ((Ra=1.399×10^{-6}) (Ozima & Podosek, 2002) and expressed as [x Ra].

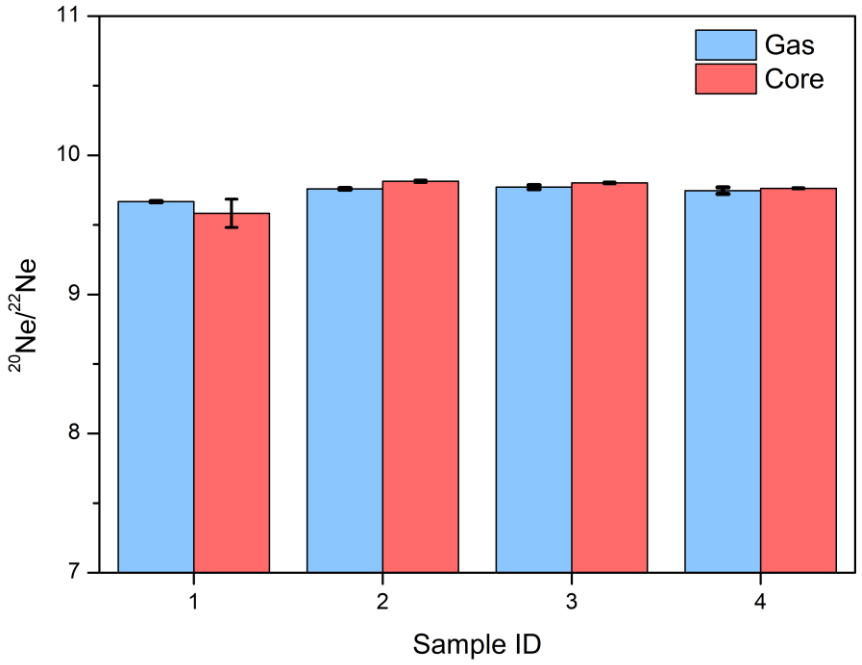

Figure 4.7 Ne ratios (± 1σ) in gas mixture in the headspace gas and crystalline rock porewater.

The mixing process is confirmed by the He ratio concordance in headspace gas and crystalline porewater , and the noble gas isotopic equilibration is confirmed by both He and Ne isotope ratios from individual experiments. The anomalous He signatures in headspace gas and crystalline rock porewater can attribute to the noble gas spike in which ^{4}He is enriched. The enriched ^{4}He in the noble gas spike makes the $^{3}He/^{4}He$ value drop from the atmospheric value of 1.399×10^{-6} to values in the magnitude of 10^{-7} (Figure 4.6 and Table 4.2). Three tests were conducted for He ratio of the spike gas, the $^{3}He/^{4}He$ ratio average value of the noble gas spike is 2.259×10^{-7}. In Figure 4.6 and Table 4.2, all He ratios are between the atmospheric value and spike He ratio, and He ratios of headspace gas and crystalline core porewater are almost consistent. This implies that mixing and equilibration happened during experiments. The average

$^{20}Ne/^{22}Ne$ value of the noble gas spike was attained as well from three tests those yield 9.82. $^{20}Ne/^{22}Ne$ values of headspace gas and rock porewater do not shift a lot from the atmospheric value of 9.8, but are a bit smaller than the atmospheric value. The depletion of $^{20}Ne/^{22}Ne$ is suspected as a result of small intensities of Ne isotopes (Sample 1 in Figure 4.7). $^{21}Ne/^{22}Ne$ values of headspace gas and porewater are not only consistent in headspace gas and porewater but also close to air $^{21}Ne/^{22}Ne$ value which is 0.029 (Table 4.2).

He and Ne concentrations were acquired as well with the mass spectrometer sensitivity and noble gas signal intensities (Table 4.3). Under conditions of equilibrium saturation, the partial pressure of He and Ne in the porewaters should be equal to their partial pressures in the headspace gas, when calculated with their respective Bunsen coefficient at the experimental temperature. In contrast, we find that the partial pressures of He and Ne calculated for the porewaters are greater than those in the headspace gas. Taking the reaction conditions and noble gas solubility into account, it is a matter of course that He and Ne have lower abundances in the hot water at 90 °C. Theoretically, noble gas concentrations in the porewater should be positively correlated with the noble gas partial pressure in the headspace. However, this positive correlation does not show up in these experiments. This abnormal phenomenon is due to the formation of residual unsaturated porosity (RUP) in the fissures of the rock that water could not reach because of the capillary effect. Compared with noble gases dissolved in the water, the dead angles keep a considerable amount of gas in them and will get equilibrated with water ultimately.

4.5.3 Mass balance

Although the long time and high temperature facilitate the re-distribution of noble gases in the closed reaction system, the dissolved noble gases are still negligible compared with those in the headspace. It can be simplified that there are constantly two components involved in the interaction in headspace gas, one is remaining air, the other is the noble gas spike. Before the mixing process, the noble gas spike outflow was set at 15 psi (≈air pressure) to ensure the water and air in the reaction chamber would not be sucked out because of the pressure difference.

Theoretically, in a case where the element in components A and B has not only different concentrations but also different isotope compositions, both the concentration and isotope composition of the element in a mixture M need to be accounted for. Here, we assume air as component A, and noble gas spike as component B. At the equilibrium, the factions of air and noble gas spike can be calculated with the following equations (Faure & Mensing, 2004):

$$\left(\frac{^3He}{^4He}\right)_M = \left(\frac{^3He}{^4He}\right)_{Air} f_{Air} \left(\frac{He_{Air}}{He_M}\right) + \left(\frac{^3He}{^4He}\right)_{Spike} f_{Spike} \left(\frac{He_{Spike}}{He_M}\right) \quad (4.3)$$

$$f_{Air} + f_{Spike} = 1 \quad (4.4)$$

He concentrations and ratios of the two components are listed below:

Component air: C_{He}= 5.24×10^{-6} cm^3/cm^3 $^3He/^4He$=1.399×10^{-6} $^3He/^4He$ (R/Ra)=1

Component spike: C_{He}= 5×10^{-3} cm^3/cm^3 $^3He/^4He$=2.259×10^{-7} $^3He/^4He$ (R/Ra)=0.1615

The fractions of air in the gas mixture after interaction were calculated with equation

(4.3) and the initial conditions above. The results are presented in Figure 4.6. The air fractions in the headspace gas mixture are large than 95%, which suggests that a tiny amount of the noble gas spike can dominate the He ratio of the gas mixture. Besides, the air fractions in the headspace gas (Figure 4.6) have a positive correlation with the He ratio.

These two-components mixing fraction calculation was not conducted to Ne ratios and concentration, because though there is a difference between Ne concentrations of air and noble gas spike (1.82×10^{-5} cm^3/cm^3 and 5×10^{-3} cm^3/cm^3, respectively), there is no obvious difference between their Ne isotope ratios. In addition, the small-signal intensity and big analytical errors make the Ne calculation not accurate enough.

The weights of water saturated in crystalline rocks were acquired by weighing cores before and after baking. As shown in Table 4.4, the RUP volumes in core samples competed, ranging from 0 cc to 0.026 cc. In the closed reaction system, even though the RUP accounts for a very small amount of the total pore space, the gas reserved in it after equilibrium has the same partial pressure as that in the headspace gas. This small volume makes a big difficulty for the total re-saturation of the crystalline rock samples.

Table 4.4 He Mass Balance Calculation in the closed reaction system

Sample ID	Extracted water (cc)	Total ^{4}He in rock (cc)	^{4}He partial pressure at 293 K (cc/cc_{volume})	^{4}He partial pressure at 363 K (cc/cc_{volume})	^{4}He Bunsen Coefficient at 363 K ($cc/cc_{H2O}/atm$)	RUP(cc)
1	1.36	6.923E-06	1.38E-04	1.71E-04	0.010703081	0.026
2	0.76	9.651E-07	4.50E-05	5.58E-05	0.010703081	0.009
3	0.97	6.440E-06	1.54E-04	1.91E-04	0.010703081	0.023
4	1.30	3.468E-06	1.95E-04	2.42E-04	0.010703081	0.000

4.6 Conclusions

This study on the crystalline rock porewater isotopes and noble gases demonstrates our ability to extract and reliably analyze porewater isotopes and dissolved noble gases in crystalline rock full-round cores. The porewater stable isotopes ^{2}H and ^{18}O suggest negligible influence from the vacuum distillation extraction protocol. The close match of noble gas ratios in headspace gas and crystalline porewater suggests that equilibrium was achieved in the benchmarking experimental system and that noble gases can be reliably extracted from crystalline rock by heating under vacuum at 150 °C.

The consistency of noble gas ratios between gas and liquid phases confirms the reproducibility of noble gas ratios from crystalline rock porewater. The noble gas standard samples for crystalline rock porewater can be prepared with the re-saturated crystalline rock. However, this is only accurate for noble gas ratios, more factors such as dead angles should be taken into account for noble gas concentration work.

Generally, this study benchmarks the porewater stable isotopes and dissolved noble gases extraction method from crystalline rocks. The vacuum distillation extraction

method has negligible influence on $\delta^{2}H$ and $\delta^{18}O$ values compared with saturation water. Noble gas results suggests that the vacuum heating extraction is an effective method to extract porewater noble gases. With these extraction methods, the in-situ porewater stable isotopes and noble gases can be accurately measured in laboratory.

Acknowledgments

This work was supported by the Nuclear Waste Management Organization (NWMO), Toronto, Canada. Acknowledgment to China Scholarship Council (CSC) for the financial support on Ende Zuo's Ph.D. project (No. 201606170089).

References

Andrews, J. (1992). *Mechanisms for noble gas dissolution by groundwaters.* Paper presented at the Isotopes of noble gases as tracers in environmental studies.

Bauer, S. J., Gardner, W. P., & Lee, H. (2016). Release of radiogenic noble gases as a new signal of rock deformation. *Geophysical Research Letters, 43*(20), 10,688-610,694.

Bauer, S. J., & Hyunwoo Lee, U. (2017). Noble Gas Release and Flow Through a Granite and Basalt: Sandia National Lab.(SNL-NM), Albuquerque, NM (United States).

Clauer, N., Zwingmann, H., Liewig, N., & Wendling, R. (2012). Comparative 40Ar/39Ar and K–Ar dating of illite-type clay minerals: A tentative explanation for age identities and differences. *Earth-Science Reviews, 115*(1-2), 76-96.

Clever, H. L. (2015). *Helium and neon: gas solubilities* (Vol. 1): Elsevier.

de Magalhães, H. P., Brennwald, M. S., & Kipfer, R. (2017). Diverging effects of isotopic fractionation upon molecular diffusion of noble gases in water: mechanistic insights through ab initio molecular dynamics simulations. *Environmental Science: Processes & Impacts, 19*(3), 405-413.

Faure, G., & Mensing, T. M. (2004). *Isotopes: Principles and Applications, 3rd Edition*.

Gerber, C., Vaikmäe, R., Aeschbach, W., Babre, A., Jiang, W., Leuenberger, M., . . . Raidla, V. (2017). Using 81Kr and noble gases to characterize and date groundwater and brines in the Baltic Artesian Basin on the one-million-year

timescale. *Geochimica et cosmochimica acta, 205*, 187-210.

Greene, S., Battye, N., Clark, I., Kotzer, T., & Bottomley, D. (2008). Canadian Shield brine from the Con Mine, Yellowknife, NT, Canada: Noble gas evidence for an evaporated Palaeozoic seawater origin mixed with glacial meltwater and Holocene recharge. *Geochimica et cosmochimica acta, 72*(16), 4008-4019.

Hassanipak, A., & Wampler, J. (1996). Radiogenic argon released by stepwise heating of glauconite and illite: The influence of composition and particle size. *Clays and Clay Minerals, 44*(6), 717-726.

Kietäväinen, R., Ahonen, L., Kukkonen, I. T., Hendriksson, N., Nyyssönen, M., & Itävaara, M. (2013). Characterisation and isotopic evolution of saline waters of the Outokumpu Deep Drill Hole, Finland–Implications for water origin and deep terrestrial biosphere. *Applied geochemistry, 32*, 37-51.

Kietäväinen, R., Ahonen, L., Kukkonen, I. T., Niedermann, S., & Wiersberg, T. (2014). Noble gas residence times of saline waters within crystalline bedrock, Outokumpu Deep Drill Hole, Finland. *Geochimica et cosmochimica acta, 145*, 159-174.

Lehmann, B. E., Waber, H. N., Tolstikhin, I., Kamensky, I., Gannibal, M., Kalashnikov, E., & Pevzner, B. (2003). Helium in solubility equilibrium with quartz and porefluids in rocks: A new approach in hydrology. *Geophysical Research Letters, 30*(3).

Meier, D., Waber, H., Gimmi, T., Eichinger, F., & Diamond, L. W. (2015). Reconstruction of in-situ porosity and porewater compositions of low-

permeability crystalline rocks: Magnitude of artefacts induced by drilling and sample recovery. *Journal of contaminant hydrology, 183*, 55-71.

Morikawa, N. (2004). Dissolved helium distribution in deep groundwaters from the Tono area, central Japan: a tool for tracing groundwater flow in fractured granite. *Limnology, 5*(2), 61-69.

Oxburgh, E., O'nions, R., & Hill, R. (1986). Helium isotopes in sedimentary basins. *Nature, 324*(6098), 632-635.

Ozima, M., & Podosek, F. A. (2002). *Noble gas geochemistry*: Cambridge University Press.

Podosek, F., Honda, M., & Ozima, M. (1980). Sedimentary noble gases. *Geochimica et cosmochimica acta, 44*(11), 1875-1884.

Purkamo, L., Bomberg, M., Nyyssönen, M., Kukkonen, I., Ahonen, L., Kietäväinen, R., & Itävaara, M. (2013). Dissecting the deep biosphere: retrieving authentic microbial communities from packer-isolated deep crystalline bedrock fracture zones. *FEMS microbiology ecology, 85*(2), 324-337.

Rufer, D., Waber, H., Eichinger, F., & Pitkänen, P. (2017). Helium in porewater and rocks of crystalline bedrock from the Fennoscandian Shield, Olkiluoto (Finland). *Procedia earth and planetary science, 17*, 762-765.

Selvadurai, A., Blain-Coallier, A., & Selvadurai, P. A. (2020). Estimates for the Effective permeability of intact granite obtained from the Eastern and western flanks of the Canadian Shield. *Minerals, 10*(8), 667.

Tolstikhin, I., Lehmann, B., Loosli, H., & Gautschi, A. (1996). Helium and argon

isotopes in rocks, minerals, and related ground waters: A case study in northern Switzerland. *Geochimica et cosmochimica acta, 60*(9), 1497-1514.

Waber, H., Gimmi, T., & Smellie, J. (2011). Effects of drilling and stress release on transport properties and porewater chemistry of crystalline rocks. *Journal of hydrology, 405*(3-4), 316-332.

Waber, H., & Smellie, J. (2008). Characterisation of pore water in crystalline rocks. *Applied Geochemistry, 23*(7), 1834-1861.

Warr, O., Lollar, B. S., Fellowes, J., Sutcliffe, C. N., McDermott, J. M., Holland, G., . . . Ballentine, C. J. (2018). Tracing ancient hydrogeological fracture network age and compartmentalisation using noble gases. *Geochimica et cosmochimica acta, 222*, 340-362.

Weiss, R. F. (1971). Solubility of helium and neon in water and seawater. *Journal of Chemical & Engineering Data, 16*(2), 235-241.

Chapter 5 Crustal Noble Gas Isotopic Characteristics in Low-permeability Ordovician Sedimentary Rock, Eastern Flank of the Michigan Basin

Ende Zuo, Anthony Lapp, Josué J. Jautzy, Ian D. Clark*

ACS Earth and Space Chemistry

DOI: 10.1021/acsearthspacechem.1c00346

ABSTRACT

This study presents noble gas characteristics of porewater in the Ordovician low-permeability drill cores, which were vacuum-sealed in Al-foil bags and collected over a decade ago on the eastern flank of the Michigan Basin. Noble gas ratios and concentrations reveal crustal noble gas features as well as radiogenic ^{4}He, ^{40}Ar and ^{136}Xe components. The measured noble gas ratios in this study agree with measurements previously made in the Ordovician brine samples from the western flank of the Michigan Basin. However, unlike water samples from the western Michigan Basin, no mantle-featured noble gas components are found in the Ordovician rock porewater from this site. The Ordovician porewater residence time is quantitatively estimated with both He and Xe radiogenic ingrowth, yielding an average of 251 million years (m.y.). This porewater residence time estimate is comparable with the previous He accumulation time estimate at the same study site that yielded 260 m.y.. The radiogenic noble gas ingrowth demonstrates long-term confinement of porewater and concomitant gases within the Ordovician low-permeability rock investigated. The remarkable preservation of gases in these well-sealed vapor-barrier Al-foil bags provide an economic and efficient possibility for noble gas out-diffusion sampling from drill cores.

Keywords

Noble gases, Ordovician, Aquiclude, Aquitard, Porewater, Residence time, Michigan Basin

Synopsis

Noble gases in the Ordovician porewater reveal the radiogenic ingrowth and yield 251 million years as the confinement time of subsurface environment.

5.1 Introduction

Radiogenic noble gases in the crust including ^{4}He, ^{40}Ar and ^{136}Xe are generated from radioactive decay of the primordial radionuclides, uranium (U), thorium (Th) and potassium (K). The chemically inert properties of noble gases result in their accumulation and preservation in closed systems and can be used to estimate the closure time, with implications for porewater residence time. Gases or fluids from different geologic reservoirs represent distinct sources, or mixtures, which can be identified with noble gas characteristics.

In practice, noble gases have been widely applied as effective tracers to reveal the origin and transport mechanisms of gases and fluids in the crust (C. J. Ballentine et al., 2002; Castro et al., 2009; Ma et al., 2009; I. D. Clark et al., 2013; Al et al., 2015; Wen et al., 2015; Wen et al., 2016). In addition, they are often coupled to the interpretation of water stable isotopes (H and O), Cl, Br (Pinti, Castro, López-Hernández, Hernández, Richard, et al., 2019; Pinti, Castro, López-Hernández, Hernández, Shouakar-Stash, et al., 2019), CH_4, N_2, and hydrocarbons (Tolstikhin et al., 2017; Pujol et al., 2018; Kotarba et al., 2019; Li et al., 2020) in order to deduce the physical processes occurring in natural reservoirs.

In the context of nuclear waste management, noble gas characteristics can provide important information about the far-field environment surrounding a deep geological repository (DGR) and the potential for long-term isolation of radionuclides. Some studies that investigated stable isotopes in porewater, dissolved He and Cl^- transport in shale-dominated argillaceous aquitards, have concluded that the diffusional time scales are over million years (Hendry et al., 2015). Heavy noble gas (Ne, Ar, Kr and Xe) enrichments have been detected in a variety of shales since the 1980s (Podosek et al., 1980). The dating of very old porewater with an age of at least 6 million years old in sedimentary rock with radiogenic noble gases was conducted in Germany (Osenbrück et al., 1998). The first He diffusion coefficient profile in porewater of the whole clay formation was derived for the 180 million years old lower Dogger Opalinus clay, Mont Terri, Switzerland, with a minimum calculated in-situ helium accumulation age of ~ 9.1 million years (Rübel et al., 2002).

Here we discuss the results of noble gas studies undertaken in the Ordovician formations on the eastern flank of the Michigan Basin at a site considered for nuclear waste isolation. Site investigations were undertaken from August 2006 to June 2010 at the Bruce Nuclear Site (Kincardine, Ontario, Canada). An extensive dataset was collected and work on archived cores continues to date to enhance understanding of the basin evolution in southern Ontario and the

aquitard characteristics of these formations. In particular, noble gas measurements confirmed the accumulation of He in the confined Ordovician shale aquiclude for more than 260 million years (I. D. Clark et al., 2013; I. Clark et al., 2015). A subsequent study, based on compound-specific isotope analysis of biomarkers in the entire Ordovician succession at the same site, further confirmed the partitioning of this sedimentary column into two separated systems with the upper section of the Ordovician shale isolated since the Silurian, following the infiltration of evaporated Silurian seawater brine, while the underlying Ordovician limestone reached a confined state at some time after peak burial (Jautzy et al., 2018).

Drill cores were collected from the Ordovician sedimentary sequence of the Michigan Basin in southwest Ontario, Canada, as a part of site characterization activities undertaken between 2006 and 2010 (Intera Engineering Ltd.. 2011). Drill core samples were vacuum-sealed in laminated OPP/PE/Foil/PE Mil PRF-131K Class 1 vapor barrier Al foil bags following two full volume N_2 flushes, then stored at 4°C. Over time in storage, it was observed that many archived cores exhibited degassing into the foil bags, as manifested by a puffy condition rather than the initial vacuum-sealed appearance. This study and related CH_4 work undertook to sample gases from Ordovician shale and limestone core samples stored in foil bags, demonstrating that the laminated OPP/PE/Foil/PE foil bags are impermeable enough to retain all noble gases over the past decade (Jautzy et al., 2018). Compared with traditional noble gas out-diffusion metal containers, laminated OPP/PE/Foil/PE Al foil bags can significantly simplify the noble gas sampling and provide cost savings.

In this study, we not only measure He again with Al-bag sampling method, but also analyze heavy noble gases from the Ordovician rock. In addition, radioactive element (U, Th, K) concentrations were acquired from site characterization reports to calculate radiogenic noble gas production rates. U/Th-He and U-Xe ages re-determine the porewater and gas residence time within the Ordovician low-permeability rock, which provides additional support for the confining character of the Ordovician aquiclude and aquitard for both gas and liquid phases.

5.2 Materials and Methods

5.2.1 Ordovician Aquiclude and Black River Group Aquitard

The intracratonic Michigan basin, where the target strata locate, is nearly circular and centered on the lower peninsula of the state of Michigan, U.S.A (Figure 5.1). Its formation began with the late Precambrian mid-continental rifting and crustal extension (Van Schmus, 1992), followed by approximately 4800 m thick accumulation of sedimentary rock sequence in the center of the basin. In southwestern Ontario, Canada, the sedimentary sequence thickness decreases eastward to approximately 850 m at the Bruce Nuclear Site (Figure 5.1). The stratigraphy at the Bruce Nuclear Site from borehole bottom to ground surface comprises: Precambrian granitic gneiss; Cambrian sandstone; Ordovician siltstone and sandstone; Ordovician argillaceous limestone; Ordovician shale, Silurian dolostone, argillaceous dolostone, shale and evaporate; Devonian dolostone; Pleistocene surficial overburden deposits (Figure A3.1).

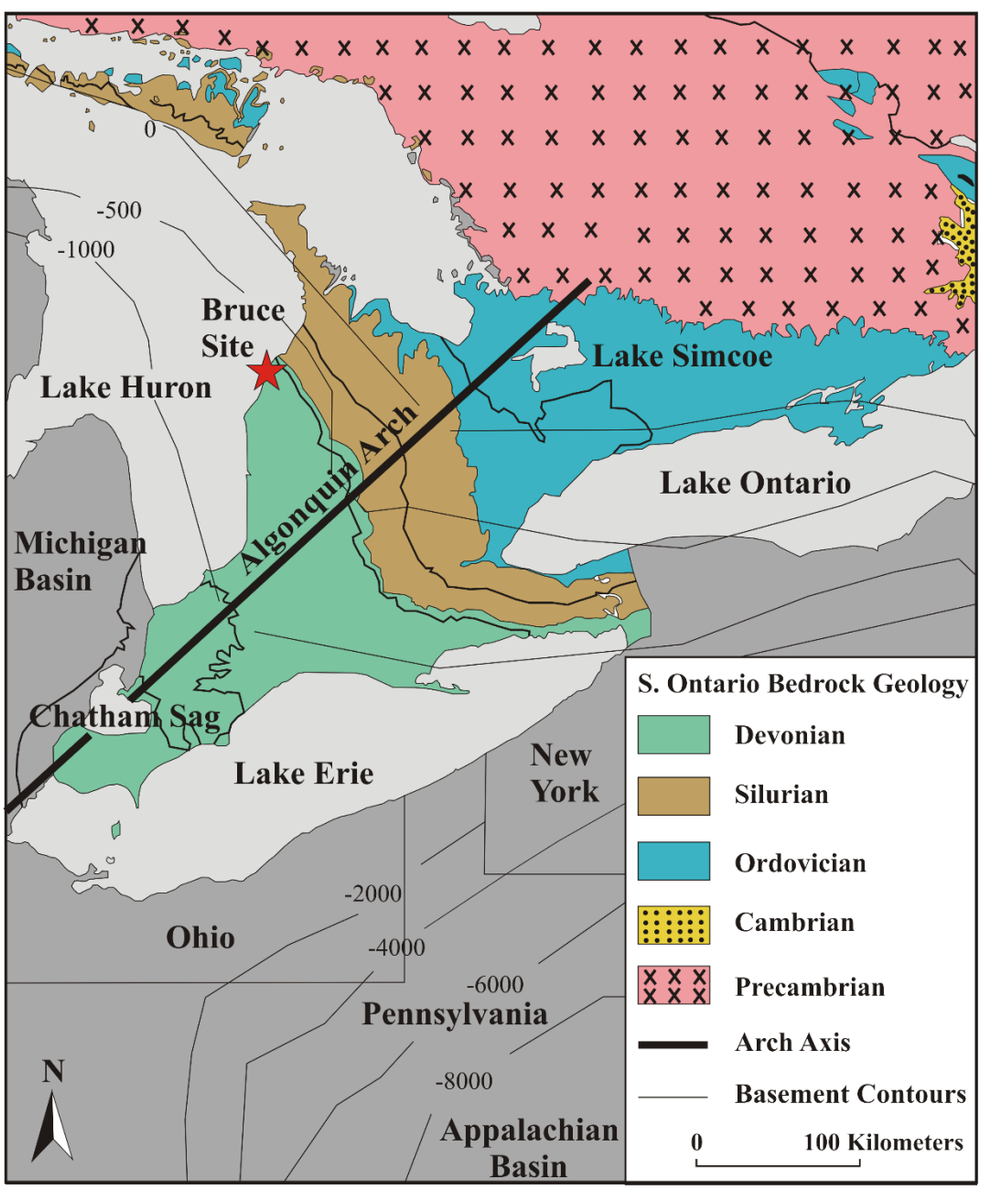

Figure 5.1 Map of southern Ontario showing the principal geological features and the location of the Bruce nuclear site (red solid star).

This study is focused on the Ordovician shale and limestone formations (Figure A3.1). The Queenston shale is both calcareous and dolomitized, particularly in the upper part (Intera Engineering Ltd.. 2011). Dolomite was also found in the Georgian Bay, Blue Mountain and Collingwood shales. Halite was frequently detected as fracture-infill and grain-boundary materials in the Ordovician shales (Intera Engineering Ltd.. 2011). The Ordovician shales have the largest content of clay (up to 70 wt %), while it is less than 20 wt % in the Ordovician limestones (Intera Engineering Ltd.. 2011).

The Ordovician shales, Cobourg and Sherman Fall argillaceous limestones are very sparsely fractured to unfractured (Intera Engineering Ltd.. 2011). The average estimates of horizontal hydraulic conductivity of the Ordovician shale and Cobourg, Sherman Fall and Kirkfield limestone formations range from 4×10^{-15} to 3×10^{-14} m/s, with vertical hydraulic conductivity approximately 10 times less than horizontal (Intera Engineering Ltd.. 2011). The overlying shale and limestone formations are classified as aquiclude. In the Coboconk, Gull River and Shadow Lake limestone formations (Black River Group), the average estimates of horizontal hydraulic conductivity range from 2×10^{-12} to 2×10^{-11} m/s, with vertical hydraulic conductivity potentially 10 to 1000 times less than horizontal hydraulic conductivity (Intera Engineering Ltd.. 2011). These limestone formations with smaller hydraulic conductivity are classified as aquitard.

5.2.2 Sampling

Six continuously cored boreholes were drilled from 2006 to 2010. All the core samples were vacuum-sealed in laminated OPP/PE/Foil/PE Mil PRF-131K Class 1 vapor barrier Al-foil bags following two full volume N_2 flushes and then stored at 4°C. At the moment of sampling (March 2017), gas out-diffusion had occurred to create headspace in the foil bags to allow sampling to proceed. Noble gas samples were collected with 3/8” refrigeration-grade annealed copper tubes using a custom-made and transportable vacuum line (Figure A3.2). The vertical depths of core samples from different drill boreholes were calibrated to the same datum (DGR 1/2), ranging from 508.93 to 852.7 mBGS. In addition, one passive Cu-tube diffusion sampler with duplicate was available from the Cambrian sandstone groundwater acquired in 2008. The working principle of diffusion sampler is described in detail by Aeschbach-Hertig and Solomon (Aeschbach-Hertig & Solomon, 2013). The sampling procedure of noble gases by diffusion sampler is elaborated in Text

A3.1.

5.2.3 Sample Analysis

Noble gas samples in Cu tubes were purified and separated using a multi-stage ultra-high vacuum processing line (Figure A3.3) in the Noble Gas and Tritium Laboratory at the University of Ottawa. Water vapor was removed with a U-shape polished stainless steel trap in an ethanol bath at 190 K. N_2, O_2, H_2, hydrocarbons and other active gases (e.g., CO, CO_2) were removed with two SAES ST 172 getters (Zr-V-Fe); one at room temperature (293 K) and the other at 573 K.

Following purification, noble gas separation was conducted with multiple stainless steel and activated charcoal finger traps (SSTs and ACTs in Figure A3.3) and a modified Advanced Research Systems (ARS) DE-204 cryocooler. Because of the high abundance of Ar in air standards and samples, the layered effect of Ar and Kr adsorption onto a charcoal finger is a common issue (Beyerle et al., 2000; Stanley et al., 2009; Mathouchanh & Aeschbach-Hertig, 2015). To solve this issue, we utilized two sequential polished stainless steel wool traps (SST1 and SST2 in Figure A3.3) at liquid N_2 temperature (77 K). Repeated air standard analysis yielded comparable sensitivity and steady ratios for Ar, Kr and Xe, demonstrating trapping > 95% Kr and > 99% Xe. After isolation of the stainless steel traps, Ar was isolated on two activated charcoal traps (ACT1 and ACT2 in Figure A3.3) immersed in liquid N_2 at 77K. Subsequently, He and Ne were drawn down on the ARS activated charcoal cryocooler at 5 K, and then individually released into the mass spectrometer at 30 K and 80 K. Subsequently, Kr and Xe were trapped onto the cryocooler at 125 K and then released into the mass spectrometer at 210 K and 325 K, respectively. The last step involved releasing Ar by heating the charcoal cold fingers (ACT1 and ACT2) and performing appropriate chops according to the spinning rotor vacuum gauge (SRG) reading for analysis. All noble gases were analyzed on the magnetic sector static vacuum Thermo Scientific Helix SFT mass spectrometer using a Faraday detector, except for ^3He, which was measured using an electron multiplier in ion counting mode.

5.3 Results and Discussion

5.3.1 Radioelement Concentrations and noble gas isotope ratio characteristics

Radioelement (U, Th, K) concentration results from previous work performed during site characterization activities at the Bruce Nuclear Site are summarized below (Figure 5.2) and the data sources are the Nuclear Waste Management Organization (NWMO) technical reports (Activation Laboratories Ltd.. ; SGS Laboratories., 2010a, 2010b). The noble gas isotopic ratio and concentration data performed in this study are presented in Table A2.1 and Table A2.2. Noble gas radiogenic ingrowth estimates have been calculated using these earlier elemental chemistry concentrations for the rock units and the noble gas data derived from this study.

U concentrations in the Ordovician rock samples range from 0.4 ppm to 4.2 ppm with lower concentrations measured in the limestones than in the shale formations (Figure 5.2). While a similar trend can be observed for Th, the concentrations are on average three times higher than the U concentrations (Figure 5.2). Th concentrations range from 1.1 ppm in the limestones to as high as 18 ppm in Blue Mountain shale samples. The concentrations of both U and Th in the Cambrian sandstone groundwater plot between the values measured in the Ordovician shale and limestone samples. K concentrations are represented in (wt %) in the rock, and are higher in the Ordovician shales relative to the limestones (as expected given the differences in mineral composition of these formations), with values between 4.7% and 0.53% (Figure 5.2). K is enriched in the Cambrian sandstone groundwater compared with those in limestone but is not as abundant as K concentrations in the Ordovician shale.

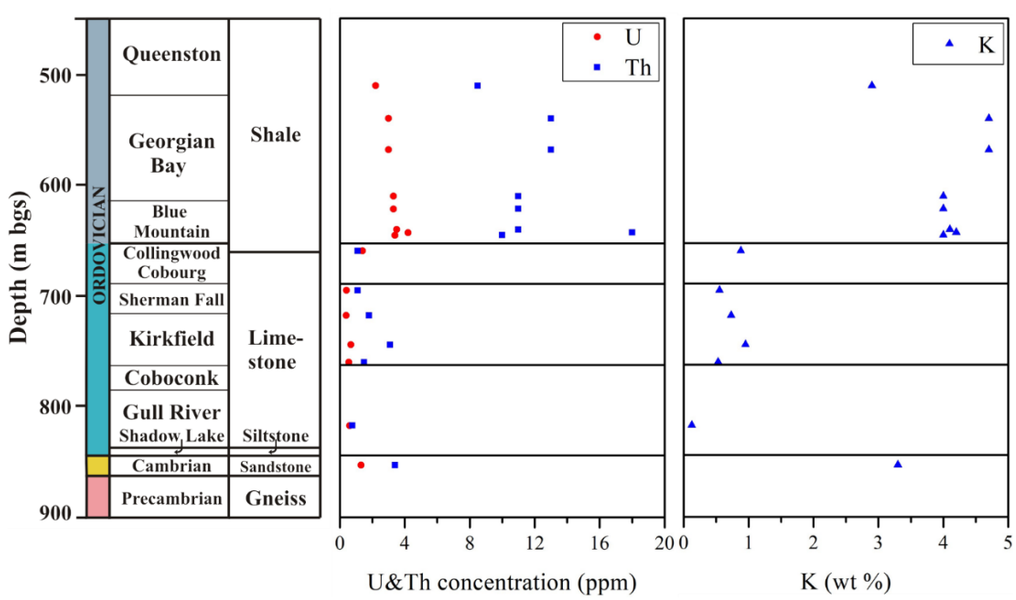

Figure 5.2 U, Th and K concentration vertical profile in the Ordovician and Cambrian rock samples.

Noble gas isotope ratios for the Ordovician rock out-diffusion gas samples and one Cambrian sandstone groundwater diffusion sampler (collected during site activities) are summarized in Table A2.1. He isotope ratios ($^3He/^4He$) in core samples are normalized to air [xRa = $(^3He/^4He)_{sample}$ /$(^3He/^4He)_{air}$; where $(^3He/^4He)_{air}$ is 1.399×10^{-6}] (Ozima & Podosek, 2002). The xRa is relatively uniform (0.02 Ra to 0.03 Ra) in the Ordovician shales, and shifts up to 0.05 Ra in the Ordovician limestones and then drops back to 0.022 Ra in the Cambrian sandstone groundwater (Figure 5.3). The shift in xRa occurs below the Ordovician shales near the interface between the Cobourg limestone and Sherman Fall limestone, in agreement with the He isotopic profile of step-heated subcores in the previous research (I. D. Clark et al., 2013). The air-normalized $^3He/^4He$ values in the Ordovician rock porewaters all fall within the typical crustal production range of 0.01-0.05 Ra(Oxburgh et al., 1986). This is in agreement with the measured (xRa = 0.020 to 0.035) and calculated authigenic He ratios of step-heated subcoresin the previous research at the same site (I. D. Clark et al., 2013). The $^4He/^{20}Ne$ ratios in the Ordovician formations also calculated from noble gas concentrations (Table A2.2), vary from 15.96±0.016 to 731.51±1.065, with higher values in the Ordovician shale samples. The maximum $^4He/^{20}Ne$ ratio of 1914.56±0.332 can be found in the Cambrian sandstone groundwater. Compared to the typical radiogenic production rate of ^4He in the crust (4.13×10^{-13} cm^3 STP/g year) (C. J. Ballentine & Burnard, 2002), the contribution from radiogenic ^{20}Ne (production rate =1.49×10^{-21} cm^3 STP/g year) (Leya & Wieler, 1999) is negligible. Therefore, the variation of $^4He/^{20}Ne$ values is deduced as a result of different (U+Th) concentrations in the formations, which are the producers of radiogenic ^4He. Compared with air saturated water (ASW) $^4He/^{20}Ne$ value at 18 °C [$(^4He/^{20}Ne)_{ASW}$=0.267] (Ozima & Podosek, 2002), it is obvious that He in the Ordovician and Cambrian strata is dominated by a crustal component.

Ne ratios ($^{20}Ne/^{22}Ne$) mostly distribute along the atmospheric value [$(^{20}Ne/^{22}Ne)_{air}$=9.8] (Ozima & Podosek, 2002) (Figure 5.3), with few exceptions which are within analytical error (±1σ). Due to the very high He concentrations in the gas samples (Table A2.2), Ne signals on the Faraday detector were consistently much lower, with larger analytical errors than those in air standards, and likely contributed to uncertainty in the Ne concentrations and Ne ratios.

Compared with the atmospheric Ar ratio 295.5 (Ozima & Podosek, 2002), the measured $^{40}Ar/^{36}Ar$ values demonstrate ^{40}Ar enrichment with an average value 307.6 in the Ordovician shales and limestones, with a minimum in Sherman Fall limestone (295.9±0.55) and maximum in Blue Mountain shale (343.6±0.90) (Table A2.1, Figure 5.3). However, Ar ratios in the Ordovician

rocks are much smaller than that in Cambrian groundwater. The relatively low excess ^{40}Ar in the Ordovician formations can likely be attributed to the limited release of radiogenic Ar to the porewaters. The weathering of K-bearing minerals has been confirmed as an important factor influencing Ar release (Andrews et al., 1989; Seltzer et al., 2021). This may due to minimal lattice damage given the weak energy of β decay compared with the release of ^{4}He from α decay of ^{238}U, and given the larger atomic radius of ^{40}Ar when compared to ^{4}He. This results in the preferential retention of radiogenic ^{40}Ar over ^{4}He in the clay minerals. This interpretation is supported by a heating experiment performed on one Blue Mountain shale sample that had been exposed to air for several years. The crushed shale sample was heated to 400 °C for 12 hours which is sufficient to release radiogenic ^{40}Ar from clay minerals (Grim & Bradley, 1940; Clauer et al., 2012). The resulting $^{40}Ar/^{36}Ar$ ratio from the heating experiment is 1366.5 (Table A2.1), showing minimal porewater out-diffusion at room temperature and demonstrating that most radiogenic ^{40}Ar is retained within clay minerals under such conditions. In contrast, the high radiogenic ^{40}Ar in the Cambrian sandstone groundwater ($^{40}Ar/^{36}Ar$=728.4) suggests allochthonous contributions from the underlying granitic shield.

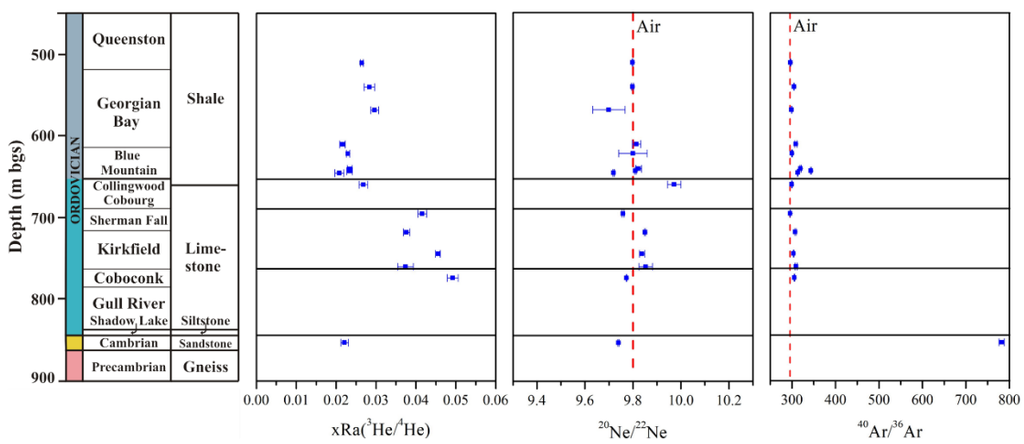

Figure 5.3 He, Ne and Ar isotope ratios (±1 σ uncertainties) in the Ordovician shale, limestone porewaters and Cambrian groundwater from the eastern flank of the Michigan Basin. He ratios ($^{3}He/^{4}He$) are normalized to atmospheric $^{3}He/^{4}He$ value [xRa = $(^{3}He/^{4}He)_{sample}/(^{3}He/^{4}He)_{air}$], where $(^{3}He/^{4}He)_{air}$ is 1.399×10^{-6}. $(^{20}Ne/^{22}Ne)_{air}$ and $(^{40}Ar/^{36}Ar)_{air}$ are 9.8 and 295.5, respectively (red dashed lines) (Ozima & Podosek, 2002).

Kr isotope ratios ($^{86}Kr/^{84}Kr$) are coincident with that of air (0.305) (Ozima & Podosek, 2002) throughout the Ordovician and Cambrian formations (Figure 5.4), and this can be due to the very low production rate of ^{86}Kr (2.74×10^{-22} cm^3 STP/g year) (C. J. Ballentine & Burnard, 2002) in the upper crust, which is even lower than ^{136}Xe production rate (1.79×10^{-21} cm^3 STP/g year) (C. J. Ballentine & Burnard, 2002). According to the production rates of radiogenic ^{86}Kr (2.74×10^{-22} cm^3 STP/g year) and ^{84}Kr (4.18×10^{-23} cm^3 STP/g year) (C. J. Ballentine & Burnard, 2002), 21 billion

years is needed to see 10% ingrowth (0.305 to 0.335) on the $^{86}Kr/^{84}Kr$ value of water in the upper crust. In contrast with Kr, fissionogenic ^{129}Xe and ^{136}Xe, normalized to atmospheric ^{130}Xe, present significant enrichments in the profile at the study site (Figure 5.4). In the Georgian Bay and Blue Mountain shales, gas samples show enrichments over atmospheric values for both $^{129}Xe/^{130}Xe$ and $^{136}Xe/^{130}Xe$. The maximum $^{129}Xe/^{130}Xe$, $^{136}Xe/^{130}Xe$ values are found in the Ordovician shale with ratios of 6.597±0.0255 and 2.245±0.0090, respectively, compared to atmospheric ratios of 6.496 and 2.176 (Ozima & Podosek, 2002). No evident Xe isotope ratio anomaly was detected in the Ordovician limestone formations. The second largest $^{136}Xe/^{130}Xe$ ratio was measured in the Cambrian sandstone groundwater, although with no pronounced ^{129}Xe ingrowth (Figure 5.4). The presence of fissiogenic ^{136}Xe has strong correlation with the concentration of parental element U in the Ordovician formations.

From the enrichments of radiogenic ^{4}He, ^{40}Ar and ^{136}Xe, we conclude that the noble gases may have been retained in the Ordovician shales and limestones for millions of years. The difference in radiogenic noble gas isotope ratios between the Ordovician sediments and the Cambrian sandstone supports previous conclusions regarding the isolation of the fluids from deep groundwater (I. D. Clark et al., 2013; Al et al., 2015; I. Clark et al., 2015). The results imply confinement of the sedimentary system over a large portion of the Phanerozoic eon, and the excess concentration of radiogenic radioisotopes should yield estimates of time since porewater isolation. Quantitative estimation of confinement is necessary for better understanding of the Ordovician aquiclude and aquitard hydrogeological properties.

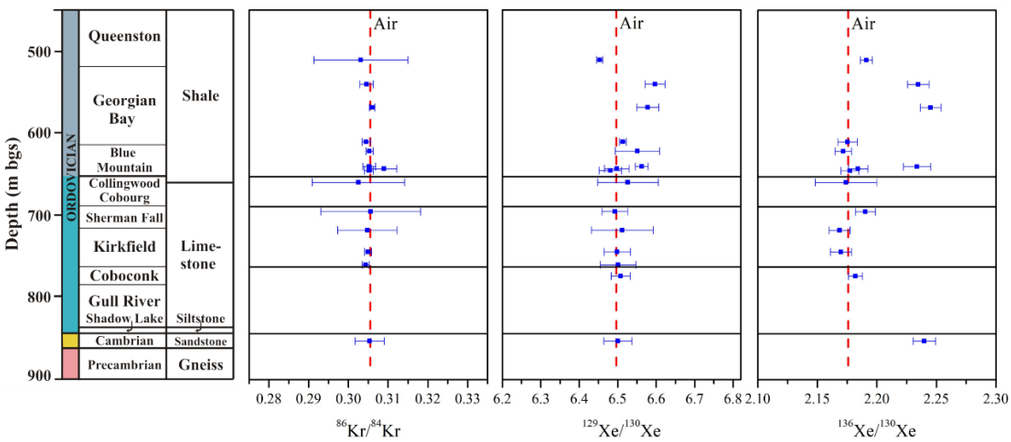

Figure 5.4 Kr and Xe isotope ratios (±1 σ uncertainties) in the Ordovician shale, limestone porewaters and Cambrian groundwater from the eastern flank of the Michigan Basin. $(^{86}Kr/^{84}kr)_{air}$, $(^{129}Xe/^{130}Xe)_{air}$ and $(^{136}Xe/^{130}Xe)_{air}$ are 0.305, 6.496 and 2.176, respectively (red dashed lines) (Ozima & Podosek, 2002).

5.3.2 Porewater residence time estimation

Noble gas concentrations in the drill core porewater were calculated from calibrated volumes of gas encapsulated in Cu tubes and are summarized in Table A2.2.

In this study, all the samples had undergone degassing over 10 years, supporting the total out-diffusion of all (mainly CH_4) gas from porewater in the rock. So the release factors of all noble gases from porewater are equal to 1.

The fractions of noble gases in the Cu tubes were then normalized to cc_{STP} gas diffused out per gram rock (cc_{STP}/g rock) with measured volumes of gas sampling system as shown in Figure A3.2. The weights of core samples were acquired from the logging records on the foil bags. This can be expressed as:

$$C_{rock}=\frac{C_i \times V_{sampling}}{M_{rock}} \tag{5.1}$$

Where C_{rock} is the volume of noble gas i diffused from 1 gram rock, also described as noble gas i concentration in unit mass rock, in cc_{STP}/g rock; C_i is the concentration of noble gas i in the Cu tube samples; $V_{sampling}$ is the total volume of the sampling system in cc; and M_{rock} is the weight of the rock sample in the foil bag, the unit is g.

The $^4He/^{20}Ne$ ratio (15.96 to 731.51) demonstrates that He in the Ordovician and Cambrian porewater is dominated by crustal production, which means atmospheric He contribution can be neglected. In contrast with He, without the obvious mantle-featured He and Ne ratios, it is concluded that heavy noble gas components degassed from the Ordovician sedimentary rock porewater are composed of two main end members: ancient atmospheric and crustal/radiogenic components. Radiogenic ^{136}Xe ($^{136}Xe^*$) is calculated as follows (C. Ballentine et al., 1991):

$$^{136}Xe^* = {}^{136}Xe_{measured} \times \left(1 - \left(\frac{^{136}Xe}{^{130}Xe}\right)_{air} \Big/ \left(\frac{^{136}Xe}{^{130}Xe}\right)_{measured}\right) \tag{5.2}$$

The radiogenic components are computed with the equations above and shown in Table A2.3. Based on parent radioisotope (U and Th) concentrations, the radiogenic production rate can be calculated. Then the radiogenic noble gas concentration per unit mass of rock is divided by production rate to derive an estimate of ingrowth time. Radiogenic ^4He from α-decay of actinides can yield an age estimate based on a production rate calculated from the concentration of U and Th in the host rock, according to:

$$^4He = 8\times\left[^{238}U\right]\times(e^{\lambda_{238}t}-1)+7\times\left[^{235}U\right]\times(e^{\lambda_{235}t}-1)+6\times\left[^{232}Th\right]\times(e^{\lambda_{232}t}-1) \tag{5.3}$$

Where ^{4}He is the radiogenic ^{4}He concentration that would be produced within a rock over time, t; [^{238}U], [^{235}U], [^{232}Th] are concentrations in ppm of the parent elements; λ_{238}, λ_{235}, λ_{232} are the decay constants for the three radioisotopes, 1.55×10^{-10} yr^{-1}, 9.85×10^{-10} yr^{-1} and 4.95×10^{-11} yr^{-1}, respectively (Faure & Mensing, 2004; Yoshioka et al., 2005).

The U-Xe age is calculated using the following equation (Eikenberg et al., 1993):

$$t_{(U-Xe)}=\frac{1}{\lambda_{\alpha}+\lambda_{sf}}\ln\left[\frac{^{136}Xe_{sf}\times\left(\lambda_{\alpha}+\lambda_{sf}\right)}{^{238}U\times Y_{sf}\times\lambda_{sf}}+1\right] \quad (5.4)$$

Where λ_{α} is the α-decay constant of ^{238}U which is 1.55×10^{-10} yr^{-1} (Yoshioka et al., 2005); λ_{sf} is the ^{238}U spontaneous fission decay constant that is 8.51×10^{-17} yr^{-1} (Yoshioka et al., 2005); Y_{sf} is the mass yield of ^{136}Xe from ^{238}U spontaneous fission, which is 6.3% (Young & Thode, 1960); and $^{136}Xe_{sf}$ is the concentration of fissionogenic ^{136}Xe.

The related parameters and calculation for U/Th-He and U-Xe noble gas dating are summarized in Table A2.3. To accurately normalize the noble gas concentration to per gram rock, only the fully extracted samples were selected for age calculation. Six fully extracted samples were chosen for U/Th-He age calculation, and two samples were used for U-Xe age calculation. The errors on U/Th-He and U-Xe ages are derived uniquely from uncertainty in the noble gas analysis on the mass spectrometer and do not consider sampling uncertainties, which should be considered to be on the order of a few percent. The minimum porewater residence time is constrained by the in-situ radiogenic ^{4}He production rate. Atmospheric He inherited from the infiltrated brines in the shales is insignificant. The porewater residence time is calculated by using measured ^{4}He (Table A2.2) divided by the ^{4}He production rate (Equation 5.3). In the low-permeability Ordovician shales and limestones, the estimate for porewater residence time with ^{4}He is 246±0.184 m.y. (Table A2.3). The ^{136}Xe ingrowth is only detected in Ordovician shale formations, which means the U-Xe dating method can only be applied to the Ordovician shale. The calculated U-Xe age is 255±1.07 m.y. (Table A2.3), giving a close estimation of porewater residence time to the U/Th-He method. All the porewater residence time estimations determined in this study are remarkably close to the 260 m.y. He accumulation time proposed previously (I. D. Clark et al., 2013).

5.3.3 Conclusions

In this study we measured noble gas isotope ratios and concentrations from low-permeability Ordovician sedimentary rocks from the eastern flank of the Michigan Basin to contribute to

investigations of these formations as barriers for nuclear waste isolation. Overall, three main conclusions can be made:

a. Measured noble gas isotopic ratios show enrichments in ^{4}He, ^{40}Ar and ^{136}Xe relative to their atmospheric components. In contrast to the crust-mantle dominated noble gas features from the western flank of the Michigan Basin (Castro et al., 2009; Ma et al., 2009), He isotopic ratios (0.02-0.05 Ra) from our study site show only crustal dominated noble gas features. Ar isotope ratios show only minor enrichments in the Ordovician aquiclude and aquitard, due to the retention of radiogenic ^{40}Ar by clay minerals. Xe ingrowth is only measurable in the Georgian Bay and Blue Mountain U-enriched shales.

b. The noble gas isotopic ratio anomalies in the Ordovician aquiclude and aquitard clearly reveal the accumulation of radiogenic noble gases in a confined environment. Further, the distinction in the measured ratios between the Ordovician shale aquiclude and the underlying limestone aquitard and the Cambrian sandstone groundwater indicates a lack of exchange between these gas and fluid reservoirs.

c. The concordance of age estimates for the two different radiogenic systems is encouraging and provides an average mean residence time of some 250 m.y. (U/Th-He: 246±0.184 m.y. and U-Xe: 255±1.07 m.y.), in agreement with the estimation of 260 m.y. from a previous He study at the same study site (I. D. Clark et al., 2013).

In summary, this study provides a new method to estimate porewater residence time using fissiogenic^{136}Xe in a closed system. In addition, an economic and efficient noble gas capsulation method for rock out-diffusion gases is verified by using well-sealed vapor-barrier Al-foil bags which maintain integrity for more than 7 years. The U-^{136}Xe age estimate supports our ^{4}He age determinations, demonstrating the very high integrity of these formations as barriers to fluid flow and the isolation of nuclear waste.

Acknowledgments

We thank Laura Kennell-Morrison (NWMO) and Dylan Luhowy (NWMO) for their help and coordination in advance of and during sampling, ensuring the samples could be successfully collected for this and related work. Great appreciation for Shilong Liu (Zhejiang University) for his help with the improvement of figure aesthetics. This work was supported by the Nuclear Waste Management Organization (NWMO), Toronto, Canada. Part of the research described in this paper was performed at the AEL-AMS laboratory, a national research facility hosted at the University of Ottawa, which is supported by the Canada Foundation for Innovation (CFI), the Major Science Initiatives (MSI), and the University of Ottawa. Acknowledgment to China Scholarship Council (CSC) for the financial support on Ende Zuo's Ph.D. project (No. 201606170089).

References

Activation Laboratories Ltd.. Geochemical and SEM/EDS Analysis of DGR-1 and DGR-2 Core: Ancaster, Ontario, Canada.

Aeschbach-Hertig, W., & Solomon, D. K. (2013). Noble gas thermometry in groundwater hydrology. *The noble gases as geochemical tracers*, 81-122.

Al, T. A., Clark, I. D., Kennell, L., Jensen, M., & Raven, K. G. (2015). Geochemical evolution and residence time of porewater in low-permeability rocks of the Michigan Basin, Southwest Ontario. *Chemical Geology, 404*, 1-17.

Andrews, J., Hussain, N., & Youngman, M. (1989). Atmospheric and radiogenic gases in groundwaters from the Stripa granite. *Geochimica et cosmochimica acta, 53*(8), 1831-1841.

Ballentine, C., O'nions, R., Oxburgh, E., Horvath, F., & Deak, J. (1991). Rare gas constraints on hydrocarbon accumulation, crustal degassing and groundwater flow in the Pannonian Basin. *Earth and Planetary Science Letters, 105*(1-3), 229-246.

Ballentine, C. J., Burgess, R., & Marty, B. (2002). Tracing fluid origin, transport and interaction in the crust. *Reviews in Mineralogy and geochemistry, 47*(1), 539-614.

Ballentine, C. J., & Burnard, P. G. (2002). Production, release and transport of noble gases in the continental crust. *Reviews in Mineralogy and geochemistry, 47*(1), 481-538.

Beyerle, U., Aeschbach-Hertig, W., Imboden, D. M., Baur, H., Graf, T., & Kipfer, R. (2000). A mass spectrometric system for the analysis of noble gases and tritium from water samples. *Environmental Science & Technology, 34*(10), 2042-2050.

Castro, M. C., Ma, L., & Hall, C. M. (2009). A primordial, solar He-Ne signature in crustal fluids of a stable continental region. *Earth and Planetary Science Letters, 279*(3-4), 174-184.

Clark, I., Ilin, D., Jackson, R., Jensen, M., Kennell, L., Mohammadzadeh, H., . . . Raven, K. (2015). Paleozoic-aged microbial methane in an Ordovician shale and carbonate aquiclude of the Michigan Basin, southwestern Ontario. *Organic Geochemistry, 83*, 118-126.

Clark, I. D., Al, T., Jensen, M., Kennell, L., Mazurek, M., Mohapatra, R., & Raven, K. (2013). Paleozoic-aged brine and authigenic helium preserved in an Ordovician shale aquiclude. *Geology, 41*(9), 951-954.

Clauer, N., Zwingmann, H., Liewig, N., & Wendling, R. (2012). Comparative 40Ar/39Ar and K–Ar dating of illite-type clay minerals: A tentative explanation for age identities and differences. *Earth-Science Reviews, 115*(1-2), 76-96.

Eikenberg, J., Signer, P., & Wieler, R. (1993). U-Xe, U-Kr, and U-Pb systematics for dating uranium minerals and investigations of the production of nucleogenic neon and argon. *Geochimica et cosmochimica acta, 57*(5), 1053-1069.

Faure, G., & Mensing, T. M. (2004). *Isotopes: Principles and Applications, 3rd Edition*.

Grim, R. E., & Bradley, W. F. (1940). Investigation of the effect of heat on the clay minerals illite and montmorillonite. *Journal of the American Ceramic Society, 23*(8), 242-248.

Hendry, M., Solomon, D., Person, M., Wassenaar, L., Gardner, W., Clark, I., . . . Hasegawa, T. (2015). Can argillaceous formations isolate nuclear waste? Insights from isotopic, noble gas, and geochemical profiles. *Geofluids, 15*(3), 381-386.

Intera Engineering Ltd.. (2011). Descriptive Geosphere Site Model. In Intera Engineering Ltd. (Ed.): Toronto, Ontario, Canada.

Jautzy, J. J., Ahad, J. M., Jensen, M., & Clark, I. D. (2018). Molecular and isotopic evaluation of the maturation history of the organic matter in an Ordovician aquiclude (Michigan Basin): Evidence for late diagenetic biodegradation. *Organic Geochemistry, 125*, 129-141.

Kotarba, M. J., Sumino, H., & Nagao, K. (2019). Origin of hydrocarbon and noble gases, carbon dioxide and molecular nitrogen in Devonian, Pennsylvanian and Miocene strata of the Polish Lublin and Ukrainian Lviv basins, southern part of the Upper Silesian Coal Basin and western part of the Carpathian Foredeep (Poland). *Applied Geochemistry, 108*, 104371.

Leya, I., & Wieler, R. (1999). Nucleogenic production of Ne isotopes in Earth's crust and upper mantle induced by alpha particles from the decay of U and Th. *Journal of Geophysical Research: Solid Earth, 104*(B7), 15439-15450.

Li, Y., Qin, S., Wang, Y., Holland, G., & Zhou, Z. (2020). Tracing interaction between hydrocarbon and groundwater systems with isotope signatures preserved in the Anyue gas field, central Sichuan Basin, China. *Geochimica et cosmochimica acta, 274*, 261-285.

Ma, L., Castro, M. C., & Hall, C. M. (2009). Crustal noble gases in deep brines as natural tracers of vertical transport processes in the Michigan Basin. *Geochemistry Geophysics Geosystems, 10*.

Mathouchanh, E., & Aeschbach-Hertig, W. (2015). *Krypton separation from argon for Atom Trap Trace Analysis of 85 Kr and 81 Kr.* MSc Thesis, University Paris SUD, France and University of Heidelberg, Germany.

Osenbrück, K., Lippmann, J., & Sonntag, C. (1998). Dating very old pore waters in impermeable

rocks by noble gas isotopes. *Geochimica et cosmochimica acta, 62*(18), 3041-3045.

Oxburgh, E., O'nions, R., & Hill, R. (1986). Helium isotopes in sedimentary basins. *Nature, 324*(6098), 632-635.

Ozima, M., & Podosek, F. A. (2002). *Noble gas geochemistry*: Cambridge University Press.

Pinti, D. L., Castro, M. C., López-Hernández, A., Hernández, M. A. H., Richard, L., Hall, C. M., . . . Rodríguez-Rodríguez, M. H. (2019). Cerro Prieto geothermal field (Baja California, Mexico)–a fossil system? Insights from a noble gas study. *Journal of Volcanology and Geothermal Research, 371*, 32-45.

Pinti, D. L., Castro, M. C., López-Hernández, A., Hernández, M. A. H., Shouakar-Stash, O., Richard, L., . . . Ramírez-Montes, M. (2019). Signature of ongoing brine reinjection on noble gas isotopes and fluid chemistry at Las Tres Vírgenes geothermal field, Mexico. *Journal of Volcanology and Geothermal Research, 377*, 33-42.

Podosek, F., Honda, M., & Ozima, M. (1980). Sedimentary noble gases. *Geochimica et cosmochimica acta, 44*(11), 1875-1884.

Pujol, M., Van den Boorn, S., Bourdon, B., Brennwald, M., & Kipfer, R. (2018). Physical processes occurring in tight gas reservoirs from Western Canadian Sedimentary Basin: Noble gas signature. *Chemical Geology, 480*, 128-138.

Rübel, A. P., Sonntag, C., Lippmann, J., Pearson, F., & Gautschi, A. (2002). Solute transport in formations of very low permeability: Profiles of stable isotope and dissolved noble gas contents of pore water in the Opalinus Clay, Mont Terri, Switzerland. *Geochimica et cosmochimica acta, 66*(8), 1311-1321.

Seltzer, A. M., Krantz, J. A., Ng, J., Danskin, W. R., Bekaert, D. V., Barry, P. H., . . . Severinghaus, J. P. (2021). The triple argon isotope composition of groundwater on ten-thousand-year timescales. *Chemical Geology, 583*, 120458.

SGS Laboratories. (2010a). Mineralogy and Geochemistry of DGR-3 Core: Mississauga, Ontario, Canada.

SGS Laboratories. (2010b). Mineralogy and Geochemistry of DGR-4 Core: Mississauga, Ontario, Canada.

Stanley, R. H. R., Baschek, B., Lott III, D. E., & Jenkins, W. J. (2009). A new automated method for measuring noble gases and their isotopic ratios in water samples. *Geochemistry, Geophysics, Geosystems, 10*(5). doi: 10.1029/2009gc002429

Tolstikhin, I. N., Ballentine, C. J., Polyak, B. G., Prasolov, E. M., & Kikvadze, O. E. (2017). The noble gas isotope record of hydrocarbon field formation time scales. *Chemical Geology, 471*, 141-152.

Van Schmus, W. (1992). Tectonic setting of the Midcontinent Rift system. *Tectonophysics, 213*(1-2), 1-15.

Wen, T., Castro, M. C., Ellis, B. R., Hall, C. M., & Lohmann, K. C. (2015). Assessing compositional variability and migration of natural gas in the Antrim Shale in the Michigan Basin using noble gas geochemistry. *Chemical Geology, 417*, 356-370.

Wen, T., Castro, M. C., Nicot, J. P., Hall, C. M., Larson, T., Mickler, P., & Darvari, R. (2016). Methane Sources and Migration Mechanisms in Shallow Groundwaters in Parker and Hood Counties, Texas-A Heavy Noble Gas Analysis. *Environmental Science & Technology, 50*(21), 12012-12021.

Yoshioka, T., Tsuruta, T., Iwano, H., & Danhara, T. (2005). Spontaneous fission decay constant of 238U determined by SSNTD method using CR-39 and DAP plates. *Nuclear Instruments and Methods in Physics Research Section A: Accelerators, Spectrometers, Detectors and Associated Equipment, 555*(1-2), 386-395.

Young, B. G., & Thode, H. (1960). Absolute yields of the xenon and krypton isotopes in U238 spontaneous fission. *Canadian Journal of Physics, 38*(1), 1-9.

For Table of Contents Only (Abstract Art)

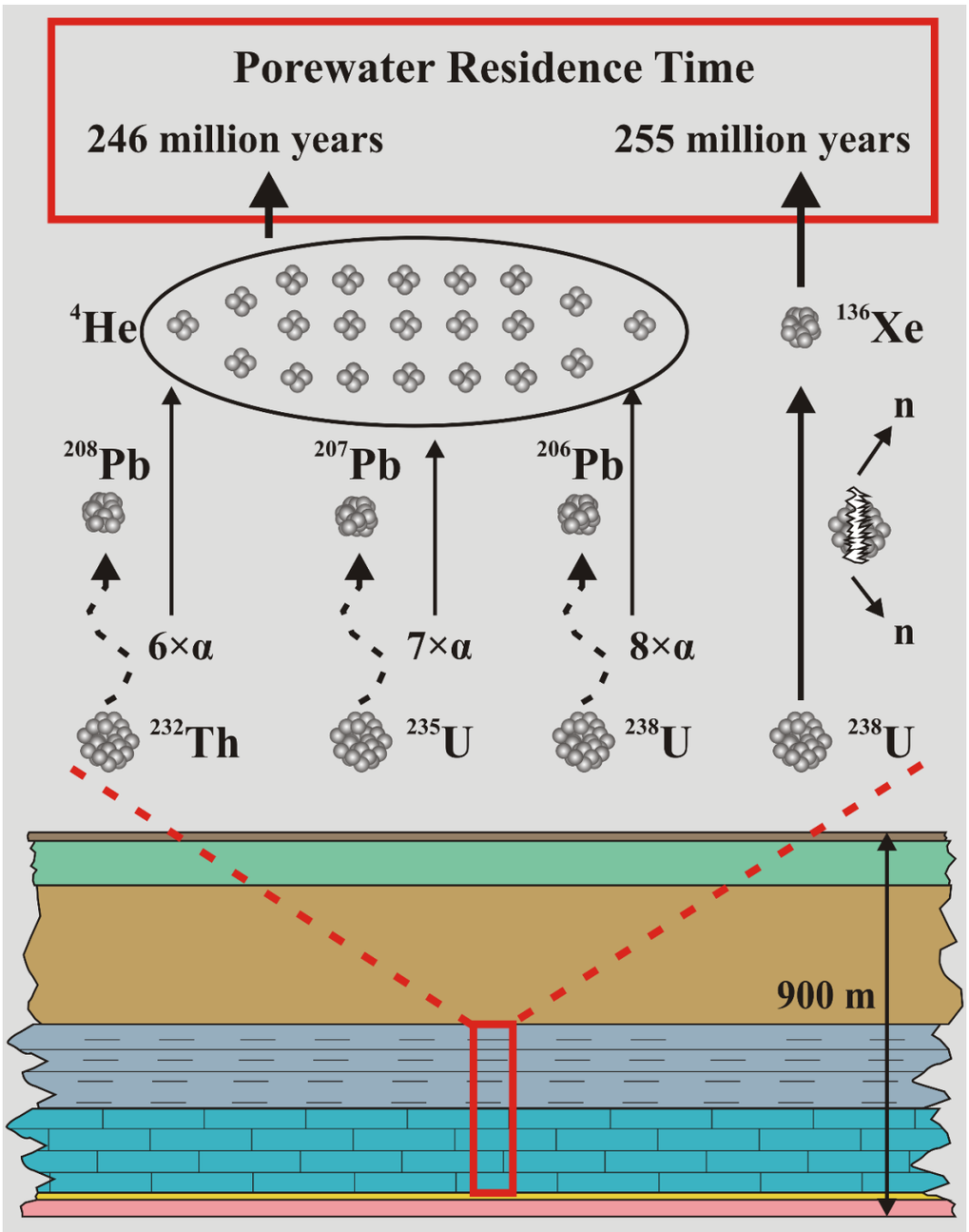

Chapter 6 Summary and Prospect

6.1 Summary

This thesis has been dedicated to the building of noble gas processing and analysis line, noble gas methodology development and applications of noble gases in crystalline and sedimentary rock porewaters.

From air standard measurements, the noble gas processing line gives steady and consistent noble gas sensitivities and isotope ratios. The noble gas sensitivity data verify the reproducibility and robustness of the procedure and processing line. All precisions of noble gas isotope ratios are less than 1% except for He ratio which is less than 1.4%. The performance parameters such as precision of noble gas isotope ratios of the processing line are comparable with other labs around the world.

In this thesis, the iterative trapping method using polished stainless steel wool achieves better than 95% Kr trapping efficiency. This iterative Kr trapping method not only provides two freeze-thaw thermal cycles for Ar-Kr separation but also keeps Ar away from the custom-made ARS activated charcoal coldhead In addition, compared with processing lines in other labs, the analysis time is 4.5 hours which is comparable to the time reported in the literatures (Stanley et al., 2009). The remnant magnetism on pole pieces of Helix SFT after heavy noble gas analysis is resolved with an inversed tuning protocol.

The extraction of noble gases from crystalline porewater is difficult because of the low porosity of crystalline rock and potential contributions from fluid inclusions and minerals. Porewater stable isotopes and noble gases were applied to trace resaturation and porewater extraction processes. The crystalline rock porewater was extracted with the vacuum-distillation method at 150 ℃. Results suggest negligible fractionation occurred on ^{2}H and ^{18}O during the vacuum distillation extraction process. He and Ne isotopic ratios were identical between the headspace gas and rock porewater, which demonstrates reliability of the vacuum-distillation extraction method. The extraction temperature was appropriate to volatilize porewater including noble gases without disturbing the radiogenic components in minerals.

Our noble gas method was also applied to archived Ordovician sedimentary aquitards. The vacuum out-diffusion method was used to extract porewater noble gases in archived cores from Ordovician shale aquiclude and limestone aquitard which have been sealed in Al-foil bags for 7 years. This is the first time to use Al-foil bags as long-term containers for noble gas storage. This

attempt gives an economic and effective way to strip noble gases from sedimentary rock porewater. More importantly, crustal noble gas features and geogenic noble gas components (^{4}He*, ^{40}Ar*, ^{136}Xe*) were found from the sedimentary aquitards. Xe geogenic ingrowth is only measurable in the U-enriched shales. This study complements and furthers previous noble gas work at the same field site by utilizing both He and Xe geogenic ingrowth to calculate the Ordovician porewater residence time. The concordance of age estimates for the two different radiogenic systems provides an average residence time of some 250 m.y. (U/Th-He: 246 ±0.184 m.y. and U-Xe: 255 ±1.07 m.y.), in agreement with the estimation of 260 m.y. from a previous He study at the same study site (Clark et al., 2013). The distinction in the measured ratios between the Ordovician shale aquiclude and the underlying limestone aquitard and the Cambrian sandstone groundwater indicates a lack of mass exchange between these gas and fluid reservoirs. Most importantly, this provides a new geochronometer ^{136}Xe that is useful for estimating porewater residence time in aquitards.

6.2 Prospect

Noble gas isotopes are becoming more and more important in the study of groundwater interactions of the geospheres. The mass exchange among spheres comprises complicated processes. The improvement of the analysis techniques and methodology therefore advances this knowledge.

As demonstrated in this thesis, the noble gas processing line and noble gas procedure have been applied in geologic research. Some aspects of the processing line are found to still need improvement. The first concern is the compositions of the gas samples, as the sedimentary rock samples are enriched in hydrocarbons which are harmful to the SEAS getters. An extra hydrocarbon getter is necessary to remove most of the hydrocarbons before the gas is introduced into the SEAS getters. Secondly, 95% trapping efficiency for Kr is a remarkable achievement with limited material, but the more Kr the better for Kr isotopic ratios, especially for ^{78}Kr and ^{80}Kr. A processing line with both stainless steel coldhead and activated charcoal coldhead will give better Kr trapping efficiency.

Despite the successful noble gas analysis on the Helix SFT by peak jumping, a multi-collector noble gas spectrometer is a better choice to run heavy noble gases. For instance, Kr has 6 isotopes and Xe has 9 isotopes which will make their measurements and data integration time much longer relative to He, Ne and Ar. The longer data collection time will result in a larger analytical error and interfere with the extrapolation for the measured noble gas intensity. A multi-collector noble gas mass spectrometer is a better selection for heavy noble gas measurements. In our lab, a Helix MC Plus is functional with a new noble gas processing line. Without the peak jumping, it is helpful to attain more steady heavy noble gas sensitivities and isotopic ratios.

The new geochronometer ^{136}Xe provides new information on sedimentary aquitards and deep geological repository selection for nuclear waste. One of the main parts of our future work is to make the ^{238}U—^{136}Xe dating method more routine.

With the more powerful processing line and multi-collector noble gas mass spectrometer, we plan to run more sedimentary and crystalline rock samples, including new sedimentary rock samples that have been collected from new boreholes at the South Bruce field site.

References

Clark, I. D., Al, T., Jensen, M., Kennell, L., Mazurek, M., Mohapatra, R., & Raven, K. (2013). Paleozoic-aged brine and authigenic helium preserved in an Ordovician shale aquiclude. *Geology, 41*(9), 951-954.

Stanley, R. H. R., Baschek, B., Lott III, D. E., & Jenkins, W. J. (2009). A new automated method for measuring noble gases and their isotopic ratios in water samples. *Geochemistry, Geophysics, Geosystems, 10*(5). doi: 10.1029/2009gc002429

Appendices

Appendix 1 Supporting Information for Chapter 3

Text A1.1 Tuning protocol for removing remnant magnetism after heavier noble gas measurements on the Helix SFT

The following tests show that the pole pieces remain magnetised even after 2 hours, the ^{3}He-^{4}He coincidence scans hold. A mass jump test to Argon and back to Helium at the end also show obvious change in coincidence scans. This confirms that magnetising the pole pieces before any helium mass calibration is done will allow the long term run of helium alone as well as He-Ne analysis in the same sample run. This is true providing the system is kept at a higher mass (Ne or Ar) when it is idle and the user jumps to a higher mass once in a while to keep the pole pieces magnetised.

1. In the beginning, conduct He mass calibration and ^{3}He-^{4}He coincidence scan with HD.

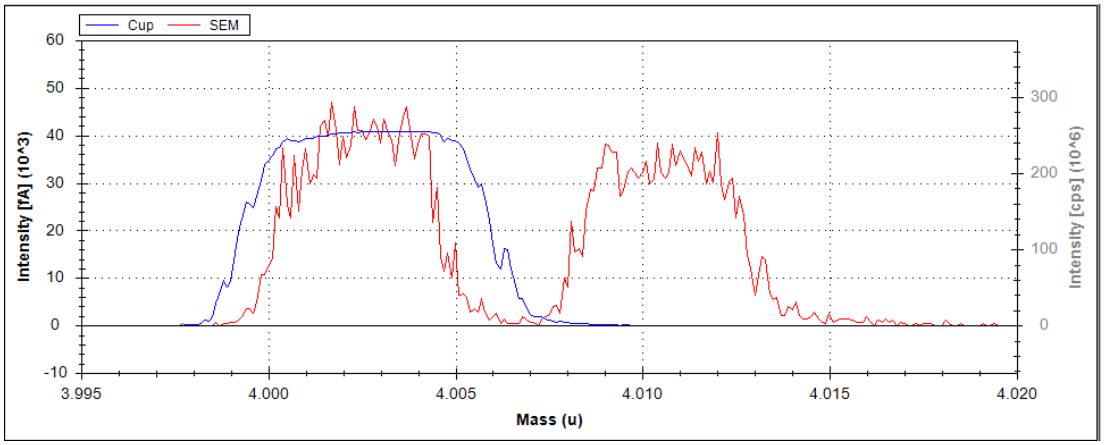

2. Switched to Ne configuration for 5 minutes.

3. **Time = 0 min:** Switched back to He configuration, ^{3}He-^{4}He coincidence scan. He peaks significantly shift to smaller mass.

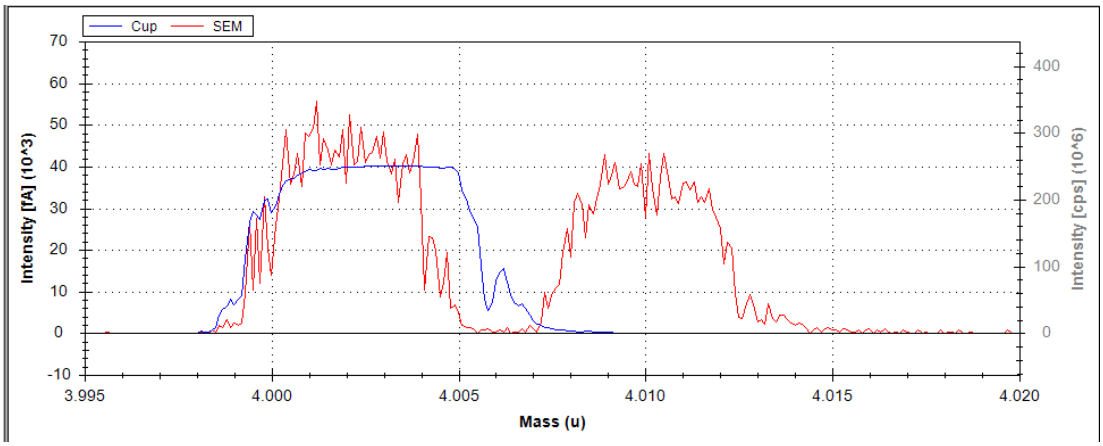

4. **Time = 165 min:** Switched to Ne configuration.

5. **Time = 185 min:** New air aliquot is injected into the SFT. Switched to He configuration

6. **Time = 190 min:** ^{3}He-^{4}He coincidence scan.

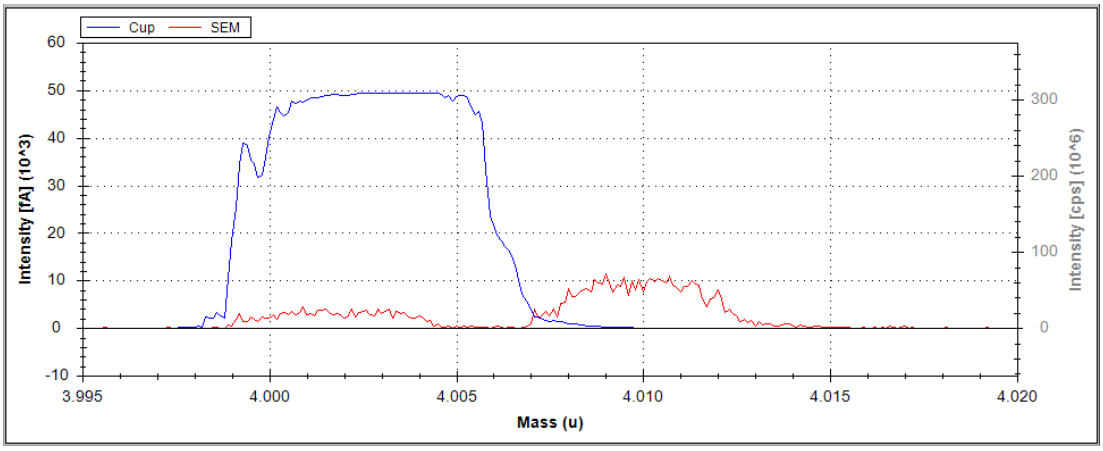

7. **Time = 195 min:** Switched to Ar configuration

8. **Time = 210 min:** Switched back to He configuration. ^{3}He-^{4}He coincidence scan. A prominent peak position return happened after switched to Ar configuration.

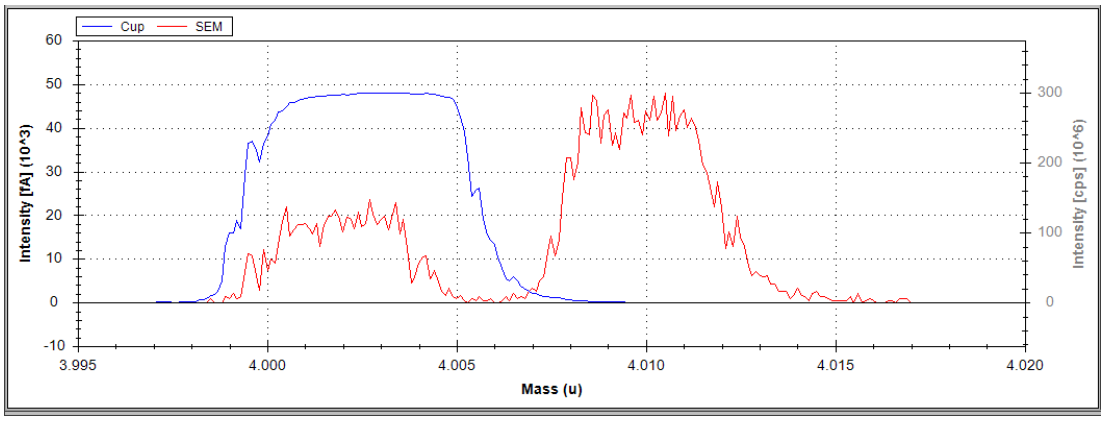
Cup
SEM
Intensity [fA] (10^3)
Intensity [cps] (10^6)
Mass (u)
60
50
40
30
20
10
0
-10
300
200
100
0
3.995
4.000
4.005
4.010
4.015
4.020

Table A1.1 He-Ne and Kr-Xe releasing profile with temperature of the modified ARS cryostat

Temperature (K)	^{4}He	^{20}Ne	Temperature (K)	^{84}Kr	^{132}Xe
	(%) Released			(%) Released	
10	0.00	0.00	100	0.01	0.01
12	0.13	0.00	105	0.01	0.01
14	4.52	0.00	110	0.04	0.01
16	40.88	0.00	115	0.39	0.01
18	82.09	0.00	120	1.92	0.01
20	93.89	0.00	125	4.34	0.01
22	98.21	0.01	130	6.80	0.01
24	99.96	0.02	140	13.82	0.01
26	100.00	0.05	150	23.05	0.34
28	99.67	0.15	160	37.53	0.34
30	98.47	0.87	170	52.80	0.84
35		26.82	180	69.64	0.84
40		83.78	190	86.19	1.13
42		93.32	195	91.78	1.43
44		97.05	200	94.83	1.92
46		98.61	205	97.72	2.52
48		99.42	210	100.00	3.94
50		99.72	212	99.96	5.07
55		100.00	214		6.16
58		99.79	216		7.53
60		99.23	218		9.78
			220		12.09
			230		20.37
			240		34.41
			250		56.97
			260		82.44
			265		95.17
			270		100.00
			272		99.31

Table A1.2 ^{20}Ne and ^{40}Ar signal intensity released together with Kr at Kr releasing temperature of the ARS cryostat.

Analysis Number	^{20}Ne released with Kr (fA)	^{40}Ar released with Kr (fA)
1	1371.30	3941.00
2	3583.00	11052.00
3	1627.00	4590.00
4	3222.00	10412.00
5	3187.00	9576.00
6	3167.00	9395.00
7	2446.00	9144.00
8	3493.00	11313.00
9	3199.00	9945.00
10	1375.00	5678.00
11	1216.57	4029.00
12	2119.45	8210.00
13	2264.13	8549.32
14	2169.80	6044.00
15	2561.00	6984.00

Table A1.3 Noble gas sensitivities from measurements on the Helix SFT mass spectrometer.

Analysis No.	Sensitivity (A/Torr)				
	He	Ne	Ar	Kr	Xe
1	1.80E-04	9.00E-05	2.59E-04	4.74E-04	1.02E-03
2	1.73E-04	8.18E-05	2.31E-04	4.53E-04	1.02E-03
3	1.77E-04	1.07E-04	2.44E-04	5.07E-04	1.03E-03
4	1.67E-04	1.10E-04	2.26E-04	5.25E-04	1.00E-03
5	1.71E-04	1.11E-04	2.37E-04	5.13E-04	9.72E-04
6	1.67E-04	9.77E-05	2.31E-04	4.92E-04	1.02E-03
7	1.79E-04	1.01E-04	2.31E-04	4.76E-04	9.74E-04
8	1.78E-04	1.00E-04	2.28E-04	5.35E-04	9.81E-04
9	1.82E-04	1.07E-04	2.18E-04	5.21E-04	1.01E-03
10	1.72E-04	1.02E-04	2.34E-04	4.97E-04	1.07E-03
11	1.79E-04	1.05E-04	2.26E-04	5.10E-04	1.05E-03
12	1.75E-04	1.05E-04	2.28E-04	5.37E-04	1.05E-03
13	1.79E-04	9.04E-05	2.08E-04	4.90E-04	1.04E-03
14	1.70E-04	9.17E-05	2.08E-04	5.25E-04	1.06E-03
15	1.60E-04	8.55E-05	2.42E-04	5.55E-04	1.01E-03
16	1.61E-04	8.99E-05	2.16E-04	5.10E-04	9.95E-04
17	1.60E-04	9.37E-05	2.26E-04	5.33E-04	9.78E-04
18	1.81E-04	1.00E-04	2.19E-04	5.00E-04	9.97E-04
19	1.73E-04	9.66E-05	2.27E-04	5.15E-04	1.03E-03
20	1.61E-04	9.41E-05	2.11E-04	5.14E-04	9.72E-04
Average	1.72E-04	9.79E-05	2.28E-04	5.09E-04	1.01E-03
STDEV	7.51E-06	8.14E-06	1.26E-05	2.42E-05	3.04E-05

Table A1.4 He signal intensities and isotopic ratios from measurements on Helix SFT

Analysis No.	^{3}He (fA)	STDEV	^{4}He (fA)	STDEV	^{3}He/^{4}He	Error
1	0.166	0.0005	124331	4.5	1.33E-06	4.09E-09
2	0.141	0.0015	103437	25.0	1.36E-06	1.48E-08
3	0.156	0.0014	115963	21.4	1.34E-06	1.19E-08
4	0.163	0.0008	118537	36.1	1.37E-06	6.95E-09
5	0.156	0.0015	115089	5.2	1.36E-06	1.28E-08
6	0.160	0.0009	116750	151.6	1.37E-06	7.76E-09
7	0.152	0.0006	110281	53.5	1.38E-06	5.22E-09
8	0.136	0.0008	99541	7.0	1.37E-06	7.65E-09
9	0.133	0.0008	99473	173.7	1.34E-06	8.29E-09
10	0.148	0.0005	110102	56.4	1.34E-06	4.50E-09
11	0.166	0.0003	124126	154.7	1.33E-06	3.26E-09
12	0.134	0.0015	99907	239.8	1.34E-06	1.50E-08
13	0.156	0.0003	116968	154.7	1.33E-06	3.46E-09
14	0.116	0.0015	86674	239.8	1.34E-06	1.73E-08
15	0.143	0.0007	106574	13.6	1.34E-06	6.19E-09
16	0.145	0.0005	110407	224.6	1.32E-06	5.52E-09
17	0.129	0.0015	97751	15.1	1.32E-06	1.49E-08
18	0.133	0.0019	100850	145.7	1.32E-06	1.86E-08
19	0.124	0.0013	93630	191.4	1.33E-06	1.46E-08
20	0.159	0.0011	117801	194.9	1.35E-06	9.63E-09
Average					1.34E-06	
Stdev					1.8657E-08	
Precision (%)					1.39	

Table A1.5 Ne signal intensities and isotopic ratios from measurements on Helix SFT

Analysis No.	^{20}Ne (fA)	STDEV	^{21}Ne (fA)	STDEV	^{22}Ne (fA)	STDEV	^{20}Ne/^{22}Ne	Error	^{21}Ne/^{22}Ne	Error
1	209526.6	55.44	627.3	0.18	21886.5	7.97	9.57	0.004	0.0287	0.00001
2	215183.1	14.00	643.4	0.21	22428.3	7.40	9.59	0.003	0.0287	0.00001
3	212617.7	38.83	638.6	0.12	22169.2	4.49	9.59	0.003	0.0288	0.00001
4	222810.9	483.13	677.8	3.25	23274.4	25.69	9.57	0.023	0.0291	0.00014
5	216215.2	176.08	648.9	1.01	22667.7	0.94	9.54	0.008	0.0286	0.00004
6	214303.0	14.50	643.3	0.15	22420.5	1.24	9.56	0.001	0.0287	0.00001
7	184370.3	36.56	551.2	0.35	19171.7	3.17	9.62	0.002	0.0288	0.00002
8	167085.0	627.74	501.8	1.74	17497.3	76.47	9.55	0.055	0.0287	0.00016
9	174578.1	17.26	522.5	0.33	18209.0	2.20	9.59	0.001	0.0287	0.00002
10	203010.1	16.24	607.3	0.27	21151.5	1.90	9.60	0.001	0.0287	0.00001
11	215454.6	19.98	646.1	0.08	22564.4	1.53	9.55	0.001	0.0286	0.00000
12	205420.0	24.21	616.3	0.13	21558.0	5.66	9.53	0.003	0.0286	0.00001
13	199378.4	58.78	598.4	0.14	20913.6	9.93	9.53	0.005	0.0286	0.00002
14	169425.1	28.70	507.8	0.21	17733.5	2.69	9.55	0.002	0.0286	0.00001
15	179105.5	27.63	535.1	0.14	18660.3	2.23	9.60	0.002	0.0287	0.00001
16	174646.8	23.81	523.1	0.22	18244.5	3.84	9.57	0.002	0.0287	0.00001
17	148587.4	17.12	445.8	0.17	15549.1	1.67	9.56	0.002	0.0287	0.00001
18	144047.2	30.75	431.0	0.16	15031.5	3.31	9.58	0.003	0.0287	0.00001
19	153220.1	476.17	463.5	1.13	15987.5	54.77	9.58	0.044	0.0290	0.00012
20	175665.5	178.92	526.0	0.64	18317.6	20.38	9.59	0.014	0.0287	0.00005
Average							9.5714		0.0287	
Stdev							0.0244		0.0001	
Precision (%)							0.26		0.45	

Table A1.6 Ar signal intensities and isotopic ratios from measurements on Helix SFT

Analysis No.	^{36}Ar (fA)	STDEV	^{38}Ar (fA)	STDEV	^{40}Ar (fA)	STDEV	^{38}Ar/^{36}Ar	Error	^{40}Ar/^{36}Ar	Error
1	102.1	0.26	19.79	0.20	30400.4	26.33	0.194	0.0020	297.8	0.81
2	101.3	0.16	19.48	0.19	30165.1	21.46	0.192	0.0019	297.9	0.51
3	102.6	0.65	19.19	0.27	30649.0	51.24	0.187	0.0029	298.6	1.97
4	93.5	0.30	17.71	0.24	27929.3	17.87	0.189	0.0027	298.6	0.99
5	754.6	0.30	145.18	0.17	224206.7	10.48	0.192	0.0002	297.1	0.12
6	694.7	0.27	132.90	0.20	206434.4	16.03	0.191	0.0003	297.1	0.12
7	719.8	0.45	138.35	0.17	215175.6	13.34	0.192	0.0003	298.9	0.19
8	674.4	0.26	128.51	0.10	201452.6	12.40	0.191	0.0002	298.7	0.11
9	660.8	0.43	126.24	0.16	196974.7	16.28	0.191	0.0003	298.1	0.20
10	706.8	1.70	133.77	0.40	210717.7	154.30	0.189	0.0007	298.1	0.75
11	751.4	1.26	142.26	0.10	224653.6	71.78	0.189	0.0003	299.0	0.51
12	717.2	1.66	136.16	0.46	214422.2	89.02	0.190	0.0008	299.0	0.70
13	722.2	1.60	136.66	0.12	215098.7	69.88	0.189	0.0005	297.8	0.67
14	665.2	1.65	125.67	0.24	198684.2	106.73	0.189	0.0006	298.7	0.76
15	670.3	1.96	127.11	0.28	200382.3	50.76	0.190	0.0007	298.9	0.88
16	777.0	1.45	147.94	0.42	232177.8	101.95	0.190	0.0006	298.8	0.57
17	686.5	1.41	131.29	0.38	204970.0	75.59	0.191	0.0007	298.6	0.63
18	713.3	1.52	135.72	0.43	212986.0	88.70	0.190	0.0007	298.6	0.65
19	688.8	2.25	130.31	0.11	205420.9	116.30	0.189	0.0006	298.2	0.99
20	812.1	2.25	153.64	0.11	242194.2	116.30	0.189	0.0005	298.2	0.84
Average							0.190		298.34	
Stdev							0.002		0.56	
Precision (%)							0.83		0.19	

Note: New chops for Ar was applied from 5th air standard measurement.

Table A1.7a Kr signal intensities with standard deviations from measurements on Helix SFT

Analysis No.	^{78}Kr (fA)	STDEV	^{80}Kr (fA)	STDEV	^{82}Kr (fA)	STDEV	^{83}Kr (fA)	STDEV	^{84}Kr (fA)	STDEV	^{86}Kr (fA)	STDEV
1	333.58	1.14	2152.88	11.50	10895.10	59.23	10776.08	36.71	53308.52	98.77	16241.51	49.12
2	339.45	1.01	2203.41	10.43	11194.49	53.58	11118.17	50.08	54895.67	205.25	16720.67	63.16
3	331.14	0.53	2142.53	0.45	10886.59	4.32	10793.41	14.80	53390.31	156.89	16261.62	37.99
4	309.87	0.47	2014.66	0.70	10237.91	1.90	10163.56	10.17	50239.64	101.20	15315.56	15.23
5	334.51	0.75	2163.30	0.62	11004.58	2.13	10914.46	13.90	54033.40	92.10	16452.09	35.14
6	322.86	1.28	2094.53	4.06	10649.75	23.29	10579.78	24.35	52336.48	126.26	15941.69	42.25
7	308.22	0.78	1996.58	3.70	10143.59	19.90	10044.23	32.46	49730.44	204.00	15144.83	66.73
8	318.23	0.21	2076.88	1.62	10568.75	11.26	10444.26	13.66	51496.55	110.01	15695.12	42.52
9	288.74	0.62	1872.88	0.42	9513.50	3.50	9438.63	18.00	46628.18	137.44	14185.23	42.36
10	344.70	0.35	2230.40	1.21	11345.06	2.81	11253.50	11.98	55774.92	116.31	16977.33	21.54
11	364.06	0.73	2351.79	1.77	11999.04	41.20	11859.77	8.66	58611.56	85.15	17836.67	29.27
12	327.93	1.23	2124.99	5.82	10830.32	27.91	10755.84	19.28	53240.10	31.13	16232.91	14.68
13	344.68	0.73	2225.99	2.01	11329.77	5.57	11232.02	15.09	55469.37	122.15	16893.75	30.18
14	268.06	0.39	1755.89	0.58	8930.94	1.69	8860.38	10.57	43712.84	106.74	13316.68	30.72
15	250.18	0.15	1621.03	0.93	8242.67	4.24	8170.00	8.49	40412.91	112.06	12306.54	30.58
16	279.82	1.24	1815.31	2.78	9225.33	14.14	9142.97	20.57	45208.51	142.62	13769.61	50.56
17	246.63	0.61	1597.97	2.01	8123.19	14.06	8053.20	17.75	39817.35	141.98	12131.55	34.60
18	279.29	0.50	1808.08	0.71	9186.95	7.98	9110.99	16.91	44988.57	130.41	13699.92	32.02
19	256.20	0.29	1659.79	2.68	8434.22	8.63	8352.84	11.35	41261.55	84.37	12591.79	29.06
20	320.31	0.34	2072.40	0.95	10532.19	2.98	10422.53	14.41	51488.90	87.73	15696.90	25.84

Table A1.7b Kr isotope ratios from measurements on Helix SFT

Analysis No.	$^{78}Kr/^{84}Kr$	Error	$^{80}Kr/^{84}Kr$	Error	$^{82}Kr/^{84}Kr$	Error	$^{83}Kr/^{84}Kr$	Error	$^{86}Kr/^{84}Kr$	Error
1	0.006258	0.000024	0.0404	0.0002	0.20438	0.00117	0.20215	0.00078	0.3047	0.0011
2	0.006183	0.000030	0.0401	0.0002	0.20392	0.00124	0.20253	0.00119	0.3046	0.0016
3	0.006202	0.000021	0.0401	0.0001	0.20391	0.00060	0.20216	0.00066	0.3046	0.0011
4	0.006168	0.000016	0.0401	0.0001	0.20378	0.00041	0.20230	0.00046	0.3049	0.0007
5	0.006191	0.000017	0.0400	0.0001	0.20366	0.00035	0.20199	0.00043	0.3045	0.0008
6	0.006169	0.000029	0.0400	0.0001	0.20349	0.00066	0.20215	0.00067	0.3046	0.0011
7	0.006198	0.000030	0.0401	0.0002	0.20397	0.00093	0.20197	0.00105	0.3045	0.0018
8	0.006180	0.000014	0.0403	0.0001	0.20523	0.00049	0.20281	0.00051	0.3048	0.0011
9	0.006192	0.000023	0.0402	0.0001	0.20403	0.00061	0.20242	0.00071	0.3042	0.0013
10	0.006180	0.000014	0.0400	0.0001	0.20341	0.00043	0.20177	0.00047	0.3044	0.0007
11	0.006211	0.000015	0.0401	0.0001	0.20472	0.00076	0.20235	0.00033	0.3043	0.0007
12	0.006160	0.000023	0.0399	0.0001	0.20342	0.00054	0.20203	0.00038	0.3049	0.0003
13	0.006214	0.000019	0.0401	0.0001	0.20425	0.00046	0.20249	0.00052	0.3046	0.0009
14	0.006132	0.000017	0.0402	0.0001	0.20431	0.00050	0.20270	0.00055	0.3046	0.0010
15	0.006191	0.000018	0.0401	0.0001	0.20396	0.00058	0.20216	0.00060	0.3045	0.0011
16	0.006189	0.000034	0.0402	0.0001	0.20406	0.00072	0.20224	0.00078	0.3046	0.0015
17	0.006194	0.000027	0.0401	0.0002	0.20401	0.00081	0.20225	0.00085	0.3047	0.0014
18	0.006208	0.000021	0.0402	0.0001	0.20421	0.00062	0.20252	0.00070	0.3045	0.0011
19	0.006209	0.000014	0.0402	0.0001	0.20441	0.00047	0.20244	0.00050	0.3052	0.0009
20	0.006221	0.000012	0.0402	0.0001	0.20455	0.00035	0.20242	0.00044	0.3049	0.0007
Average	0.006193		0.0401		0.20408		0.20229		0.3046	
Stdev	0.000026		0.0001		0.00045		0.00026		0.0002	
Precision (%)	0.42		0.27		0.22		0.13		0.07	

Table A1.8a Xe signal intensities and standard deviations from measurements on Helix SFT

Analysis No.	^{128}Xe (fA)	STDEV	^{129}Xe (fA)	STDEV	^{130}Xe (fA)	STDEV	^{131}Xe (fA)	STDEV	^{132}Xe (fA)	STDEV	^{134}Xe (fA)	STDEV	^{136}Xe (fA)	STDEV
1	308.00	1.38	4155.81	11.91	630.85	1.34	3250.45	7.37	4115.56	12.61	1610.96	4.11	1367.14	2.20
2	303.11	1.38	4108.07	12.13	623.63	1.24	3217.81	5.57	4069.95	10.20	1592.77	3.43	1352.06	1.87
3	299.67	1.15	4045.40	10.11	614.59	1.01	3171.45	4.73	4009.62	10.12	1569.47	3.33	1333.74	1.60
4	297.78	1.50	4037.41	11.69	614.37	1.12	3172.26	5.45	4011.63	9.83	1570.45	3.60	1334.06	1.80
5	282.06	1.50	3831.89	11.24	582.48	1.31	3003.36	6.14	3797.00	11.88	1486.14	3.72	1262.00	1.95
6	276.76	1.61	3737.09	17.53	568.41	2.48	2932.19	12.21	3713.23	16.07	1452.07	5.21	1232.03	4.17
7	270.02	1.31	3659.53	12.11	555.32	1.20	2869.77	6.11	3629.66	11.96	1421.89	3.87	1206.90	1.48
8	290.65	0.44	3955.49	6.25	605.79	1.08	3135.87	6.95	3973.11	8.47	1540.53	3.54	1311.31	3.27
9	298.63	0.77	4055.79	6.89	620.12	0.57	3205.21	2.78	4070.59	7.29	1585.96	2.65	1348.61	1.47
10	291.29	0.74	3943.86	6.68	600.41	0.54	3105.30	2.81	3932.02	6.39	1538.74	2.81	1307.65	1.07
11	297.53	0.90	4039.88	9.74	617.04	1.24	3194.64	6.24	4052.27	7.98	1579.52	2.82	1343.42	1.20
12	269.91	1.43	3744.93	9.13	573.05	1.50	2970.93	6.49	3763.75	11.90	1466.71	3.80	1248.04	1.66
13	314.14	1.56	4264.84	24.11	650.59	3.35	3354.86	19.77	4275.55	23.25	1669.39	9.05	1415.49	6.52
14	250.17	1.43	3471.11	9.13	531.15	1.50	2753.70	6.49	3488.55	11.90	1359.47	3.80	1156.79	1.66
15	220.34	1.56	2991.32	24.11	456.32	3.35	2353.07	19.77	2998.83	23.25	1170.89	9.05	992.81	6.52
16	243.23	1.25	3313.03	10.34	506.61	1.16	2620.82	5.97	3317.23	9.43	1294.34	2.90	1101.81	1.61
17	178.25	1.17	2420.66	11.34	369.66	1.12	1915.97	6.75	2426.04	10.15	947.08	3.52	805.67	1.69
18	229.16	1.13	3116.18	10.83	476.28	1.14	2462.47	5.34	3120.85	8.34	1218.52	2.52	1036.02	1.25
19	207.46	0.87	2810.23	6.38	429.33	0.94	2213.22	5.18	2812.88	7.20	1097.07	2.42	931.07	1.48
20	252.23	0.71	3426.59	7.00	522.25	0.43	2702.21	3.70	3428.27	7.90	1337.61	2.91	1138.63	0.98

Table A1.8b Xe isotope ratios from measurements on Helix SFT

Analysis No.	$^{128}Xe/^{130}Xe$	Error	$^{129}Xe/^{130}Xe$	Error	$^{131}Xe/^{130}Xe$	Error	$^{132}Xe/^{130}Xe$	Error	$^{134}Xe/^{130}Xe$	Error	$^{136}Xe/^{130}Xe$	Error
1	0.488	0.0024	6.59	0.02	5.15	0.02	6.52	0.02	2.55	0.01	2.167	0.006
2	0.486	0.0024	6.59	0.02	5.16	0.01	6.53	0.02	2.55	0.01	2.168	0.005
3	0.488	0.0020	6.58	0.02	5.16	0.01	6.52	0.02	2.55	0.01	2.170	0.004
4	0.485	0.0026	6.57	0.02	5.16	0.01	6.53	0.02	2.56	0.01	2.171	0.005
5	0.484	0.0028	6.58	0.02	5.16	0.02	6.52	0.03	2.55	0.01	2.167	0.006
6	0.487	0.0035	6.57	0.04	5.16	0.03	6.53	0.04	2.55	0.01	2.168	0.012
7	0.486	0.0026	6.59	0.03	5.17	0.02	6.54	0.03	2.56	0.01	2.173	0.005
8	0.480	0.0011	6.53	0.02	5.18	0.01	6.56	0.02	2.54	0.01	2.165	0.007
9	0.482	0.0013	6.54	0.01	5.17	0.01	6.56	0.01	2.56	0.00	2.175	0.003
10	0.485	0.0013	6.57	0.01	5.17	0.01	6.55	0.01	2.56	0.01	2.178	0.003
11	0.482	0.0017	6.55	0.02	5.18	0.01	6.57	0.02	2.56	0.01	2.177	0.005
12	0.471	0.0028	6.54	0.02	5.18	0.02	6.57	0.03	2.56	0.01	2.178	0.006
13	0.483	0.0035	6.56	0.05	5.16	0.04	6.57	0.05	2.57	0.02	2.176	0.015
14	0.471	0.0030	6.54	0.03	5.18	0.02	6.57	0.03	2.56	0.01	2.178	0.007
15	0.483	0.0049	6.56	0.07	5.16	0.06	6.57	0.07	2.57	0.03	2.176	0.021
16	0.480	0.0027	6.54	0.03	5.17	0.02	6.55	0.02	2.55	0.01	2.175	0.006
17	0.482	0.0035	6.55	0.04	5.18	0.02	6.56	0.03	2.56	0.01	2.179	0.008
18	0.481	0.0026	6.54	0.03	5.17	0.02	6.55	0.02	2.56	0.01	2.175	0.006
19	0.483	0.0023	6.55	0.02	5.16	0.02	6.55	0.02	2.56	0.01	2.169	0.006
20	0.483	0.0014	6.56	0.01	5.17	0.01	6.56	0.02	2.56	0.01	2.180	0.003
Ave	0.483		6.56		5.17		6.55		2.56		2.173	
Stdev	0.005		0.02		0.01		0.02		0.01		0.005	
Precision (%)	0.95		0.30		0.20		0.28		0.21		0.22	

Appendix 2 Supporting Information for Chapter 5

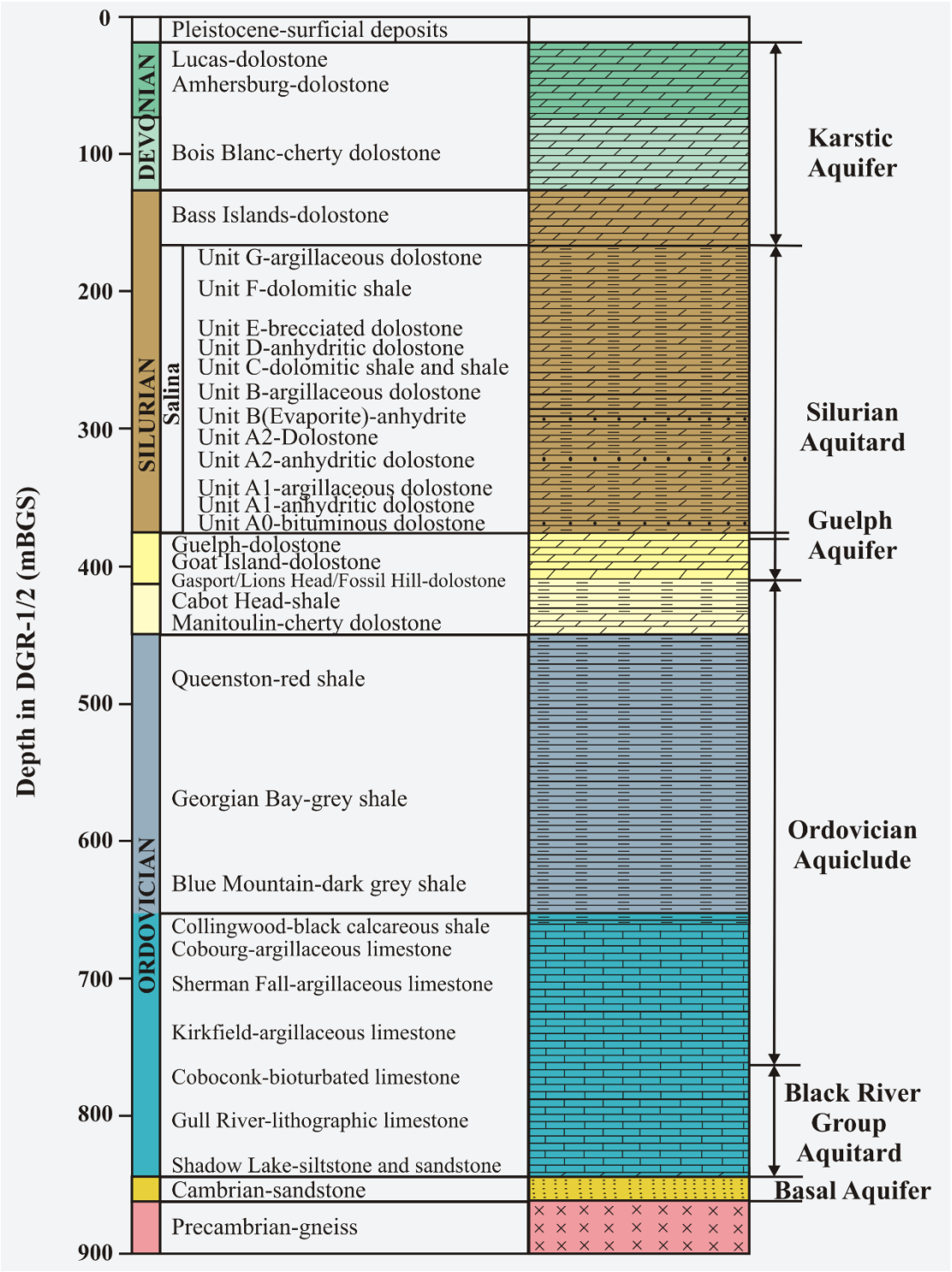

Figure A2.1 Stratigraphy of Bruce Nuclear Site. In this study, all samples' true vertical depths are calibrated to the same datum (DGR 1/2 boreholes) ((Intera Engineering Ltd.. 2011).

Intera Engineering Ltd.. (2011). Descriptive Geosphere Site Model. In Intera Engineering Ltd.

(Ed.): Toronto, Ontario, Canada.

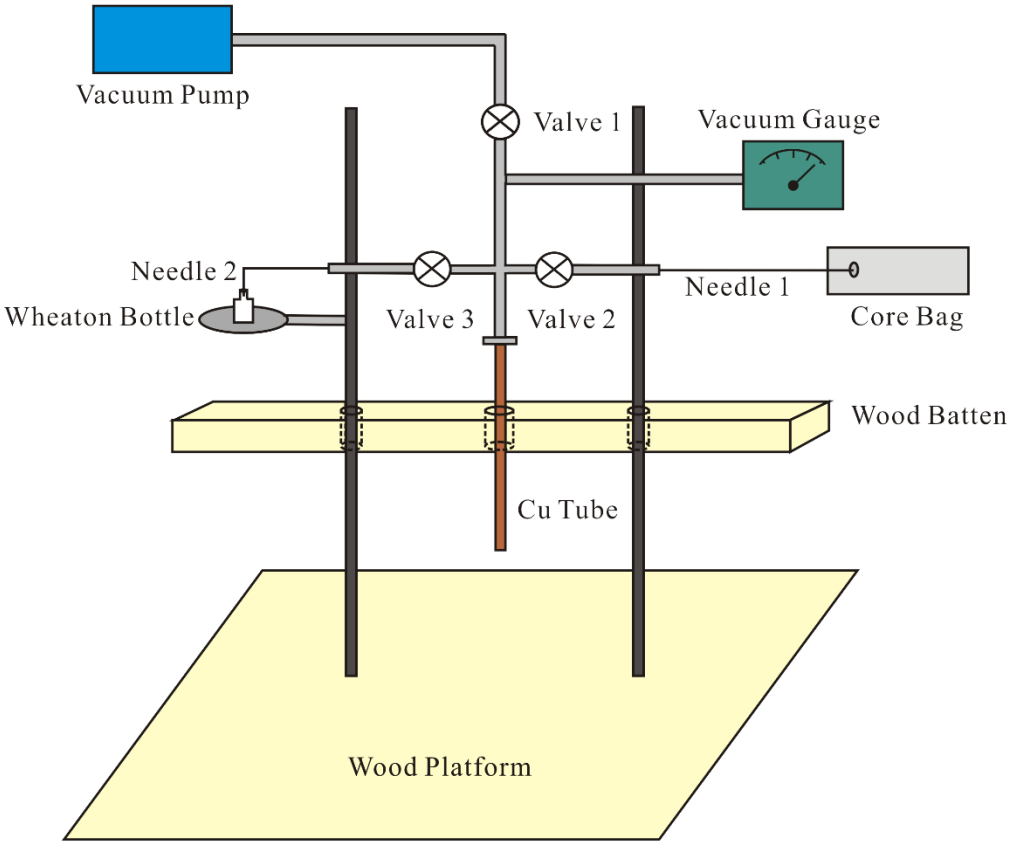

Figure A2.2 Schematic of the gas sampling system. The Vacuum pump is a rotary vane vacuum pump; Valves are Swagelok shut-off gas ball valves; Cu tube is 3/8” refrigeration-grade annealed copper tube; Needles are stainless steel made and gas-tight; the Vacuum Gauge is a Pirani vacuum gauge; Core sample in the vapor barrier foil is connected with Needle 1 via a butyl septum.

Text A2.1. Sampling Procedure

Before sampling, we attached a butyl septum to the core bag surface. Following that, a copper tube was connected via an Ultra-Torr fitting and a Wheaton bottle via a needle to the manifold. In order to pre-evacuate the sampling container and the vacuum line, Needle 1 was inserted midway through the butyl septum without puncturing the core bag. Full evacuation of the sampling apparatus was then performed with a rotary pump for 15 minutes with all valves open. The vacuum integrity of the system is ensured by monitoring vacuum stability on a Pirani vacuum gauge when the line is isolated from the rotary pump. Valve 1 (Figure S2) was then closed, and Valve 2 and Valve 3 were opened to let the gas equilibrate between the core bag and the extraction line for 5 minutes. Subsequently, Valve 3 was switched off and the copper tube immediately cold-weld sealed using a pinch-off clamp for future analysis.
The Cambrian groundwater dissolved gas sample was attained with a “high-pressure internal diffusion sampler” which has eight ports, six of those are interconnected with semipermeable silicon tubing allowing for gas exchange across the membrane into Cu tubes swaged outside. The other two ports allow for the inflow and outflow of groundwater. The Cambrian aquifer is confined by 450 m of Ordovician limestone and shale. The sampler was attached to the shut-in well head which maintained aquifer pressures at surface. The well was flushing discharge from the Cambrian sandstone aquifer for several days prior to shut in. The sampler was under well head pressure, maintained by a ball valve at the exit port. The valve was cracked open to allow a minimum flow of approximately 1 L/min. There was no effervescence observed in the gas-exchange chamber during sampling. The diffusion sampler was left for the 60+ hour duration before the copper tubes were clamped.

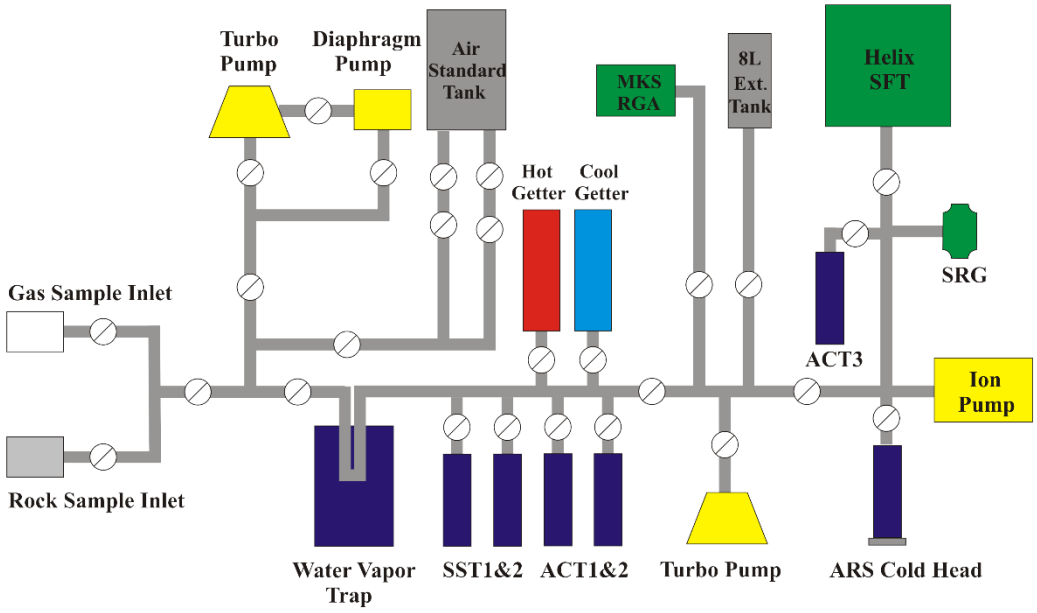

Figure A2.3 Schematic of the Noble gas preparation line at the University of Ottawa. (SST: stainless steel trap; ACT: activated charcoal trap; SRG: spinning rotor vacuum gauge)

Table A2.1 Noble gas isotoptic ratios (±1 σ uncertainties) in Ordovician shale, limestone porewater and Cambrian sandstone groundwater from the study site on the eastern flank of the Michigan Basin

Sample	Formation	Depth (mBGS)	Lithology	$^{3}He/^{4}He$	1σ	R/Ra	1σ	$^{20}Ne/^{22}Ne$	1σ	$^{40}Ar/^{36}Ar$	1σ	$^{86}Kr/^{84}Kr$	1σ	$^{129}Xe/^{130}Xe$	1σ	$^{136}Xe/^{130}Xe$	1σ
DGR5-551.07	Queenston	509	Shale	3.70E-08	4.59E-10	0.026	0.0003	9.80	0.002	296.4	0.8	0.3031	0.0118	6.453	0.008	2.191	0.005
DGR3-550.49	Georgian Bay	539	Shale	3.96E-08	1.85E-09	0.028	0.0013	9.80	0.004	304.7	0.9	0.3046	0.0016	6.597	0.026	2.235	0.009
DGR3-578.85	Georgian Bay	567	Shale	4.15E-08	1.36E-09	0.030	0.0010	9.70	0.068	299.2	0.7	0.3060	0.0007	6.578	0.028	2.245	0.009
DGR6-687.68	Blue Mountain	609	Shale	3.02E-08	9.49E-10	0.022	0.0007	9.81	0.018	308.6	2.5	0.3045	0.0011	6.513	0.009	2.175	0.008
DGR6-701.36	Blue Mountain	620	Shale	3.21E-08	5.84E-10	0.023	0.0004	9.80	0.060	300.1	1.0	0.3053	0.0009	6.509	0.027	2.172	0.007
DGR6-723.67	Blue Mountain	639	Shale	3.27E-08	8.55E-10	0.023	0.0006	9.82	0.012	319.8	1.4	0.3052	0.0016	6.562	0.017	2.234	0.011

DGR5-689.77	Blue Mountain	642	Shale	3.27E-08	1.02E-09	0.023	0.0007	9.81	0.003	343.6	0.9	0.3089	0.0032	6.498	0.032	2.184	0.008
DGR6-729.74	Blue Mountain	644	Shale	2.91E-08	1.60E-09	0.021	0.0011	9.72	0.003	313.1	1.0	0.3051	0.0011	6.481	0.029	2.177	0.007
DGR6-747.74	Coburg	658	Limestone	3.76E-08	1.49E-09	0.027	0.0011	9.97	0.028	299.5	0.8	0.3025	0.0116	6.526	0.079	2.174	0.026
DGR3-705.45	Sherman Fall	694	Limestone	5.82E-08	1.56E-09	0.042	0.0011	9.76	0.004	295.9	0.6	0.3056	0.0125	6.493	0.033	2.190	0.008
DGR-728.38	Sherman Fall	717	Limestone	5.27E-08	1.09E-09	0.038	0.0008	9.85	0.002	307.6	1.6	0.3048	0.0075	6.512	0.080	2.170	0.009
DGR3-756.00	Kirkfield	744	Limestone	6.37E-08	8.27E-10	0.046	0.0006	9.84	0.011	303.3	1.1	0.3050	0.0009	6.499	0.034	2.170	0.009
DGR3-771.83	Kirkfield	760	Limestone	5.23E-08	2.76E-09	0.037	0.0020	9.85	0.028	309.4	2.2	0.3044	0.0009	6.501	0.046	2.178	0.006
DGR6-886.99	Coboconk	773	Limestone	6.89E-08	1.90E-09	0.049	0.0014	9.77	0.002	305.4	1.0	0.3220	0.0025	6.508	0.024	2.182	0.006
DGR2-852.70	Cambrian	853	Sandstone	3.09E-08	1.32E-09	0.022	0.0009	9.74	0.002	782.4	6.1	0.3053	0.0037	6.501	0.037	2.240	0.009

DGR4-570.96_Heating 400 ℃	*Georgian Bay*	*571*	*Shale*	*1.50E-08*	*5.55E-10*	*0.0107*	*0.0004*	*11.54*	*0.073*	*1366.5*	*21.2*	*0.3050*	*0.0035*	*6.365*	*0.030*	*2.182*	*0.009*
Air (Ozima & Podosek, 2002)				1.40E-06		1		9.8		295.5		0.3052		6.496		2.176	

Table A2.2 Noble gas concentrations (cc_{STP}/cc gas) degassed from Ordovician shale, limestone porewater and Cambrian sandstone groundwater from the study site on the eastern flank of the Michigan Basin.

Sample	Formation	Depth (m)	Lithology	^{4}He (cc_{STP}/cc)	Error	^{20}Ne (cc_{STP}/cc)	Error	^{40}Ar (cc_{STP}/cc)	Error	^{84}Kr (cc_{STP}/cc)	Error	^{130}Xe (cc_{STP}/cc)	Error
DGR5-551.07	Queenston	509	Shale	4.342E-04	1.598E-08	3.625E-06	4.799E-10	3.330E-03	1.743E-06	1.799E-07	4.557E-09	1.087E-09	7.997E-13
DGR3-550.49	Georgian Bay	539	Shale	1.006E-03	2.413E-08	1.302E-05	3.892E-09	1.845E-02	4.897E-06	4.255E-07	1.683E-09	2.789E-09	5.756E-12
DGR3-578.85	Georgian Bay	567	Shale	1.505E-04	6.268E-09	2.217E-06	8.993E-09	1.253E-03	7.439E-07	8.601E-08	1.203E-10	4.519E-10	9.645E-13
DGR6-687.68	Blue Mountain	609	Shale	4.121E-05	4.650E-08	4.032E-07	4.415E-10	2.058E-04	7.660E-08	3.829E-08	6.173E-10	9.014E-10	6.013E-13
DGR6-701.36	Blue Mountain	620	Shale	1.979E-05	1.824E-08	1.174E-07	3.323E-10	1.448E-04	3.091E-07	1.256E-09	9.787E-12	6.487E-10	4.102E-12
DGR6-723.67	Blue Mountain	639	Shale	1.216E-03	1.401E-06	1.662E-06	1.482E-09	1.621E-03	2.336E-06	4.421E-08	1.489E-10	7.036E-10	1.306E-12

DGR5-689.77	Blue Mountain	642	Shale	9.522E-04	1.192E-06	5.103E-06	1.111E-09	1.344E-03	5.109E-07	8.613E-08	6.679E-10	7.136E-10	2.274E-12
DGR6-729.74	Blue Mountain	644	Shale	1.048E-03	9.640E-07	2.009E-06	2.797E-10	2.393E-03	1.389E-06	3.866E-08	8.799E-11	1.112E-09	3.449E-12
DGR6-747.74	Coburg	658	Limestone	7.640E-04	3.125E-07	1.201E-05	2.679E-08	6.340E-03	3.309E-06	1.127E-07	2.422E-09	2.724E-09	2.291E-11
DGR3-705.45	Sherman Fall	694	Limestone	5.892E-05	6.032E-08	3.691E-06	7.609E-10	2.197E-03	9.303E-07	1.707E-07	5E-09	8.642E-10	2.795E-12
DGR-728.38	Sherman Fall	717	Limestone	1.262E-04	3.478E-08	1.759E-06	5.205E-09	1.005E-03	5.046E-07	6.267E-08	1.845E-09	3.498E-10	2.916E-12
DGR3-756.00	Kirkfield	744	Limestone	7.763E-05	4.059E-09	1.475E-06	1.664E-09	1.401E-03	2.483E-07	4.777E-08	1.04E-10	3.193E-10	1.157E-12
DGR3-771.83	Kirkfield	760	Limestone	4.825E-06	4.114E-10	1.030E-07	2.676E-10	5.155E-05	2.096E-08	4.674E-08	1.792E-10	4.487E-11	7.229E-14
DGR6-886.99	Coboconk	773	Limestone	1.059E-04	1.032E-07	2.489E-06	2.360E-10	1.166E-03	2.295E-06	7.043E-08	5.368E-10	4.692E-10	1.039E-12
DGR2-852.7	Cambrian	853	Sandstone	4.559E-03	3.620E-07	2.381E-06	3.667E-10	1.913E-03	1.896E-06	4.221E-08	4.273E-10	3.124E-10	1.234E-12

Table A2.3 Noble gas dating for Ordovician shale and limestone porewater from the Bruce site on the eastern flank of the Michigan Basin

U/Th-He dating

Sample ID	Formation	Depth (m)	Rock type	Core weight(g)	U (ppm)	Th (ppm)	Radiogenic ^{4}He (atoms/g rock)	Error	^{4}He production rate (atoms/g rock/yr)	^{4}He Age (yr)	Error	Average ^{4}He Age (yr)	Error
DGR5-551.07	Queenston	508.93	Shale	2861.3	2.2	8.5	3.853E+15	1.381E+11	1.368E+07	2.815E+08	1.009E+04		
DGR3-550.49	Georgian Bay	538.59	shale	2861.3	3	13	6.420E+15	1.496E+11	1.975E+07	3.251E+08	7.578E+03		
DGR5-698.77	Blue Mountain	641.90	shale	4172.8	4.2	18	5.793E+15	7.080E+12	2.749E+07	2.107E+08	2.575E+05		
DGR3-705.45	Sherman Fall	694.25	limestone	3471.5	0.41	1.1	5.034E+14	4.939E+11	2.177E+06	2.312E+08	2.268E+05	2.46E+08	1.47E+05
DGR3-728.38	Sherman Fall	717.18	limestone	3112.4	0.4	1.8	5.958E+14	9.972E+11	2.684E+06	2.220E+08	3.715E+05		
DGR3-756.00	Kirkfield	743.70	limestone	3232.1	0.68	3.1	9.519E+14	4.750E+10	4.594E+06	2.072E+08	1.034E+04		

U-Xe dating

Sample ID	Formation	Depth (m)	Rock type	Core weight(g)	U (ppm)	Th (ppm)	Radiogenic ^{136}Xe (atoms/g rock)	Error	^{4}He production rate (atoms/g rock/yr)	^{136}Xe Age (yr)	Error	Average ^{136}Xe Age (yr)	Error
DGR3-578.85	Georgian Bay	566.95	shale	2742.1	3	13	8.822E+06	2.826E+04	1.975E+07	2.148E+08	6.994E+05	2.55E+08	1.07E+06
DGR6-723.67	Blue Mountain	639.22	shale	2742.1	3.5	11	1.422E+07	6.799E+04	1.983E+07	2.948E+08	1.442E+06		

Ozima, M., & Podosek, F. A. (2002). *Noble gas geochemistry*: Cambridge University Press.